

**Second Strain Gradient Continuum Model for the Mechanics of
Fiber-Reinforced Composites**

by

Md Hafijur Rahman

A thesis submitted in partial fulfillment of the requirements for the degree of

Master of Science

Department of Mechanical Engineering
University of Alberta

© Md Hafijur Rahman, 2022

Abstract

The mechanics of composite materials is a subject of intense study due to their versatile and tailorable mechanical properties. A composite material consists of at least two different phases; one is called the reinforcing phase and the other one in which it is embedded is called the matrix phase. Due to the presence of multi-phase and fiber-matrix interface, the characterization of local behaviors of a composite is computationally expensive. The continuum mechanics offers the necessary mathematical framework to accommodate the overall microscopic behaviors of the reinforcement phase into the model of deformations. In this thesis, the mechanics of fiber-reinforced composite materials are presented within the framework of the second strain gradient theory. A continuum-based model is developed for the analysis of elastic materials reinforced with unidirectional and bidirectional fibers and subjected to finite plane deformations. Moreover, the continuously distributed unidirectional fiber-composite system is transformed into the randomly distributed short fiber-composite system by introducing the shear lag parameter and krenchel orientation factor into the model. The mechanics of randomly distributed short fiber-composite system is also presented. The Euler equilibrium equations and the associated boundary conditions are obtained via the variational principle and iterative integration by parts. In particular, the energy density function is augmented to accommodate the first, second, and third gradient of deformations into the models of continuum deformation. The complete expressions of Piola-type triple stress and its coupled triple force arising in the third gradient of continuum deformations are formulated, which, in turn, yield the unique deformation maps in the presence of admissible boundary conditions of higher or-

der. The solutions of the resulting systems of differential equations are obtained via the custom-built numerical scheme from which smooth and dilatational shear angle distributions are predicted throughout the entire domain of interest. It is also observed that the third gradient constitutive parameter is associated with the volume dilatation of third-gradient continua, which may be appeared in the form of shear band inclination angle. In addition, the fiber aspect ratio and the third gradient constitutive parameter are observed to be related to the effective Young's modulus of a randomly distributed short-fiber composite system. The obtained numerical results are compared with the results in the dedicated literature, which show a good agreement.

Preface

This thesis is performed as a part of the research project under the supervision of Professor Chun Il Kim.

Chapter 2 of this thesis has been submitted to Continuum Mechanics and Thermodynamics journal entitled “A third gradient based continuum model for the mechanics of continua reinforced with extensible bidirectional fibers resistant to flexure”.

Chapter 3 of this work is ready to be submitted soon.

*“To my dear parents, and Wife **Orna Khandoker**” for their support and sacrifices*

Acknowledgements

Firstly, I would like to express my very special gratitude to Professor Chun Il Kim for his support, patience, motivation, and in-depth knowledge. His guidance helped me in all the time of M.Sc. research.

I also would like to thank my thesis committee: Dr. Ge Li, Dr. Zengtao Chen and Dr. Hyo-jick Choi.

Also special thanks to Mr. Suprabha Islam, for his development of nano-fiber reinforced composite system which is discussed in chapter 3. Also, Mr. Suprabha assisted with the numerical tools that was used for generating the shear angle distributions plots.

Finally, I must express my special gratitude to my parents for providing me continuous encouragement during my graduate studies.

Table of Contents

1	Introduction	1
1.1	Composite material and its Background	1
1.1.1	History of composite materials	2
1.1.2	Classification of composite materials	3
1.2	Hyperelastic material models	4
1.2.1	Neo-Hookean model	4
1.2.2	Mooney-Rivlin model	5
1.3	Analysis of composite materials	6
1.3.1	Higher-gradient continuum theory	7
1.3.2	Strain gradient theory	8
1.3.3	Micropolar theory	9
1.3.4	Nonlocal elasticity theory	10
1.3.5	Classical theory vs Higher-order theory	10
1.4	Applications of higher-order gradient theory	13
1.5	Thesis Objectives	14
1.6	Structure of thesis	15
2	A third gradient based continuum model for the mechanics of continua reinforced with extensible bidirectional fibers resistant to flexure	17
2.1	Kinematics	17
2.2	Equilibrium	23
2.3	Boundary conditions	27
2.3.1	Example: Neo-Hookean materials	32
2.3.2	Example: Mooney-Rivlin materials	35
2.4	Finite element analysis of the sixth-order coupled PDE	37
2.5	Results and discussion	44
2.5.1	Application of third gradient of deformation theory	49
2.6	Conclusions	55

3	A second strain gradient based continuum model for the composite reinforced with extensible nano-fibers resistant to flexure	57
3.1	Kinematics	57
3.1.1	Defining energy potential for the unidirectional continuous fiber composite system	58
3.1.2	Development of randomly oriented short fiber composite system	60
3.2	Equilibrium and Boundary Conditions	63
3.2.1	Example: Neo-Hookean materials	69
3.2.2	Example: Mooney-Rivlin materials	70
3.3	Custom-built FEA of the nonlinear coupled PDE	71
3.4	Results and discussion	77
3.5	Conclusions	87
4	Conclusions & Future Works	89
4.1	Conclusions	89
4.2	Future Work	91
	Bibliography	93

List of Tables

2.1	Shear band inclination angle obtained from [89, 95] and proposed third gradient model	53
3.1	Interfacial parameters and properties of graphene [100]	78

List of Figures

1.1	Materials used for the Boeing 787 Dreamliner passenger airplane [9] .	3
1.2	Bone modeling using micropolar elasticity. Picture taken from [62] . .	10
1.3	First vs. second gradient elasticity comparison. Picture taken from [68]	11
1.4	Shear angle distribution: first gradient (left), second gradient (right). Picture taken from [67]	12
1.5	Shear angle distribution: first gradient (left), second gradient (middle), third gradient (right). Picture taken from [69]	12
2.1	Schematic of the problem	43
2.2	Deformation Configuration when $\frac{t_1}{\mu} = 10$, $\frac{E_1}{\mu} = 10$, $\frac{C_1}{\mu} = 5$ and $\frac{A_1}{\mu} = 5$	45
2.3	Deformed configuration with variation of $\frac{E_1}{\mu}$ when $\frac{t_1}{\mu} = 10$, $\frac{C_1}{\mu} = 5$, and $\frac{A_1}{\mu} = 5$	45
2.4	Deformed configuration with variation of $\frac{A_1}{\mu}$ when $\frac{t_1}{\mu} = 10$, $\frac{E_1}{\mu} = 10$, and $\frac{C_1}{\mu} = 5$	46
2.5	Deformed configuration with variation of triple force (a) when $\frac{t_1}{\mu} = 5$, $\frac{E_1}{\mu} = 10$, $\frac{C_1}{\mu} = 5$ and $\frac{A_1}{\mu} = 5$, (b) Zoomed section	46
2.6	Comparison with the existing result [67]	46
2.7	Deformation contour $\sqrt{\chi_1^2 + \chi_2^2}$ (a) $\frac{A_1}{\mu} = 5$, (b) $\frac{A_1}{\mu} = 10$, (c) $\frac{A_1}{\mu} = 50$ when $\frac{t_1}{\mu} = 10$, $\frac{E_1}{\mu} = 10$, and $\frac{C_1}{\mu} = 5$	47
2.8	Shear angle and shear strain distribution for various triple stress pa- rameter when $\frac{t_1}{\mu} = 10$, $\frac{E_1}{\mu} = 10$ and $\frac{C_1}{\mu} = 5$	49
2.9	Material structure (a) Close packed array, (b) Loose packed array . .	51
2.10	Shear angle distribution for various triple force $\mathbf{r} : \mathbf{r} < \mathbf{0}$ (left) and $\mathbf{r} > \mathbf{0}$ (right)	52
2.11	Shear angle distribution with the average shear angle of the domain .	54
2.12	Variation of shear band inclination angle α with triple stress parameter $\frac{A_1}{\mu}$ and drucker prager coefficient a presented in [89, 95]	55

3.1	Schematic of the problem and demonstration of the model development (a) continuous unidirectional fiber, (b) aligned short fiber, (c) randomly distributed fiber	58
3.2	A typical strain distribution along the fiber length, and its dependence on the fiber aspect ratio	61
3.3	Strain distribution along the fiber length for (a) Pristine, (b) Hydroxylated and (c) TSW-defected cases with various aspect ratios S	78
3.4	Deformation configuration: $\frac{t}{\mu} = 10$, $\frac{E}{\mu} = 100$, $\frac{C}{\mu} = 10$, $\frac{A}{\mu} = 10$, $S = 100$	79
3.5	Deformed configuration with variation of $\frac{E}{\mu}$ when $\frac{t}{\mu} = 10$, $\frac{C}{\mu} = 10$, $\frac{A}{\mu} = 10$, $S = 100$	80
3.6	Deformed configuration with variation of S when $\frac{t}{\mu} = 10$, $\frac{E}{\mu} = 100$, $\frac{C}{\mu} = 10$, $\frac{A}{\mu} = 10$	80
3.7	Deformed configuration with variation of $\frac{A}{\mu}$ when $\frac{t}{\mu} = 10$, $\frac{E}{\mu} = 100$, $\frac{C}{\mu} = 10$, $S = 100$	81
3.8	Comparison with the existing results [67]	81
3.9	Deformation contour $\sqrt{\chi_1^2 + \chi_2^2}$ (a) $S = 100$, (b) $S = 1000$, (c) $S = 5000$ when $\frac{t}{\mu} = 10$, $\frac{E}{\mu} = 100$, $\frac{C}{\mu} = 10$, $\frac{A}{\mu} = 10$	83
3.10	Shear angle distribution for various fiber aspect ratios S ((a) $S = 100$, (b) $S = 1000$, (c) $S = 5000$) when $\frac{t}{\mu} = 10$, $\frac{E}{\mu} = 100$, $\frac{C}{\mu} = 10$, $\frac{A}{\mu} = 10$	84
3.11	Variation of effective Young's modulus of composite with fiber aspect ratio S	85
3.12	Variation of effective Young's modulus of composite with triple stress parameter $\frac{A}{\mu}$	86

Chapter 1

Introduction

This chapter begins with a brief introduction to the composite material and, subsequently, fiber-reinforced composites. In section 1.1, we discuss the background of composite materials and their common classifications. In section 1.2, we briefly discuss the hyperelastic material models that are usually used as the matrix phase of composites. In section 1.3, we discussed the various approach to analyze the mechanics of fiber-reinforced composite materials. In section 1.4, we illustrate the application of higher-order theory. Furthermore, We will demonstrate the objectives of this thesis in section 1.5. Lastly, we present a brief structure of this thesis in section 1.6.

1.1 Composite material and its Background

‘Composite materials’, also briefly referred to as ‘Composites’, consist of two or more constituents that are combined at a macroscopic level and are not soluble in each other. The physical and chemical properties of composite materials differ from their constituents. One constituent is called the reinforcing phase material, which may be appeared in the form of fibers, particles, or flakes, and the other one in which the reinforcing phase is embedded is called the matrix. The matrix is the continuous material phase, while reinforcement is the dispersed material phase. The matrix provides structural integrity and works as a binder to keep the reinforcement phase in place. The matrix transfers load to and between fibers. In particular, the reinforcement

phase adds tensile strength to the matrix material [1]. The physical properties of composite materials depend on the volume fraction of their constituents, individual properties of constituents, fiber orientation, fiber length, bonding between fiber and matrix, etc. So it is possible to tailor the properties of a composite and make it specialized to do a certain job, for instance, to become stronger, lighter, or resistant to electricity.

1.1.1 History of composite materials

The Mesopotamians are credited with using composite materials for the first time. In 3400 B.C., these people glued wood strips at different angles to make plywood. Following this, the Egyptians began to manufacture death masks out of linen or papyrus soaked in plaster at around 2181 B.C. [2]

In 1200 A.D., the Mongols constructed composite bows using wood, bamboo, bone, cattle tendons, horn, and silk which were quite effective at the time. This bows made Genghis Khan military superior on earth until the invention of gunpowder [3].

During the 1900s, synthetic resins started to take a solid form by using polymerization, which led to the creation of various plastics such as polyester, phenolic, and vinyl. The famous Belgian chemist Leo Baekeland invented Bakelite which did not conduct electricity and was heat resistant. [3, 4].

In 1935, Owens Corning combined fiberglass with a plastic polymer and invented a remarkably strong and light structure. The Fiber Reinforced Polymers (FRP) industry as we know it today began with this. [4]. The FRP industry transitioned from research to manufacturing following World War II. A fully composite frame car was created and tested by the year 1947. Later on, in 1961, carbon fiber composites were used commercially, and by the mid-nineties, the composite started to replace the traditional materials [5, 6]. In the case of manufacturing Boyeing 787 Dreamliner, 50 percent of major structures are made of Carbon Fiber Reinforced Polymer, and 15 percent of titanium alloy, resulting in 20 percent fuel saving due to reduced weight

(See Figure 1.1).

The versatile and tailorable mechanical properties of composite materials make them useful in every aspect of modern society, including home appliances, agriculture, space, chemical, and automotive industries [6–8]. Currently, it is anticipated that the size of the global market for composite materials will increase from USD 88.80 billion in 2021 to USD 144.5 billion by 2028 with a CAGR (Compound Annual Growth Rate) of 6.66 percent from 2021 to 2028.

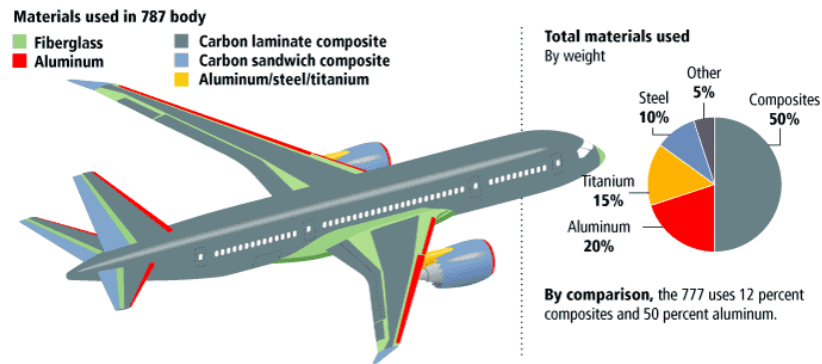


Figure 1.1: Materials used for the Boeing 787 Dreamliner passenger airplane [9]

1.1.2 Classification of composite materials

Classification of composite materials has been presented in literature [10] at two different stages:

1. Based on the matrix material types, the composites are classified as follows

- Polymer matrix composites (PMC)
- Ceramic matrix composites (CMC)
- Metal matrix composites (MMC)
- Carbon fiber/carbonaceous matrix composites (CCC)
- Particulate-reinforced metal matrix composites (PMMC)
- Fiber-reinforced polymeric composites (FRPC)

2. The second criterion is based on the reinforcement material. The composites are subdivided into the following categories as

- Particulate reinforced composites (PRC)
- Flake reinforced composite
- Fiber reinforced composites (FRC) (continuous fibers, short fibers, whiskers)

The main discussion in this thesis is about the Fiber reinforced composites (FRC). Usually, the fiber's radius is far less than its length, and they increase the strength of the composites under tensile and shear loading. The necessary mathematical framework for both continuous fibers and discretely distributed short fibers is presented in this thesis.

1.2 Hyperelastic material models

The necessary mathematical framework for the continuum description of fiber-reinforced composite materials is attained by assuming the fibers are densely embedded into the matrix material. The stress-strain relationship of matrix material can be either linear or nonlinear. For many cases, it is necessary to use a nonlinear stress-strain relationship to predict the mechanical behavior more accurately, and the hyperelasticity models serve this purpose [11]. The strain energy density function is widely used in continuum mechanics to derive the stress-strain relationship of the hyperelastic matrix material. In this section, we briefly discuss the well-established hyperelastic matrix material models.

1.2.1 Neo-Hookean model

The Neo-Hookean model is a hyperelastic material model that can be used for predicting the nonlinear stress-strain behavior of materials and is similar to Hooke's law. In general, the relationship between applied stress and strain is initially linear, but at a certain point, the stress-strain curve changes to nonlinear. Ronald Rivlin

[12] proposed this model in 1948 to predict the deformation of plastics and rubber-like substances. The strain energy density function for a compressible Neo-Hookean material is as follows:

$$W = C_1(I_1 - 3 - 2 \ln J) + D_1(J - 1)^2, \quad (1.1)$$

where C_1 and D_1 are material constants, and I_1 is the first invariant (trace), of the right Cauchy-Green deformation tensor, i.e.,

$$I_1 = \lambda_1^2 + \lambda_2^2 + \lambda_3^2, \quad (1.2)$$

where λ_i are the principal stretches. J is the determinant of deformation gradient F , i.e.,

$$J = \det(F) = \lambda_1 \lambda_2 \lambda_3. \quad (1.3)$$

For an incompressible material ($J = 1$) the strain energy density function becomes

$$W = C_1(I_1 - 3). \quad (1.4)$$

It is to be noted that, the Neo-Hookean model does not consider the dissipative release of energy as heat during deformation and assumes the perfect elasticity at all stages. It is usually used for small deformations and is typically accurate only for strains less than 20% [13].

1.2.2 Mooney-Rivlin model

In 1940, Melvin Mooney [14] proposed a hyperelastic material model. Following that, in 1948, Ronald Rivlin [12] expressed the strain energy function in terms of first and second invariants of the Cauchy-Green deformation tensor. The strain energy density function for a Mooney-Rivlin hyperelastic material is as follows:

$$W = C_1(\bar{I}_1 - 3) + C_2(\bar{I}_2 - 3), \quad (1.5)$$

where C_1 and C_2 are empirically determined material constants, and \bar{I}_1 and \bar{I}_2 are the first and the second invariant of the deviatoric component of the Cauchy-Green deformation tensor defined as

$$\begin{aligned}\bar{I}_1 &= J^{-\frac{2}{3}}I_1, \\ \bar{I}_2 &= J^{-\frac{4}{3}}I_2,\end{aligned}\tag{1.6}$$

where J and I_1 are defined in Eq. (1.3) and Eq. (1.2) respectively, and I_2 is defined as

$$I_2 = \lambda_1^2\lambda_2^2 + \lambda_2^2\lambda_3^2 + \lambda_3^2\lambda_1^2.\tag{1.7}$$

For an incompressible material ($J = 1$) the strain energy density function becomes

$$W = C_1(I_1 - 3) + C_2(I_2 - 3).\tag{1.8}$$

Mooney-Rivlin model is related to the linear elastic shear modulus G , which can be expressed as follows [15]:

$$G = 2(C_1 + C_2)\tag{1.9}$$

Several hyperelastic material models are present in the literature, amongst which the Ogden model, Arruda-Boyce model, Yeoh model, and Full and reduced Polynomial model are notable. In this thesis, we used both Neo-Hookean and Mooney-Rivlin models to characterize the matrix material. However, only the Neo-Hookean model is considered for the model implementation.

1.3 Analysis of composite materials

The general approach to analyze the mechanics of composite materials leads to two major branches of research [16]. The first approach is the direct investigation of local behaviors of an individual fiber—matrix system, including interfacial region. The interaction of the fibers with one another and with the surrounding matrix is well explored in [17–19] to comprehend the mechanical properties of fiber-reinforced composite materials. However, studies based on interface properties could not forecast

how a fiber-reinforced composite will react to external pressures and/or displacements. Later, microstructures and element interaction were added to the constitutive equation to predict the microscopic behavior of composites under boundary stresses [20–22]. Although the direct approach to investigate the local behavior is computationally expensive, this approach was used successfully to analyze the mechanics of composite materials [16].

The second approach is the development of continuum theory by incorporating the properties of fibers into the model of deformations. Adkins and Rivlin [23] introduced the idea of considering fibers as a constraint to the extension of composite materials along the directions of aligned fibers. Spencer et al. [20] extended Adkins and Rivlin’s [23] concept to propose a continuum model for fiber-reinforced composite materials in which the deformation history dictates the principal axes of anisotropy. The mathematical framework of generalized continuum theories using Navier-Cauchy’s approach is discussed in [24–27]. The issue with the Cauchy-Navier format is its inability to encompass the generalized Micro-Structured continua [28–31]. Mindlin [32] adopts the concept of variational principles to obtain the equilibrium equation. In this work, Mindlin formulated a linear theory describing the responses of an elastic solid in which the potential energy density is a function of the first and second gradient of continuum deformations. Later on, the concept has been widely adopted in the analysis of micro-structured solids [33–39].

1.3.1 Higher-gradient continuum theory

We have discussed in section 1.3 the usefulness of continuum theories in analyzing micro-structured continua. This section will briefly discuss the higher-gradient continuum theories and their suitability in the analysis of fiber-reinforced composites.

Higher-gradient theories can be categorized into three major groups [40]:

- strain gradient elasticity

- micropolar elasticity
- nonlocal elasticity

The strain gradient theories can be sub-categorized into the following groups:

- first and second strain gradient theories
- couple stress theory
- modified couple stress theory
- modified strain gradient theory

1.3.2 Strain gradient theory

In the strain gradient theories, the strain energy is a function of both strains and the gradient of strains. The primary continuum theories describing the mechanical responses under various loading conditions consider the composites as anisotropic materials whose response function depends only on the first gradient of deformation [41, 42]. Due to some of its limitations, i.e., the first gradient theory can't capture large deformations, Rivlin [43] formulated a new method incorporating up to the second order of deformation gradient into the model. Later, Adkins and Rivlin [23] provided a mathematical framework to analyze large deformations and considered the fibers as a constraint to the extension of isotropic materials along the directions of aligned fibers. The proposed model [23] is further developed in [44–47]. In [47], Spencer developed a more comprehensive model for the fiber-reinforced composite, which closely connects with nonlinear anisotropic elasticity. A few applications of the proposed theory [47] in the analysis of biological materials can be found in [48]. However, all the previous developments [44–47] consider the fibers as infinitesimally thin and thus infinitely flexible and exclude the fibers bending resistance. Later, Spencer and Soldatos [49] incorporated fiber bending stiffness into the continuum model by assuming that strain-energy density depends not only on the deformation

and the fiber vectors but also on the gradients of the deformed fiber vectors. Thus the fiber curvature is included in the continuum model via the second gradient of deformation. A similar continuum theory is discussed for liquid crystals [50] and large deformations of elastic membranes with bending stiffness [51]. Using the concept of variational principle to obtain the Euler equilibrium equation, Mindlin [32] formulated a continuum model for the deformation of an elastic solid in which the potential energy density is a function of the strain and its first and second gradients. Steigmann [52] modeled the fibers as continuously distributed spatial rods of the Kirchhoff type and formulated a theory of fiber-reinforced composites where the fiber's resistance to bending and shear is incorporated. A similar mathematical framework can also be found in [53–56]. In addition, several higher-order theories have been proposed to analyze the micro-structured continua; for example, couple stress theory [34, 35, 57], modified couple stress theory [58], modified strain gradient theory [59], etc.

1.3.3 Micropolar theory

The micropolar elasticity, also known as Cosserat elasticity, describes the static deformation of each point by a displacement vector and an independent rotation vector along with non-symmetric strain and stress. According to micropolar elasticity, a material element can have microrotation without undergoing a micro displacement [60]. It incorporates both couple stress and force stress. In the isotropic Cosserat solid, there are six elastic constants, in contrast to the classical elastic solid in which there are two independent elastic constants (Lame's constants). These constants are experimentally determinable.

The micropolar elasticity was proposed by Cosserat brothers more than a hundred years ago and later developed by others (see, for example, [37, 61]). Nowadays, micropolar elasticity is widely used in modeling bones, cracks in fracture mechanics, foams, porous media, beam lattices, etc [62]. Figure 1.2 depicts the micropolar modeling of bone structure. In general, micropolar elasticity has the following consequences

over the classical elasticity theory:

- it can accommodate size effects, i.e., the effect of microstructure, whereas classical elasticity doesn't [62]
- the stress concentration factor estimated from micropolar elasticity for a circular hole is smaller than the classical value [63]
- in wave propagation analysis, the pace of dilational waves in the Cosserat medium is independent of frequency [63]

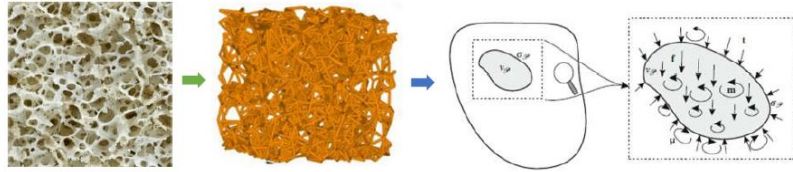


Figure 1.2: Bone modeling using micropolar elasticity. Picture taken from [62]

1.3.4 Nonlocal elasticity theory

Kroner [64] presented the nonlocal elasticity hypothesis, which was further improved by Eringen and Edelen [65]. In this theory, the points undergo translational motion as in the classical case, but the stress at a point depends on the strain in a region near that point, and the size effect is thus accounted for by constitutive equations with a nonlocal parameter. Nonlocal elasticity theory was initially formulated in an integral form and later reformulated by Eringen [66] in a differential form by considering a specific kernel function. Compared to the integral model, the differential one is widely used for nanostructures due to its simplicity [40].

1.3.5 Classical theory vs Higher-order theory

The classical theory or the first-order deformation gradient theory assumes the stress as a function of strain only, whereas the higher-order deformation gradient theory includes both strain and strain gradient into the constitutive equation of stress. The

mathematical relationships of stress-strain for classical and higher-order gradient continua are defined in Eqs. (1.10) and (1.11) respectively as

$$\sigma = f(\varepsilon), \quad (1.10)$$

$$\sigma = f(\varepsilon, \nabla\varepsilon). \quad (1.11)$$

In the case of fiber-reinforced composite materials analysis, the classical theory doesn't append the fiber's bending energy into the strain energy potential function that demonstrates the stress-strain relationship. Mathematically, we can express the strain energy potential function for the first gradient continua as

$$W(\mathbf{F}, \varepsilon(\mathbf{F})) = W(\mathbf{F}) + W(\varepsilon(\mathbf{F})), \quad (1.12)$$

where $W(\mathbf{F})$ is the energy potential of matrix, $W(\varepsilon(\mathbf{F}))$ is the fiber's energy potential pertaining to the extension. The mechanical response (i.e., shear angle distribution) of first-gradient continua under the extension test is shown in Figure 1.3. It is shown that the transition zones (from the red area to the green area and again from the green area to the blue area) are sharp, which doesn't correspond to the experimental results. In the actual case, there exists some gradient in the transition areas, and the transitions are smooth, continuous, and dilatational [67].

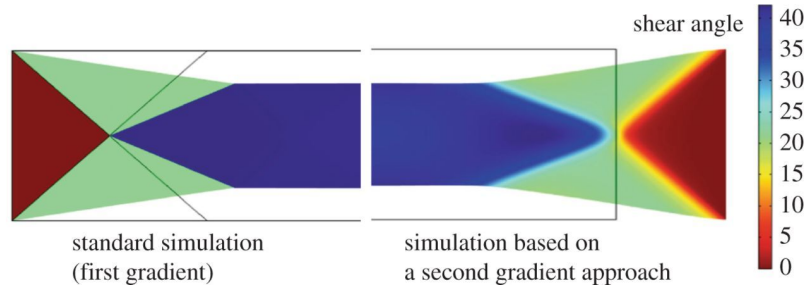


Figure 1.3: First vs. second gradient elasticity comparison. Picture taken from [68]

In the case of second-order theory, the strain energy potential is augmented as

$$W(\mathbf{F}, \varepsilon(\mathbf{F}), \mathbf{g}(\mathbf{G})) = W(\mathbf{F}) + W(\varepsilon(\mathbf{F})) + W(\mathbf{g}(\mathbf{G})), \quad (1.13)$$

to incorporate the bending energy of fiber into the model of deformations. The fiber bending energy ($W(\mathbf{g}(\mathbf{G}))$) can be computed via the computation of geodesic curvature, which is related to the second gradient of deformation. The shear angle distribution (see, Figures 1.3 and 1.4) from the second gradient theory exhibits a good match with the experimental results as it can capture the gradients in transition zones. Although the shear angle distribution is smooth and continuous, it is non-dilatational. To this end, Kim et al. [69, 70] devised a third gradient theory and incorporated the rate of change in curvature into the model by augmenting the strain energy potential (see Eq. 3.3). The obtained solutions provide a smooth, continuous, and dilatational shear angle distribution (see figure 1.5).

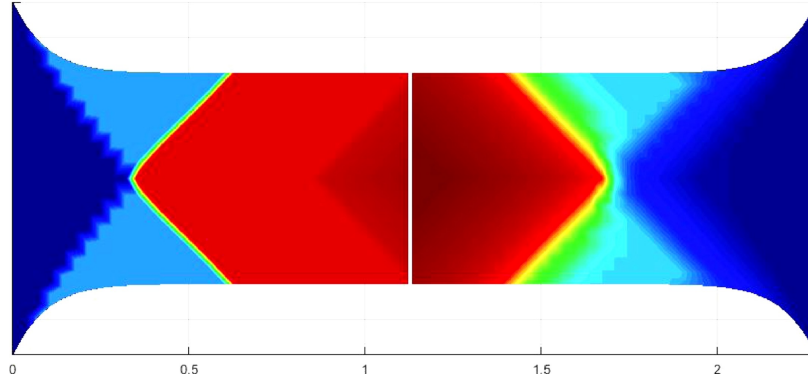


Figure 1.4: Shear angle distribution: first gradient (left), second gradient (right). Picture taken from [67]

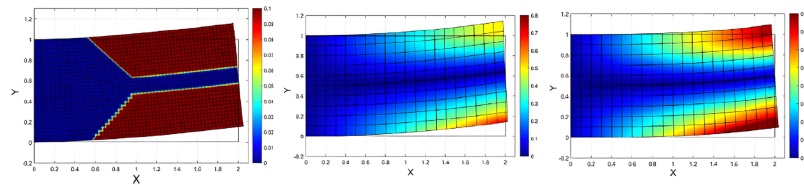


Figure 1.5: Shear angle distribution: first gradient (left), second gradient (middle), third gradient (right). Picture taken from [69]

1.4 Applications of higher-order gradient theory

We have already mentioned the applicability of higher-gradient theories to analyze the mechanical responses of micro-structured continua. In particular, higher gradient models account for singularities and can explain phenomena associated with localization, such as crack nucleation and the localization of shear stresses, amongst other examples [71, 72]. Higher gradient theories are applied to study several complicated phenomena, including buckling, interactions of multiple bodies, internal resonance due to the interactions of beams and cables with three-dimensional bodies, and wave propagation inside an inhomogeneous body [73–75].

The numerical analysis of bones and biomaterials is a very challenging problem due to complex microstructures and physical properties. Sometimes a bone can be treated as an open foam-like structure or a system of beams. Since in foam struts or in beams, there exist moments in addition to forces, this naturally leads to the model of the higher-order gradient elasticity [62]. The complex continuum modelings of bone tissues [76, 77], tendons, and ligaments [78] are obtained within the framework of the higher-gradient theory.

Recently, higher-gradient theories have gotten more attention to analyze fiber-reinforced composites, especially to obtain the shear strain distribution and deformation configuration under various boundary conditions. To this end, Kim et al. [67] devised a strain gradient elasticity theory for composites and incorporated fiber's resistance to stretch and flexure via the variational computations of the first and second gradients of deformations. In addition, Kim et al. [69, 70] formulated a third gradient continuum model, in which the energy density function depends on the first, second, and third gradients of deformation, and demonstrated that introducing an additional gradient field results in a set of mechanical interaction forces on the desired boundaries. The obtained third gradient models also predict smooth and dilatational shear angle distribution.

1.5 Thesis Objectives

In the previous sections (1.1-1.4), we have discussed that the first-order theory can't describe the micro-structured continua properly. Several second-order theories [24, 34, 35, 67] have been proposed to attain the experimental results more accurately. However, the second-gradient theories can't explain some complex phenomena, for example, mechanical contacts on the edges, dilatation, etc. The third gradient of deformation model or the second strain-gradient model leads to dilatational shear angle distribution throughout the domain of interest [69, 70].

The main objective of this thesis is to develop a second-strain gradient model to understand the mechanical responses of an elastic material reinforced with unidirectional or bidirectional, or randomly distributed short fibers and subjected to finite plane deformations. The complete procedure to develop the continuum model is given in chapter (2-3). We first define the kinematics of the fibers by their position and director fields, allowing them to be modeled as continuously distributed spatial rods of the Kirchhoff type [79]. Within this prescription, we develop the energy density function to account for the third gradient of continuous deformation. In particular, we consider the contact forces, couplings, double forces, and triple forces in addition to the extension and bending resistance of fibers. Then, we obtain the Euler equations and associated boundary conditions by employing iterative integrations by parts and variational formulations that emerge from the third gradient of continuum deformations. Further, we compute the rate of change in curvature, specified at locations on the convected curves of fibers, using the third gradient of the deformation map. Both Neo-Hookean and Mooney-Rivlin hyperelastic models are used to characterize the response of matrix material.

The model furnishes the governing equations as a system of sixth-order nonlinear coupled Partial Differential Equations (PDEs) from which we obtain a set of numerical solutions via the custom-built Finite Element Analysis (FEA) code. The detailed

finite element analysis procedures are given in chapter 2 to 3. Finally, we compare the obtained solutions with existing literature and find a perfect match.

1.6 Structure of thesis

This thesis consists of 4 main chapters, including the introduction and the conclusion. The first chapter briefly introduces the composite materials and the objectives of this thesis.

In chapter 2, we formulate a second strain-gradient theory for the mechanics of continua reinforced with extensible bidirectional fibers resistant to flexure. In section 2.1 to 2.3, we develop the fiber kinematics, equilibrium equation, and boundary conditions and form the governing equations as a nonlinear coupled system of partial differential equations (PDEs). The case of Neo-Hookean material reinforced with bidirectional fibers is considered for the purpose of model development which has been generalized to the case of a Mooney-Rivlin hyperelastic matrix material reinforced with bidirectional fibers. The obtained model is further applied to the case of Neo-Hookean material reinforced with unidirectional fiber for the purpose of model implementation. The resulting system of PDEs has been solved numerically and the procedures are shown in section 2.4. The following section 2.5 provides the results obtained from the proposed model and found to be consistent with those reported in the literature.

In chapter 3, we develop a second strain gradient-based continuum model for the composite reinforced with nano-fibers. We assume that the fiber's directors and accompanying deformation map remain in a plane with no out-of-plane components and that the corresponding deformations and material parameters are constrained to be independent of the out-of-plane coordinate. The kinematics of the embedded fibers are formulated by their position and director fields. The reinforcement phase is transformed from the continuously distributed unidirectional fibers to the nanofibers system using shear lag parameters[80, 81] and Krenchel orientation factors [82]. Fi-

nally, we investigate the effect of fiber aspect ratio on the mechanical response of composites.

Throughout all chapters, we use standard notation such as \mathbf{A}^T , \mathbf{A}^{-1} , \mathbf{A}^* and $tr(\mathbf{A})$. These are the transpose, the inverse, the cofactor and the trace of a tensor \mathbf{A} , respectively. The tensor product of vectors is indicated by interposing the symbol \otimes , and the Euclidian inner product of tensors \mathbf{A}, \mathbf{B} is defined by $\mathbf{A} \cdot \mathbf{B} = tr(\mathbf{A}\mathbf{B}^T)$; the associated norm is $|\mathbf{A}| = \sqrt{\mathbf{A} \cdot \mathbf{A}}$. The symbol $|\ast|$ is also used to denote the usual Euclidian norm of three-vectors. Latin and Greek indices take values in $\{1, 2\}$ and, when repeated, are summed over their ranges. Lastly, the notation $F_{\mathbf{A}}$ stands for the tensor-valued derivatives of a scalar-valued function $F(\mathbf{A})$.

Chapter 2

A third gradient based continuum model for the mechanics of continua reinforced with extensible bidirectional fibers resistant to flexure

In section 2.1, we define the kinematics of fibers. Following that, we develop the Equilibrium equation by using the virtual work statement and iterative integration by parts in section 2.2. The associated boundary conditions are derived in section 2.3 and the governing equations for the mechanics of Neo-Hookean solids and Mooney-Rivlin solids reinforced with fibers are delivered in section 2.3.1 and 2.3.2 respectively. In section 2.4, we provide a detailed Finite Element Analysis procedure to solve the obtained nonlinear Partial Differential Equations PDEs for the case of the Neo-Hookean solid. Lastly, we discuss the obtained numerical solution in section 2.5 and provide a summary of this chapter in section 2.6.

2.1 Kinematics

In the reference configuration, let \mathbf{D} and \mathbf{M} be the unit tangents to the fiber's trajectory. \mathbf{d} and \mathbf{m} are their equivalents in the deformed configuration. Following that,

the orientations of specific bidirectional fibers are determined as

$$\lambda = |\eta| = \frac{ds}{dS}, \quad \gamma = |\tau| = \frac{du}{dU} \quad \text{and} \quad \mathbf{d} = \eta\lambda^{-1}, \quad \mathbf{m} = \tau\gamma^{-1}, \quad (2.1)$$

where

$$\mathbf{FD} = \lambda\mathbf{d} \quad \text{and} \quad \mathbf{FM} = \gamma\mathbf{m}. \quad (2.2)$$

The unit tangents to the fiber's trajectory in the current configuration are \mathbf{d} and \mathbf{m} , and \mathbf{F} is the gradient of deformation function ($\boldsymbol{\chi}(\mathbf{X})$), i.e.,

$$\mathbf{F} = \nabla\boldsymbol{\chi}(\mathbf{X}). \quad (2.3)$$

Eq. (2.2) can be derived by taking the derivative of $\mathbf{r}(s(S)) = \boldsymbol{\chi}(\mathbf{X}(S))$, with respect to the arc length parameters, S , and ultimately, s , upon making the identifications $\mathbf{D} = \frac{d\mathbf{X}}{dS}$ and $\mathbf{d} = \frac{d\boldsymbol{\chi}}{ds}$ and similarly for \mathbf{M} (i.e. $\mathbf{M} = \frac{d\mathbf{X}}{dU}$ and $\mathbf{m} = \frac{d\boldsymbol{\chi}}{du}$). Here, $\frac{d(*)}{dS}$, $\frac{d(*)}{dU}$ and $\frac{d(*)}{ds}$, $\frac{d(*)}{du}$ refer to the arc length derivatives of $(*)$ along the fibers' directions in the reference and deformed configurations, respectively. In this thesis, we limit our attention to the case of initially orthogonal fibers:

$$\mathbf{M} \cdot \mathbf{D} = 0. \quad (2.4)$$

Combining Eqs. (2.2) and (2.4) embellishes a useful fiber decomposition of the deformation gradient that is

$$\mathbf{F} = \lambda\mathbf{d} \otimes \mathbf{D} + \gamma\mathbf{m} \otimes \mathbf{M}. \quad (2.5)$$

Therefore we have, for example, $\mathbf{D} = D_A\mathbf{E}_A$ and $\mathbf{d} = d_i\mathbf{e}_i$ to yield

$$\lambda d_i = F_{iA}D_A, \quad (2.6)$$

where $\{\mathbf{e}_i\}$ and $\{\mathbf{E}_A\}$ are the orthonormal bases in the current and reference configurations. Accordingly, from Eq. (2.2), the geodesic curvature of an arc ($\mathbf{r}(s, u)$) can be obtained as

$$\mathbf{g}_1 = \frac{d^2\mathbf{r}(S)}{dS^2} = \frac{d}{dS} \left(\frac{d(\mathbf{r}(S))}{dS} \right) = \frac{\partial(\mathbf{FD})}{\partial\mathbf{X}} \frac{d\mathbf{X}}{dS} = \nabla[\mathbf{FD}]\mathbf{D}, \quad (2.7)$$

and

$$\mathbf{g}_2 = \frac{d^2 \mathbf{r}(U)}{dU^2} = \frac{d}{dU} \left(\frac{d(\mathbf{r}(U))}{dU} \right) = \frac{\partial(\mathbf{F}\mathbf{M})}{\partial \mathbf{X}} \frac{d\mathbf{X}}{dU} = \nabla[\mathbf{F}\mathbf{M}]\mathbf{M}. \quad (2.8)$$

In a typical environment, most of the fibers are assumed as a straight prior to deformations. The length scales of fibers compared to the matrix materials are small and that allows us to treat the slightly curved fibers as ‘fairly straight’ [70]. Thus, the gradient fields of the unit tangent in the reference configuration are assumed as zero (i.e., $\nabla \mathbf{D} = \mathbf{0}$, and $\nabla \mathbf{M} = \mathbf{0}$). Now Eqs. (2.7) and (2.8) reduce to

$$\mathbf{g}_1 = \nabla \mathbf{F}(\mathbf{D} \otimes \mathbf{D}) \text{ and } \mathbf{g}_2 = \nabla \mathbf{F}(\mathbf{M} \otimes \mathbf{M}). \quad (2.9)$$

The commonly used conventions of the second gradient of deformations is:

$$\nabla \mathbf{F} \equiv \mathbf{G}, \quad (2.10)$$

and the compatibility condition of \mathbf{G} is as follows

$$G_{iAB} = F_{iA,B} = F_{iB,A} = G_{iBA}. \quad (2.11)$$

Combining Eqs. (2.9) and (2.10) gives

$$\mathbf{g}_1 = \mathbf{G}(\mathbf{D} \otimes \mathbf{D}) = \mathbf{g}_1(\mathbf{G}) \text{ and } \mathbf{g}_2 = \mathbf{G}(\mathbf{M} \otimes \mathbf{M}) = \mathbf{g}_2(\mathbf{G}). \quad (2.12)$$

The above kinematic settings constitute a second gradient-based energy function in the description of an elastic solid reinforced with fibers resistant to flexure;

$$W(\mathbf{F}, \mathbf{g}(\mathbf{G})) = W(\mathbf{F}) + W(\mathbf{g}(\mathbf{G})), \quad W(\mathbf{g}(\mathbf{G})) \equiv \frac{1}{2} C_1(\mathbf{F}) |\mathbf{g}_1(\mathbf{G})|^2 + \frac{1}{2} C_2(\mathbf{F}) |\mathbf{g}_2(\mathbf{G})|^2, \quad (2.13)$$

where $C_i(\mathbf{F})$ refers to the material property of fibers which are, in general, independent of the deformation gradient (i.e. $C_i(\mathbf{F}) = C_i$). Thus, we find

$$W(\mathbf{F}, \mathbf{g}(\mathbf{G})) = W(\mathbf{F}) + W(\mathbf{g}(\mathbf{G})), \quad W(\mathbf{g}(\mathbf{G})) \equiv \frac{1}{2} C_1 |\mathbf{g}_1(\mathbf{G})|^2 + \frac{1}{2} C_2 |\mathbf{g}_2(\mathbf{G})|^2. \quad (2.14)$$

In Eq. (2.14), the fiber’s bending energy is assumed to be dependent entirely on the second gradient of deformations, \mathbf{G} , which facilitates the development of the

associated mathematical framework. The concept has been widely and successfully adopted in the relevant studies (see, for example, [52, 54, 67]). For the desired applications, the above energy potential is now augmented to accommodate extensible fibers as

$$W(\mathbf{F}, \varepsilon(\mathbf{F}), \mathbf{g}(\mathbf{G})) = W(\mathbf{F}) + W(\mathbf{g}(\mathbf{G})) + W(\varepsilon(\mathbf{F})), \quad W(\varepsilon(\mathbf{F})) = \frac{1}{2}E_1\varepsilon_1^2 + \frac{1}{2}E_2\varepsilon_2^2, \quad (2.15)$$

where E_i are the elastic modulus of fiber's extension. The expressions of ε_i are given respectively as

$$\varepsilon_1 = \frac{1}{2}(\lambda^2 - 1), \quad (2.16)$$

and

$$\varepsilon_2 = \frac{1}{2}(\gamma^2 - 1). \quad (2.17)$$

The expressions of λ^2 and γ^2 can be obtained using Eqs. (2.2) and (2.4) as following:

$$\lambda^2 = \mathbf{F}\mathbf{D} \cdot \mathbf{F}\mathbf{D} = \mathbf{F}^T\mathbf{F}\mathbf{D} \cdot \mathbf{D} = (\mathbf{F}^T\mathbf{F}) \cdot \mathbf{D} \otimes \mathbf{D}, \quad (2.18)$$

and

$$\gamma^2 = \mathbf{F}\mathbf{M} \cdot \mathbf{F}\mathbf{M} = \mathbf{F}^T\mathbf{F}\mathbf{M} \cdot \mathbf{M} = (\mathbf{F}^T\mathbf{F}) \cdot \mathbf{M} \otimes \mathbf{M}. \quad (2.19)$$

Hence, Eqs. (2.16)-(2.17) can be recast as

$$\varepsilon_1 = \frac{1}{2}(\lambda^2 - 1) = \frac{1}{2}((\mathbf{F}^T\mathbf{F}) \cdot \mathbf{D} \otimes \mathbf{D} - 1), \quad (2.20)$$

and

$$\varepsilon_2 = \frac{1}{2}(\gamma^2 - 1) = \frac{1}{2}((\mathbf{F}^T\mathbf{F}) \cdot \mathbf{M} \otimes \mathbf{M} - 1). \quad (2.21)$$

In this thesis, a more comprehensive description of generalized higher-order continua is obtained by introducing the third gradient of deformations into the model of continuum deformations. For this purpose, the rate of changes in curvature (the

third gradient of deformations) at points on the fibers is computed as

$$\begin{aligned}
\boldsymbol{\alpha}_1 &= \frac{d^3 \mathbf{r}(S)}{dS^3} = \frac{d}{dS}(\nabla[\mathbf{FD}]\mathbf{D}) = \frac{\partial(\nabla[\mathbf{FD}]\mathbf{D})}{\partial \mathbf{X}} \frac{d\mathbf{X}}{dS} = [\nabla\{\nabla[\mathbf{FD}]\mathbf{D}\}] \mathbf{D} \\
&= [\nabla\{\nabla[\mathbf{FD}]\}\mathbf{D} + \nabla[\mathbf{FD}](\nabla\mathbf{D})] \mathbf{D}, \\
\boldsymbol{\alpha}_2 &= \frac{d^3 \mathbf{r}(U)}{dU^3} = \frac{d}{dU}(\nabla[\mathbf{FM}]\mathbf{M}) = \frac{\partial(\nabla[\mathbf{FM}]\mathbf{M})}{\partial \mathbf{X}} \frac{d\mathbf{X}}{dU} = [\nabla\{\nabla[\mathbf{FM}]\mathbf{M}\}] \mathbf{M} \\
&= [\nabla\{\nabla[\mathbf{FM}]\}\mathbf{M} + \nabla[\mathbf{FM}](\nabla\mathbf{M})] \mathbf{M}, \quad (2.22)
\end{aligned}$$

through which the interactions between the fibers and the surrounding matrix, contact forces between the edges may be characterized [69]. The required third gradient fields can be formulated in the same spirit as in Eqs. (2.9)-(2.10) that

$$\boldsymbol{\alpha}_1 = \nabla(\nabla\mathbf{F})(\mathbf{D} \otimes \mathbf{D} \otimes \mathbf{D}) \quad \text{and} \quad \boldsymbol{\alpha}_2 = \nabla(\nabla\mathbf{F})(\mathbf{M} \otimes \mathbf{M} \otimes \mathbf{M}), \quad (2.23)$$

$$\nabla(\nabla\mathbf{F}) = \nabla(\mathbf{G}) \equiv \mathbf{H}. \quad (2.24)$$

Combining Eqs. (2.23) and (2.24) furnishes the third gradient fields as

$$\boldsymbol{\alpha}_1 = \mathbf{H}(\mathbf{D} \otimes \mathbf{D} \otimes \mathbf{D}) = \boldsymbol{\alpha}_1(\mathbf{H}) \quad \text{and} \quad \boldsymbol{\alpha}_2 = \mathbf{H}(\mathbf{M} \otimes \mathbf{M} \otimes \mathbf{M}) = \boldsymbol{\alpha}_2(\mathbf{H}). \quad (2.25)$$

Thus, the energy potential associated with the third gradient of deformations is incorporated and yields

$$\begin{aligned}
W(\mathbf{F}, \varepsilon(\mathbf{F}), \mathbf{g}(\mathbf{G}), \boldsymbol{\alpha}(\mathbf{H})) &= W(\mathbf{F}) + W(\varepsilon(\mathbf{F})) + W(\mathbf{g}(\mathbf{G})) + W(\boldsymbol{\alpha}(\mathbf{H})), \\
W(\boldsymbol{\alpha}(\mathbf{H})) &\equiv \frac{1}{2}A_1(\mathbf{H})|\boldsymbol{\alpha}_1(\mathbf{H})|^2 + \frac{1}{2}A_2(\mathbf{H})|\boldsymbol{\alpha}_2(\mathbf{H})|^2. \quad (2.26)
\end{aligned}$$

We note here that, $A_i(\mathbf{H})$ pertaining to the third gradient of continuum deformations is assumed to be constant for the sake of simplicity (i.e., $A_i(\mathbf{H}) = A_i$). Thus

$$\begin{aligned}
W(\mathbf{F}, \varepsilon(\mathbf{F}), \mathbf{g}(\mathbf{G}), \boldsymbol{\alpha}(\mathbf{H})) &= W(\mathbf{F}) + W(\varepsilon(\mathbf{F})) + W(\mathbf{g}(\mathbf{G})) + W(\boldsymbol{\alpha}(\mathbf{H})), \\
W(\boldsymbol{\alpha}(\mathbf{H})) &\equiv \frac{1}{2}A_1|\boldsymbol{\alpha}_1(\mathbf{H})|^2 + \frac{1}{2}A_2|\boldsymbol{\alpha}_2(\mathbf{H})|^2. \quad (2.27)
\end{aligned}$$

We continue by assessing the induced energy variation of the response function with respect to \mathbf{F} , ε , \mathbf{g} and $\boldsymbol{\alpha}$ as needed for the derivation of Euler equations and the appropriate boundary conditions,

$$\dot{W}(\mathbf{F}, \varepsilon_i, \mathbf{g}_i, \boldsymbol{\alpha}_i) = W_{\mathbf{F}} \cdot \dot{\mathbf{F}} + W_{\varepsilon_i} \dot{\varepsilon}_i + W_{\mathbf{g}_i} \cdot \dot{\mathbf{g}}_i + W_{\boldsymbol{\alpha}_i} \cdot \dot{\boldsymbol{\alpha}}_i, \quad i = 1, 2, \quad (2.28)$$

where the superposed dot refers to derivatives with respect to a parameter at the particular configuration of the composite ($\epsilon = 0$) that labels a one-parameter family of deformations. The desired expression for the induced energy variation can be found using Eqs. (2.16)-(2.27) as

$$\dot{\epsilon}_1 = \frac{1}{2}(\lambda^2 - 1) \dot{} = \frac{1}{2}(\mathbf{FD} \cdot \mathbf{FD} - \mathbf{1}) \dot{} = \mathbf{FD} \cdot \dot{\mathbf{F}}\mathbf{D} = \mathbf{FD} \otimes \mathbf{D} \cdot \dot{\mathbf{F}}, \quad (2.29)$$

$$\dot{\epsilon}_2 = \frac{1}{2}(\gamma^2 - 1) \dot{} = \frac{1}{2}(\mathbf{FM} \cdot \mathbf{FM} - \mathbf{1}) \dot{} = \mathbf{FM} \cdot \dot{\mathbf{F}}\mathbf{M} = \mathbf{FM} \otimes \mathbf{M} \cdot \dot{\mathbf{F}}, \quad (2.30)$$

and

$$W_{\epsilon_i} \dot{\epsilon}_i = W_{\epsilon_1} \dot{\epsilon}_1 + W_{\epsilon_2} \dot{\epsilon}_2 = E_1 \epsilon_1 \dot{\epsilon}_1 + E_2 \epsilon_2 \dot{\epsilon}_2. \quad (2.31)$$

Using Eqs. (2.20)-(2.21) and Eqs. (2.29)-(2.30), we find

$$E_1 \epsilon_1 \dot{\epsilon}_1 = \frac{E_1}{2}(\mathbf{FD} \cdot \mathbf{FD} - \mathbf{1})\mathbf{FD} \otimes \mathbf{D} \cdot \dot{\mathbf{F}} = \frac{E_1}{2}(F_{jC}F_{jD}D_C D_D - 1)(F_{iB}D_B D_A) \dot{F}_{iA}, \quad (2.32)$$

and

$$E_2 \epsilon_2 \dot{\epsilon}_2 = \frac{E_2}{2}(\mathbf{FM} \cdot \mathbf{FM} - \mathbf{1})\mathbf{FM} \otimes \mathbf{M} \cdot \dot{\mathbf{F}} = \frac{E_2}{2}(F_{jC}F_{jD}M_C M_D - 1)(F_{iB}M_B M_A) \dot{F}_{iA}. \quad (2.33)$$

Combining Eqs. (2.32) and (2.33) gives

$$W_{\epsilon_i} \dot{\epsilon}_i = \left[\frac{E_1}{2}(F_{jC}F_{jD}D_C D_D - 1)(F_{iB}D_B D_A) + \frac{E_2}{2}(F_{jC}F_{jD}M_C M_D - 1)(F_{iB}M_B M_A) \right] \dot{F}_{iA}. \quad (2.34)$$

Using Eq. (2.12) (i.e., $\mathbf{g}_1 = \mathbf{G}(\mathbf{D} \otimes \mathbf{D})$ and $\mathbf{g}_2 = \mathbf{G}(\mathbf{M} \otimes \mathbf{M})$), the variational derivative of the energy potential with respect to the second gradient of deformations is

$$W_{\mathbf{g}_i} \cdot \dot{\mathbf{g}}_i = W_{\mathbf{g}_1} \cdot \dot{\mathbf{g}}_1 + W_{\mathbf{g}_2} \cdot \dot{\mathbf{g}}_2 = C_1 \mathbf{g}_1 \cdot \dot{\mathbf{g}}_1 + C_2 \mathbf{g}_2 \cdot \dot{\mathbf{g}}_2 = C_1 (g_1)_j \mathbf{e}_j \cdot \dot{G}_{iAB} D_A D_B \mathbf{e}_i + C_2 (g_2)_j \mathbf{e}_j \cdot \dot{G}_{iAB} M_A M_B \mathbf{e}_i. \quad (2.35)$$

This can be further simplified as

$$W_{\mathbf{g}_i} \cdot \dot{\mathbf{g}}_i = C_1 (g_1)_j \dot{G}_{iAB} D_A D_B \delta_{ij} + C_2 (g_2)_j \dot{G}_{iAB} M_A M_B \delta_{ij} = C_1 (g_1)_i \dot{G}_{iAB} D_A D_B + C_2 (g_2)_i \dot{G}_{iAB} M_A M_B. \quad (2.36)$$

The similar fashion is used to find the variational derivative of the energy potential with respect to the third gradient of deformations, i.e. using Eq. (2.25),

$$\begin{aligned} W_{\alpha_i} \cdot \dot{\alpha}_i &= W_{\alpha_1} \cdot \dot{\alpha}_1 + W_{\alpha_2} \cdot \dot{\alpha}_2 = A_1 \alpha_1 \cdot \dot{\alpha}_1 + A_2 \alpha_2 \cdot \dot{\alpha}_2 = A_1 (\alpha_1)_j \mathbf{e}_j \cdot \dot{H}_{iABC} D_A D_B D_C \mathbf{e}_i \\ &\quad + A_2 (\alpha_2)_j \mathbf{e}_j \cdot \dot{H}_{iABC} M_A M_B M_C \mathbf{e}_i, \end{aligned} \quad (2.37)$$

which is reduced as

$$\begin{aligned} W_{\alpha_i} \cdot \dot{\alpha}_i &= A_1 (\alpha_1)_j \dot{H}_{iABC} D_A D_B D_C \delta_{ij} + A_2 (\alpha_2)_j \dot{H}_{iABC} M_A M_B M_C \delta_{ij} \\ &= A_1 (\alpha_1)_i \dot{H}_{iABC} D_A D_B D_C + A_2 (\alpha_2)_i \dot{H}_{iABC} M_A M_B M_C. \end{aligned} \quad (2.38)$$

Now, from Eq. (2.28) the final expression for the induced energy potential variation is obtained as

$$\begin{aligned} \dot{W}(\mathbf{F}, \varepsilon_1, \varepsilon_2, \mathbf{g}_1, \mathbf{g}_2, \alpha_1, \alpha_2) &= W_{F_{iA}} \dot{F}_{iA} + \left[\frac{E_1}{2} (F_{jC} F_{jD} D_C D_D - 1) (F_{iB} D_B D_A) + \right. \\ &\quad \left. \frac{E_2}{2} (F_{jC} F_{jD} M_C M_D - 1) (F_{iB} M_B M_A) \right] \dot{F}_{iA} + C_1 (g_1)_i \dot{G}_{iAB} D_A D_B + C_2 (g_2)_i \dot{G}_{iAB} M_A M_B \\ &\quad + A_1 (\alpha_1)_i \dot{H}_{iABC} D_A D_B D_C + A_2 (\alpha_2)_i \dot{H}_{iABC} M_A M_B M_C. \end{aligned} \quad (2.39)$$

As a result, we have the variational form in Eq. (2.39) that is dependent on both the second and third deformation gradients. The rate of change in curvature has now been incorporated into the model via the third gradient of deformations, as can be shown. The obtained variational form (Eq. (2.39)) facilitates the relevant mathematical framework to accommodate the triple force (e.g. interaction forces) and its energy couple (Piola-type triple stress) sustained by the third-gradient continua.

2.2 Equilibrium

The derivation of the Euler equation and boundary conditions arising in the second-gradient elasticity are well established in [24, 34, 35, 67]. In this section, we discuss a variational formulation arising in the third gradient of the continuum deformation using the principles of the virtual work statement and iterated integrations by parts

[24, 33, 67]. The weak form of the equilibrium equations is given by the virtual-work statement,

$$\dot{E} = P, \quad (2.40)$$

where P is the virtual work of the applied load and the superposed dot refers to the variational and/or Gateaux derivative.

Volumetric changes in material deformations are energetically expensive processes in a typical environment, and so are constrained in most engineering analyses [52]. The following form of the augmented energy potential can be used to overcome the constraint of bulk incompressibility.

$$U(\mathbf{F}, \varepsilon_1, \varepsilon_2, \mathbf{g}_1, \mathbf{g}_2, \boldsymbol{\alpha}_1, \boldsymbol{\alpha}_2, p) = W(\mathbf{F}, \varepsilon_1, \varepsilon_2, \mathbf{g}_1, \mathbf{g}_2, \boldsymbol{\alpha}_1, \boldsymbol{\alpha}_2) - p(J - 1), \quad (2.41)$$

where J is determinant of \mathbf{F} and p is a Lagrange multiplier field. The strain energy of the system is then expressed as

$$E = \int_{\Omega} U(\mathbf{F}, \varepsilon_1, \varepsilon_2, \mathbf{g}_1, \mathbf{g}_2, \boldsymbol{\alpha}_1, \boldsymbol{\alpha}_2, p) dA, \quad (2.42)$$

where Ω is the referential domain occupied by a fiber-matrix material. Since the conservative loads are characterized by the existence of a potential L such that $P = \dot{L}$, the problem of determining equilibrium deformations is then reduced in this case to the problem of minimizing the potential energy $E - L$: Accordingly, we find

$$\dot{E} = \int_{\Omega} \dot{U}(\mathbf{F}, \varepsilon_1, \varepsilon_2, \mathbf{g}_1, \mathbf{g}_2, \boldsymbol{\alpha}_1, \boldsymbol{\alpha}_2, p) dA. \quad (2.43)$$

Using the identity $\dot{J} = J_{\mathbf{F}} \dot{\mathbf{F}} \cdot \dot{\mathbf{F}} = \mathbf{F}^* \cdot \dot{\mathbf{F}}$ along with Eqs. (2.39) and (2.41), the variational derivative of the augmented energy potential can be evaluated as

$$\begin{aligned} \dot{U} &= \dot{W} - p\dot{J} \\ &= W_{F_{iA}} \dot{F}_{iA} + \left[\frac{E_1}{2} (F_{jC} F_{jD} D_C D_D - 1) (F_{iB} D_B D_A) + \frac{E_2}{2} (F_{jC} F_{jD} M_C M_D - 1) \right. \\ &\quad \left. (F_{iB} M_B M_A) \right] \dot{F}_{iA} + C_1 (g_1)_i \dot{G}_{iAB} D_A D_B + C_2 (g_2)_i \dot{G}_{iAB} M_A M_B + A_1 (\alpha_1)_i \dot{H}_{iABC} D_A D_B D_C \\ &\quad + A_2 (\alpha_2)_i \dot{H}_{iABC} M_A M_B M_C - p F_{iA}^* \dot{F}_{iA}. \end{aligned} \quad (2.44)$$

Let us define the variation of position field $\dot{\chi}_i = u_i$. Then, Eq. (2.43) can be recast as

$$\begin{aligned} \dot{E} = \int_{\Omega} [W_{F_{iA}} u_{i,A} + [\frac{E_1}{2}(F_{jC}F_{jD}D_C D_D - 1)(F_{iB}D_B D_A) + \frac{E_2}{2}(F_{jC}F_{jD}M_C M_D - 1) \\ (F_{iB}M_B M_A)]u_{i,A} + (C_1 (g_1)_i D_A D_B + C_2 (g_2)_i M_A M_B) u_{i,AB} + (A_1 (\alpha_1)_i D_A D_B D_C \\ + A_2 (\alpha_2)_i M_A M_B M_C)u_{i,ABC} - pF_{iA}^* u_{i,A}]dA. \end{aligned} \quad (2.45)$$

Applying integration by parts on the third and fourth terms in Eq. (2.45)

$$\begin{aligned} (C_1 (g_1)_i D_A D_B + C_2 (g_2)_i M_A M_B) u_{i,AB} = [(C_1 (g_1)_i D_A D_B + C_2 (g_2)_i M_A M_B) u_{i,A}]_{,B} \\ - [(C_1 (g_1)_i D_A D_B + C_2 (g_2)_i M_A M_B)]_{,B} u_{i,A}, \end{aligned} \quad (2.46)$$

and

$$\begin{aligned} (A_1 (\alpha_1)_i D_A D_B D_C + A_2 (\alpha_2)_i M_A M_B M_C) u_{i,ABC} = [A_1 (\alpha_1)_i D_A D_B D_C \\ + A_2 (\alpha_2)_i M_A M_B M_C]u_{i,AB}]_{,C} - [(A_1 (\alpha_1)_i D_A D_B D_C + A_2 (\alpha_2)_i M_A M_B M_C)]_{,C} u_{i,AB}. \end{aligned} \quad (2.47)$$

Now putting back the values from Eqs. (2.46) and (2.47) into the Eq. (2.45) we obtain

$$\begin{aligned} \dot{E} = \int_{\Omega} [W_{F_{iA}} u_{i,A} + [\frac{E_1}{2}(F_{jC}F_{jD}D_C D_D - 1)(F_{iB}D_B D_A) + \frac{E_2}{2}(F_{jC}F_{jD}M_C M_D - 1) \\ (F_{iB}M_B M_A)]u_{i,A} + [(C_1 (g_1)_i D_A D_B + C_2 (g_2)_i M_A M_B) u_{i,A}]_{,B} - (C_1 (g_1)_i D_A D_B + \\ C_2 (g_2)_i M_A M_B)_{,B} u_{i,A} + [(A_1 (\alpha_1)_i D_A D_B D_C + A_2 (\alpha_2)_i M_A M_B M_C) u_{i,AB}]_{,C} \\ - (A_1 (\alpha_1)_i D_A D_B D_C + A_2 (\alpha_2)_i M_A M_B M_C)_{,C} u_{i,AB} - pF_{iA}^* u_{i,A}]dA. \end{aligned} \quad (2.48)$$

This can be recast as

$$\begin{aligned} \dot{E} = \int_{\Omega} [W_{F_{iA}} - pF_{iA}^* + \frac{E_1}{2}(F_{jC}F_{jD}D_C D_D - 1)(F_{iB}D_B D_A) + \frac{E_2}{2}(F_{jC}F_{jD}M_C M_D - 1) \\ (F_{iB}M_B M_A) - (C_1 (g_1)_i D_A D_B + C_2 (g_2)_i M_A M_B)_{,B}]u_{i,A}dA - \int_{\Omega} [((A_1 (\alpha_1)_i D_A D_B D_C \\ + A_2 (\alpha_2)_i M_A M_B M_C)_{,C})u_{i,AB}]dA + \int_{\partial\Omega} [(C_1 (g_1)_i D_A D_B + C_2 (g_2)_i M_A M_B) u_{i,A}] N_B dS \\ + \int_{\partial\Omega} [(A_1 (\alpha_1)_i D_A D_B D_C + A_2 (\alpha_2)_i M_A M_B M_C) u_{i,AB}] N_C dS, \end{aligned} \quad (2.49)$$

where \mathbf{N} is the rightward unit normal to the boundary $\partial\Omega$. To obtain the desired expression, we again apply integration by parts and the Green-Stoke's theorem on the second integral of the above; i.e.,

$$\begin{aligned} \int_{\Omega} \left[\left((A_1(\alpha_1)_i D_A D_B D_C + A_2(\alpha_2)_i M_A M_B M_C)_{,C} \right) u_{i,AB} \right] dA &= \int_{\Omega} \left\{ \left((A_1(\alpha_1)_i (D_A D_B D_C) \right. \right. \\ &\quad \left. \left. + A_2(\alpha_2)_i M_A M_B M_C)_{,C} \right) u_{i,A} \right\}_{,B} - \left((A_1(\alpha_1)_i D_A D_B D_C + A_2(\alpha_2)_i M_A \right. \\ &\quad \left. M_B M_C)_{,CB} \right) u_{i,A} \Big|_{\partial\Omega} dA = \int_{\partial\Omega} \left\{ \left((A_1(\alpha_1)_i D_A D_B D_C + A_2(\alpha_2)_i M_A M_B M_C)_{,C} \right) u_{i,A} \right\} N_B dS \\ &\quad - \int_{\partial\Omega} \left[\left((A_1(\alpha_1)_i D_A D_B D_C + A_2(\alpha_2)_i M_A M_B M_C)_{,CB} \right) u_{i,A} \right] dA. \quad (2.50) \end{aligned}$$

The substitution of Eq. (2.50) into Eq. (2.49) then furnishes

$$\begin{aligned} \dot{E} &= \int_{\Omega} [W_{F_{iA}} - pF_{iA}^* + \frac{E_1}{2}(F_{jC}F_{jD}D_C D_D - 1)(F_{iB}D_B D_A) + \frac{E_2}{2}(F_{jC}F_{jD}M_C M_D - 1) \\ &\quad (F_{iB}M_B M_A) - (C_1(g_1)_i D_A D_B + C_2(g_2)_i M_A M_B)_{,B} + (A_1(\alpha_1)_i D_A D_B D_C \\ &\quad + A_2(\alpha_2)_i M_A M_B M_C)_{,CB}] u_{i,A} dA + \int_{\partial\Omega} [(C_1(g_1)_i D_A D_B + C_2(g_2)_i M_A M_B) u_{i,A}] N_B dS \\ &\quad + \int_{\partial\Omega} [(A_1(\alpha_1)_i D_A D_B D_C + A_2(\alpha_2)_i M_A M_B M_C) u_{i,AB}] N_C dS \\ &\quad - \int_{\partial\Omega} \left\{ \left((A_1(\alpha_1)_i D_A D_B D_C + A_2(\alpha_2)_i M_A M_B M_C)_{,C} \right) u_{i,A} \right\} N_B dS. \quad (2.51) \end{aligned}$$

Finally, we obtain

$$\begin{aligned} \dot{E} &= \int_{\Omega} P_{iA} u_{i,A} dA + \int_{\partial\Omega} \left[\{ C_1(g_1)_i D_A D_B + C_2(g_2)_i M_A M_B - A_1((\alpha_1)_i D_A D_B D_C)_{,C} \right. \\ &\quad \left. - A_2((\alpha_2)_i M_A M_B M_C)_{,C} \} u_{i,A} N_B + (A_1(\alpha_1)_i D_A D_B D_C + A_2(\alpha_2)_i M_A M_B M_C) u_{i,AB} N_C \right] dS, \quad (2.52) \end{aligned}$$

where

$$\begin{aligned} P_{iA}(\mathbf{e}_i \otimes \mathbf{E}_A) &= [W_{F_{iA}} - pF_{iA}^* + \frac{E_1}{2}(F_{jC}F_{jD}D_C D_D - 1)(F_{iB}D_A D_B) + \frac{E_2}{2}(F_{jC}F_{jD}M_C M_D \\ &\quad - 1)(F_{iB}M_A M_B) - C_1((g_1)_i D_A D_B)_{,B} - C_2((g_2)_i M_A M_B)_{,B} \\ &\quad + A_1((\alpha_1)_i D_A D_B D_C)_{,BC} + A_2((\alpha_2)_i M_A M_B M_C)_{,BC}] (\mathbf{e}_i \otimes \mathbf{E}_A). \quad (2.53) \end{aligned}$$

2.3 Boundary conditions

In this section, we present derivations of the admissible boundary conditions which arise in the third gradient of virtual displacement. The introduction of the higher order gradient fields into the model of the continuum deformation leads to the necessary existence of their high-order energy conjugate pairs (e.g. triple forces, contact interactions) suitably imposed on the desired boundaries (see, for example, [33, 72, 83]).

To proceed, we apply integration by parts (i.e. $P_{iA}u_{i,A} = (P_{iA}u_i)_{,A} - P_{iA,A}u_i$) on the first term of Eq. (2.52) and thereby obtain

$$\begin{aligned} \dot{E} = & \int_{\partial\Omega} P_{iA}u_i N_A dS - \int_{\Omega} P_{iA,A}u_i dA + \int_{\partial\Omega} [\{C_1 (g_1)_i D_A D_B + C_2 (g_2)_i M_A M_B \\ & - (A_1 ((\alpha_1)_i D_A D_B D_C)_{,C} + A_2 ((\alpha_2)_i M_A M_B M_C)_{,C})\} u_{i,A} N_B + (A_1 (\alpha_1)_i D_A D_B D_C \\ & + A_2 (\alpha_2)_i M_A M_B M_C) u_{i,AB} N_C] dS, \end{aligned} \quad (2.54)$$

where we define

$$\begin{aligned} W_{G_{iAB}} & \equiv C_1 (g_1)_i D_A D_B + C_2 (g_2)_i M_A M_B, \text{ and} \\ W_{H_{iABC}} & \equiv A_1 (\alpha_1)_i D_A D_B D_C + A_2 (\alpha_2)_i M_A M_B M_C. \end{aligned} \quad (2.55)$$

Also, the Euler equation satisfies

$$P_{iA,A} \mathbf{e}_i = \text{Div}(\mathbf{P}) = 0. \quad (2.56)$$

Using Eqs. (2.55) and (2.56), we can recast Eq. (2.54) as

$$\dot{E} = \int_{\partial\Omega} P_{iA}u_i N_A dS + \int_{\partial\Omega} [(W_{G_{iAB}} - (W_{H_{iABC}})_{,C}) u_{i,A} N_B + W_{H_{iABC}} u_{i,AB} N_C] dS. \quad (2.57)$$

We project $\nabla \mathbf{u}$ onto the normal and tangential direction and thereby obtain

$$\nabla \mathbf{u} = \nabla \mathbf{u}(\mathbf{T} \otimes \mathbf{T}) + \nabla \mathbf{u}(\mathbf{N} \otimes \mathbf{N}) = \mathbf{u}' \otimes \mathbf{T} + \mathbf{u}_{,N} \otimes \mathbf{N}, \quad (2.58)$$

such that \mathbf{u}' and $\mathbf{u}_{,N}$ are, respectively, the tangential and normal derivatives of \mathbf{u} on $\partial\Omega$, i.e.,

$$u'_i = u_{i,A}T_A, \quad u_{i,N} = u_{i,A}N_A, \quad (2.59)$$

where $\mathbf{T} = \mathbf{X}'(S) = \mathbf{k} \times \mathbf{N}$ defines the unit tangent to $\partial\Omega$, and \mathbf{N} is the associated unit normal to the boundary. Thus, invoking Eqs. (2.58)–(2.59), $u_{i,A}$ can be decomposed into

$$u_{i,A} = \frac{\partial u_i}{\partial X_A} = \frac{du_i}{dS} \frac{dS}{dX_A} + \frac{du_i}{dN} \frac{dN}{dX_A} = u'_i T_A + u_{i,N} N_A, \quad (2.60)$$

and similarly for $u_{i,AB}$

$$\begin{aligned} u_{i,AB} = & u''_i T_A T_B + u'_i (T'_A T_B + T_{A,N} N_B) + u'_{i,N} (T_A N_B + N_A T_B) + u_{i,N} (N'_A T_B \\ & + N_{A,N} N_B) + u_{i,NN} N_A N_B. \end{aligned} \quad (2.61)$$

Substituting Eqs. (2.60) and (2.61) into Eq. (2.57), we obtain

$$\begin{aligned} \dot{E} = & \int_{\partial\Omega} P_{iA} u_i N_A dS + \int_{\partial\Omega} \left[W_{G_{iAB}} - (W_{H_{iABC}})_{,C} \right] \left(u'_i T_A + u_{i,N} N_A \right) N_B dS \\ & + \int_{\partial\Omega} W_{H_{iABC}} \left[u''_i T_A T_B + u'_i (T'_A T_B + T_{A,N} N_B) + u'_{i,N} (T_A N_B + N_A T_B) \right. \\ & \left. + u_{i,N} (N'_A T_B + N_{A,N} N_B) + u_{i,NN} N_A N_B \right] N_C dS. \end{aligned} \quad (2.62)$$

In order to extract the admissible boundary conditions from Eq. (2.62), we make use of iterated integrations by parts. For example,

$$W_{G_{iAB}} T_A N_B u'_i = (W_{G_{iAB}} T_A N_B u_i)' - (W_{G_{iAB}} T_A N_B)' u_i, \quad (2.63)$$

$$(W_{H_{iABC}})_{,C} T_A N_B u'_i = \left((W_{H_{iABC}})_{,C} T_A N_B u_i \right)' - \left((W_{H_{iABC}})_{,C} T_A N_B \right)' u_i, \quad (2.64)$$

$$\begin{aligned} W_{H_{iABC}} (T'_A T_B N_C + T_{A,N} N_B N_C) u'_i = & \left(W_{H_{iABC}} (T'_A T_B N_C + T_{A,N} N_B N_C) u_i \right)' \\ & - \left(W_{H_{iABC}} (T'_A T_B N_C + T_{A,N} N_B N_C) \right)' u_i, \end{aligned} \quad (2.65)$$

$$\begin{aligned} W_{H_{iABC}} (T_A N_B N_C + N_A T_B N_C) u'_{i,N} = & (W_{H_{iABC}} (T_A N_B N_C + N_A T_B N_C) u_{i,N})' \\ & - (W_{H_{iABC}} (T_A N_B N_C + N_A T_B N_C))' u_{i,N}, \end{aligned} \quad (2.66)$$

$$\begin{aligned}
W_{H_{iABC}}T_A T_B N_C u_i'' &= (W_{H_{iABC}}T_A T_B N_C u_i)'' + (W_{H_{iABC}}T_A T_B N_C)'' u_i \\
&\quad - 2 \left[(W_{H_{iABC}}T_A T_B N_C)' u_i \right]'. \tag{2.67}
\end{aligned}$$

Using Eqs. (2.63)-(2.67) into Eq. (2.62), we obtain

$$\begin{aligned}
\dot{E} &= \int_{\partial\Omega} P_{iA} u_i N_A dS + \int_{\partial\Omega} \left[(W_{G_{iAB}}T_A N_B u_i)' - (W_{G_{iAB}}T_A N_B)' u_i \right] dS \\
&\quad - \int_{\partial\Omega} \left[\left((W_{H_{iABC}})_{,C} T_A N_B u_i \right)' - \left((W_{H_{iABC}})_{,C} T_A N_B \right)' u_i \right] dS + \int_{\partial\Omega} [W_{G_{iAB}}N_A N_B \\
&\quad - (W_{H_{iABC}})_{,C} N_A N_B] u_{i,N} dS + \int_{\partial\Omega} [(W_{H_{iABC}}T_A T_B N_C u_i)'' + (W_{H_{iABC}}T_A T_B N_C)'' u_i \\
&\quad - 2 \left[(W_{H_{iABC}}T_A T_B N_C)' u_i \right]'] dS + \int_{\partial\Omega} \left[(W_{H_{iABC}}(T_A' T_B N_C + T_{A,N} N_B N_C) u_i \right)' \\
&\quad - (W_{H_{iABC}}(T_A' T_B N_C + T_{A,N} N_B N_C))' u_i \right] dS + \int_{\partial\Omega} W_{H_{iABC}} [u_{i,N} (N_A' T_B N_C \\
&\quad + N_{A,N} N_B N_C)] dS + \int_{\partial\Omega} [(W_{H_{iABC}}(T_A N_B N_C + N_A T_B N_C) u_{i,N})' - (W_{H_{iABC}}(T_A N_B N_C \\
&\quad + N_A T_B N_C))' u_{i,N}] dS + \int_{\partial\Omega} (W_{H_{iABC}} u_{i,NN} N_A N_B N_C) dS, \tag{2.68}
\end{aligned}$$

which can be rearranged as

$$\begin{aligned}
\dot{E} &= \int_{\partial\Omega} [P_{iA} N_A - (W_{G_{iAB}}T_A N_B)' + \left((W_{H_{iABC}})_{,C} T_A N_B \right)' + (W_{H_{iABC}}T_A T_B N_C)'' \\
&\quad - (W_{H_{iABC}}(T_A' T_B N_C + T_{A,N} N_B N_C))'] u_i dS + \int_{\partial\Omega} [W_{G_{iAB}}N_A N_B - (W_{H_{iABC}})_{,C} N_A N_B \\
&\quad + W_{H_{iABC}}(N_A' T_B N_C + N_{A,N} N_B N_C) - (W_{H_{iABC}}(T_A N_B N_C + N_A T_B N_C))'] u_{i,N} dS \\
&\quad + \int_{\partial\Omega} [\{W_{G_{iAB}}T_A N_B - (W_{H_{iABC}})_{,C} T_A N_B - 2(W_{H_{iABC}}T_A T_B N_C)'\} u_i]' dS \\
&\quad + \int_{\partial\Omega} [(W_{H_{iABC}}T_A T_B N_C u_i)''] dS + \int_{\partial\Omega} [W_{H_{iABC}}(T_A' T_B N_C + T_{A,N} N_B N_C) u_i]' dS \\
&\quad + \int_{\partial\Omega} [W_{H_{iABC}}(T_A N_B N_C + N_A T_B N_C) u_{i,N}]' dS + \int_{\partial\Omega} (W_{H_{iABC}} u_{i,NN} N_A N_B N_C) dS. \tag{2.69}
\end{aligned}$$

The above maybe further recast as

$$\begin{aligned}
\dot{E} = & \int_{\partial\Omega} [P_{iA}N_A - (C_1(g_1)_i D_A T_A D_B N_B + C_2(g_2)_i M_A T_A M_B N_B)]' + \\
& (A_1(\alpha_1)_{i,C} D_A T_A D_B N_B D_C + A_2(\alpha_2)_{i,C} M_A T_A M_B N_B M_C)' + (A_1(\alpha_1)_i D_A T_A D_B T_B D_C N_C \\
& + A_2(\alpha_2)_i M_A T_A M_B T_B M_C N_C)'' - (A_1(\alpha_1)_i D_C N_C (D_A T_A' D_B T_B + D_A T_{A,N} D_B N_B) \\
& + A_2(\alpha_2)_i M_C N_C (M_A T_A' M_B T_B + M_A T_{A,N} M_B N_B))' u_i dS \\
& + \int_{\partial\Omega} [C_1(g_1)_i D_A N_A D_B N_B + C_2(g_2)_i M_A N_A M_B N_B - A_1(\alpha_1)_{i,C} D_A N_A D_B N_B D_C \\
& - A_2(\alpha_2)_{i,C} M_A N_A M_B N_B M_C + A_1(\alpha_1)_i D_C N_C (D_A N_A' D_B T_B + D_A N_{A,N} D_B N_B) \\
& + A_2(\alpha_2)_i M_C N_C (M_A N_A' M_B T_B + M_A N_{A,N} M_B N_B) - \{A_1(\alpha_1)_i D_A D_B D_C (T_A N_B N_C \\
& + N_A T_B N_C)\}' - \{A_2(\alpha_2)_i M_A M_B M_C (T_A N_B N_C + N_A T_B N_C)\}' u_{i,N} dS \\
& + \sum \| \{C_1(g_1)_i D_A T_A D_B N_B + C_2(g_2)_i M_A T_A M_B N_B - A_1(\alpha_1)_{i,C} D_A T_A D_B N_B D_C \\
& - A_2(\alpha_2)_{i,C} M_A T_A M_B N_B M_C - 2(A_1(\alpha_1)_i D_A T_A D_B T_B D_C N_C)' \\
& - 2(A_2(\alpha_2)_i M_A T_A M_B T_B M_C N_C)\}' u_i \| + \sum \| \frac{d}{dS} [(A_1(\alpha_1)_i D_A T_A D_B T_B D_C N_C \\
& + A_2(\alpha_2)_i M_A T_A M_B T_B M_C N_C) u_i] \| + \sum \| [A_1(\alpha_1)_i (D_A T_A' D_B T_B D_C N_C + \\
& D_A T_{A,N} D_B N_B D_C N_C) + A_2(\alpha_2)_i (M_A T_A' M_B T_B M_C N_C + M_A T_{A,N} M_B N_B M_C N_C) u_i] \| \\
& + \sum \| [A_1(\alpha_1)_i (D_A T_A D_B N_B D_C N_C + D_A N_A D_B T_B D_C N_C) \\
& + A_2(\alpha_2)_i (M_A T_A M_B N_B M_C N_C + M_A N_A M_B T_B M_C N_C)] u_{i,N} \| \\
& + \int_{\partial\Omega} (A_1(\alpha_1)_i D_A N_A D_B N_B D_C N_C + A_2(\alpha_2)_i M_A N_A M_B N_B M_C N_C) u_{i,NN} dS, \quad (2.70)
\end{aligned}$$

where the double bar symbol refers to the jump across the discontinuities on the boundary $\partial\Omega$ (i.e. $\| * \| = (*)^+ - (*)^-$) and the sum refers to the collection of all discontinuities. It is concluded from Eq. (2.40) that admissible powers are of the form

$$P = \int_{\partial w_t} t_i u_i dS + \int_{\partial w} m_i u_{i,N} dS + \int_{\partial w} r_i u_{i,NN} dS + \sum f_i u_i + \sum h_i u_{i,N}. \quad (2.71)$$

By comparing Eqs. (2.70) and (2.71), we obtain

$$\begin{aligned}
t_i &= P_{iA}N_A - \frac{d}{ds}[C_1(g_1)_i D_A T_A D_B N_B + C_2(g_2)_i M_A T_A M_B N_B - \\
&A_1(\alpha_1)_{i,C} D_A T_A D_B N_B D_C - A_2(\alpha_2)_{i,C} M_A T_A M_B N_B M_C + A_1(\alpha_1)_i D_C N_C (D_A T_A' D_B T_B \\
&\quad + D_A T_{A,N} D_B N_B) + A_2(\alpha_2)_i M_C N_C (M_A T_A' M_B T_B + M_A T_{A,N} M_B N_B)] \\
&\quad + \frac{d^2}{ds^2} (A_1(\alpha_1)_i D_A T_A D_B T_B D_C N_C + A_2(\alpha_2)_i M_A T_A M_B T_B M_C N_C), \\
m_i &= C_1(g_1)_i D_A N_A D_B N_B + C_2(g_2)_i M_A N_A M_B N_B - A_1(\alpha_1)_{i,C} D_A N_A D_B N_B D_C \\
&\quad - A_2(\alpha_2)_{i,C} M_A N_A M_B N_B M_C + A_1(\alpha_1)_i D_C N_C (D_A N_A' D_B T_B + D_A N_{A,N} D_B N_B) \\
&\quad + A_2(\alpha_2)_i M_C N_C (M_A N_A' M_B T_B + M_A N_{A,N} M_B N_B) \\
&\quad - \frac{d}{ds} \{2(A_1(\alpha_1)_i D_A D_B D_C N_A T_B N_C + A_2(\alpha_2)_i M_A M_B M_C N_A T_B N_C)\}, \\
r_i &= A_1(\alpha_1)_i D_A N_A D_B N_B D_C N_C + A_2(\alpha_2)_i M_A N_A M_B N_B M_C N_C, \\
f_i &= C_1(g_1)_i D_A T_A D_B N_B + C_2(g_2)_i M_A T_A M_B N_B - A_1(\alpha_1)_{i,C} D_A T_A D_B N_B D_C \\
&\quad - A_2(\alpha_2)_{i,C} M_A T_A M_B N_B M_C - 2\frac{d}{ds}[A_1(\alpha_1)_i D_A T_A D_B T_B D_C N_C + \\
&\quad A_2(\alpha_2)_i M_A T_A M_B T_B M_C N_C] + A_1(\alpha_1)_i (D_A T_A' D_B T_B D_C N_C \\
&\quad + D_A T_{A,N} D_B N_B D_C N_C) + A_2(\alpha_2)_i (M_A T_A' M_B T_B M_C N_C + M_A T_{A,N} M_B N_B M_C N_C), \\
\frac{d}{ds}(f_i) &= \frac{d}{dS} [(A_1(\alpha_1)_i D_A T_A D_B T_B D_C N_C + A_2(\alpha_2)_i M_A T_A M_B T_B M_C N_C)], \\
h_i &= 2[A_1(\alpha_1)_i D_A N_A D_B T_B D_C N_C + A_2(\alpha_2)_i M_A N_A M_B T_B M_C N_C], \quad (2.72)
\end{aligned}$$

where t_i , m_i , and f_i are, respectively, the expression for edge tractions, edge moments, and corner forces. More importantly, the introduction of the third gradient of deformations yields new interaction boundary conditions (i.e. r_i , $\frac{d}{ds}(f_i)$ and h_i). In [69], Kim et al. proposed that these additional sets of boundary conditions can be thought of as the set of admissible contact interactions that the third-gradient continuum can sustain (see, for example, [24, 33]). Kim et al. [69] referred that the produced interaction forces are associated with the Piola-type triple stress, resulting in the triple forces that characterize mechanical contacts on the edges and points of Cauchy cuts [33, 39, 83]. In case of fiber-reinforced composite, the triple force would

refer to the impacts of local fiber-matrix interactions that can be assimilated by the computation of the third gradient of the continuum deformation on the convected curves of fibers [69, 70].

In a typical environment where fibers are aligned along the directions of either normal and/or tangential to the boundary (e.g., rectangular boundaries), we compute

$$D_A T_A D_B N_B = 0, \quad M_A T_A M_B N_B = 0 \quad \text{and} \quad T_{A,N} = T'_A = N_{A,N} = N'_A = 0. \quad (2.73)$$

Thus the boundary conditions reduce to

$$\begin{aligned} t_i &= P_{iA} N_A, \\ m_i &= \left(C_1 (g_1)_i - A_1 (\alpha_1)_{i,C} D_C \right) D_A N_A D_B N_B + \left(C_2 (g_2)_i - A_2 (\alpha_2)_{i,C} M_C \right) \\ &\quad M_A N_A M_B N_B, \\ r_i &= A_1 (\alpha_1)_i D_A N_A D_B N_B D_C N_C + A_2 (\alpha_2)_i M_A N_A M_B N_B M_C N_C, \\ f_i &= 0, \\ \frac{d}{ds}(f_i) &= 0, \\ h_i &= 0, \end{aligned} \quad (2.74)$$

and, the expression of the associated Piola-type stress in Eq. (2.53) now becomes

$$\begin{aligned} P_{iA}(\mathbf{e}_i \otimes \mathbf{E}_A) &= [W_{F_{iA}} - p F_{iA}^* + \frac{E_1}{2} (F_{jC} F_{jD} D_C D_D - 1)(F_{iB} D_A D_B) + \frac{E_2}{2} (F_{jC} F_{jD} M_C M_D - 1) \\ &\quad (F_{iB} M_A M_B) - C_1 (g_1)_{i,B} D_A D_B - C_2 (g_2)_{i,B} M_A M_B + A_1 (\alpha_1)_{i,BC} D_A D_B D_C \\ &\quad + A_2 (\alpha_2)_{i,BC} M_A M_B M_C](\mathbf{e}_i \otimes \mathbf{E}_A). \end{aligned} \quad (2.75)$$

2.3.1 Example: Neo-Hookean materials

In the case of Neo-Hookean materials, the energy density function is given by

$$W(I_1, I_3) = \frac{\mu}{2}(I_1 - 3) - \mu \log I_3 + \frac{\lambda}{2} (\log I_3)^2, \quad (2.76)$$

where μ and λ are the material constants and I_1 and I_3 are, respectively, the first and third invariants of the deformation gradient tensor. By setting $I_3 = 1$, the

incompressible model can be obtained as

$$W(I_1) = \frac{\mu}{2}(I_1 - 3) = \frac{\mu}{2}(\mathbf{F} \cdot \mathbf{F} - 3). \quad (2.77)$$

Now taking the derivative of the above with respect to \mathbf{F} and subsequently substituting it into Eq. (2.75), we find

$$\begin{aligned} P_{iA}(\mathbf{e}_i \otimes \mathbf{E}_A) &= [\mu F_{iA} - p F_{iA}^* + \frac{E_1}{2}(F_{jC}F_{jD}D_C D_D - 1)(F_{iB}D_A D_B) + \\ &\frac{E_2}{2}(F_{jC}F_{jD}M_C M_D - 1)(F_{iB}M_A M_B) - C_1(g_1)_{i,B} D_A D_B - C_2(g_2)_{i,B} M_A M_B \\ &+ A_1(\alpha_1)_{i,BC} D_A D_B D_C + A_2(\alpha_2)_{i,BC} M_A M_B M_C](\mathbf{e}_i \otimes \mathbf{E}_A). \end{aligned} \quad (2.78)$$

To obtain the Euler equation, we put the expression of Eq. (2.78) into Eq. (2.56) and obtain

$$\begin{aligned} P_{iA,A} &= \mu F_{iA,A} - p_{,A} F_{iA}^* + \frac{E_1}{2}(F_{iB,A}F_{jC}F_{jD} + F_{iB}F_{jC,A}F_{jD} + F_{iB}F_{jC}F_{jD,A})D_A D_B D_C D_D \\ &- \frac{E_1}{2}F_{iB,A}D_A D_B + \frac{E_2}{2}(F_{iB,A}F_{jC}F_{jD} + F_{iB}F_{jC,A}F_{jD} + F_{iB}F_{jC}F_{jD,A})M_A M_B M_C M_D \\ &- \frac{E_2}{2}F_{iB,A}M_A M_B - C_1(g_1)_{i,AB} D_A D_B - C_2(g_2)_{i,AB} M_A M_B \\ &+ A_1(\alpha_1)_{i,ABC} D_A D_B D_C + A_2(\alpha_2)_{i,ABC} M_A M_B M_C = 0. \end{aligned} \quad (2.79)$$

Here we use the Piola's identity $F_{iA,A}^* = 0$.

Let us now assume a fiber-reinforced material that consists of initially an orthonormal set of fibers and is subjected to finite plane deformations,

$$\mathbf{D} = \mathbf{E}_1, D_1 = 1, D_2 = 0, \mathbf{M} = \mathbf{E}_2, M_1 = 0, M_2 = 1. \quad (2.80)$$

Accordingly, Eq. (2.79) can be reduced as

$$\begin{aligned} P_{iA,A} &= \mu F_{iA,A} - p_{,A} F_{iA}^* + \frac{E_1}{2}(F_{i1,1}F_{j1}F_{j1} + F_{i1}F_{j1,1}F_{j1} + F_{i1}F_{j1}F_{j1,1}) - \frac{E_1}{2}F_{i1,1} \\ &+ \frac{E_2}{2}(F_{i2,2}F_{j2}F_{j2} + F_{i2}F_{j2,2}F_{j2} + F_{i2}F_{j2}F_{j2,2}) - \frac{E_2}{2}F_{i2,2} - C_1(g_1)_{i,11} \\ &- C_2(g_2)_{i,22} + A_1(\alpha_1)_{i,111} + A_2(\alpha_2)_{i,222} = 0, \end{aligned} \quad (2.81)$$

where

$$(g_1)_i = F_{i1,1}, (g_2)_i = F_{i2,2}, (\alpha_1)_i = F_{i1,11}, (\alpha_2)_i = F_{i2,22}, F_{iA} = \chi_{i,A}, F_{iA}^* = \varepsilon_{ij}\varepsilon_{AB}F_{jB}, \quad (2.82)$$

and ε_{ij} is a 2-D permutation, $\varepsilon_{12} = -\varepsilon_{21} = 1$, $\varepsilon_{11} = \varepsilon_{22} = 0$. Consequently, invoking Eqs. (2.80)-(2.82), together with the constraint of the bulk incompressibility (i.e., $\det \mathbf{F} = 1$), we deliver the following system of PDEs,

$$\begin{aligned} 0 = & \mu\chi_{i,AA} - p_{,A}\varepsilon_{ij}\varepsilon_{AB}\chi_{j,B} + \frac{E_1}{2}(\chi_{i,11}\chi_{j,1}\chi_{j,1} + \chi_{i,1}\chi_{j,11}\chi_{j,1} + \chi_{i,1}\chi_{j,1}\chi_{j,11}) - \frac{E_1}{2}\chi_{i,11} \\ & + \frac{E_2}{2}(\chi_{i,22}\chi_{j,2}\chi_{j,2} + \chi_{i,2}\chi_{j,22}\chi_{j,2} + \chi_{i,2}\chi_{j,2}\chi_{j,22}) - \frac{E_2}{2}\chi_{i,22} \\ & - C_1\chi_{i,11111} - C_2\chi_{i,22222} + A_1\chi_{i,1111111} + A_2\chi_{i,2222222}, \quad (2.83) \end{aligned}$$

and

$$\chi_{1,1}\chi_{2,2} - \chi_{1,2}\chi_{2,1} = 1. \quad (2.84)$$

The above system of PDE's can be solved for χ_1 , χ_2 , and p using commercial finite element analysis packages (e.g., Matlab, COMSOL, etc.).

For the special case of an unidirectional fiber (i.e., $M_A = M_B = 0$), the expression of Euler equation can be found from Eq. (2.79) as

$$\begin{aligned} P_{iA,A} = & \mu F_{iA,A} - p_{,A} F_{iA}^* + \frac{E_1}{2}(F_{iB,A}F_{jC}F_{jD} + F_{iB}F_{jC,A}F_{jD} + F_{iB}F_{jC}F_{jD,A})D_A D_B D_C D_D \\ & - \frac{E_1}{2}F_{iB,A}D_A D_B - C_1(g_1)_{i,AB}D_A D_B + A_1(\alpha_1)_{i,ABC}D_A D_B D_C = 0. \quad (2.85) \end{aligned}$$

Using same fashion as in Eqs. (2.80)-(2.84), we can deduce the following system of PDE's for the unidirectional fiber reinforcement (i.e., $M_1 = M_2 = 0$) as

$$\begin{aligned} \mu\chi_{i,AA} - p_{,A}\varepsilon_{ij}\varepsilon_{AB}\chi_{j,B} + \frac{E_1}{2}(\chi_{i,11}\chi_{j,1}\chi_{j,1} + \chi_{i,1}\chi_{j,11}\chi_{j,1} + \chi_{i,1}\chi_{j,1}\chi_{j,11}) - \frac{E_1}{2}\chi_{i,11} \\ - C_1\chi_{i,11111} + A_1\chi_{i,1111111} = 0, \quad (2.86) \end{aligned}$$

$$\begin{aligned} \text{for } i = 1, \quad \mu(\chi_{1,11} + \chi_{1,22}) - p_{,1}\chi_{2,2} + p_{,2}\chi_{2,1} + \frac{E_1}{2}(3\chi_{1,11}\chi_{1,1}\chi_{1,1} + \chi_{1,11}\chi_{2,1}\chi_{2,1} \\ + 2\chi_{2,11}\chi_{1,1}\chi_{2,1}) - \frac{E_1}{2}\chi_{1,11} - C_1\chi_{1,11111} + A_1\chi_{1,1111111} = 0, \quad (2.87) \end{aligned}$$

for $i = 2$, $\mu(\chi_{2,11} + \chi_{2,22}) + p_{,1}\chi_{1,2} - p_{,2}\chi_{1,1} + \frac{E_1}{2}(3\chi_{2,11}\chi_{2,1}\chi_{2,1} + \chi_{2,11}\chi_{1,1}\chi_{1,1} + 2\chi_{1,11}\chi_{1,1}\chi_{2,1}) - \frac{E_1}{2}\chi_{2,11} - C_1\chi_{2,1111} + A_1\chi_{2,111111} = 0$, (2.88)

and

$$\chi_{1,1}\chi_{2,2} - \chi_{1,2}\chi_{2,1} - 1 = 0. \quad (2.89)$$

2.3.2 Example: Mooney-Rivlin materials

In the case of Mooney-Rivlin materials, the energy density function is given by

$$W(\mathbf{F}) = \frac{\mu}{2}(I_1 - 3) + \frac{\kappa}{2}(I_2 - 3), \quad (2.90)$$

where I_2 is the second invariants of the deformation gradient tensor defined by

$$I_2 = \frac{1}{2} \left[(tr(\mathbf{F}^T \mathbf{F}))^2 - tr((\mathbf{F}^T \mathbf{F})^2) \right]. \quad (2.91)$$

Now, taking the derivative of $W(\mathbf{F})$ with respect to \mathbf{F} we obtain

$$W_{F_{iA}} = \frac{\mu}{2}(I_1)_{F_{iA}} + \frac{\kappa}{2}(I_2)_{F_{iA}},$$

where $(I_1)_{F_{iA}} = 2F_{iA}$, and $(I_2)_{F_{iA}} = 2F_{iB}(F_{jC}F_{jC}\delta_{AB} - F_{jA}F_{jB})$. The expression of $(I_2)_{F_{iA}}$ is derived in [84]. Thus Eq. (2.90) turns into the form

$$W_{F_{iA}} = \mu F_{iA} + \kappa F_{iB}(F_{jC}F_{jC}\delta_{AB} - F_{jA}F_{jB}), \quad (2.92)$$

and substituting it into Eq. (2.75), we find

$$\begin{aligned} P_{iA}(\mathbf{e}_i \otimes \mathbf{E}_A) = & [\mu F_{iA} + \kappa F_{iB}(F_{jC}F_{jC}\delta_{AB} - F_{jA}F_{jB}) - pF_{iA}^* + \frac{E_1}{2}(F_{jC}F_{jD}D_C D_D \\ & - 1)(F_{iB}D_A D_B) + \frac{E_2}{2}(F_{jC}F_{jD}M_C M_D - 1)(F_{iB}M_A M_B) - C_1(g_1)_{i,B} D_A D_B \\ & - C_2(g_2)_{i,B} M_A M_B + A_1(\alpha_1)_{i,BC} D_A D_B D_C + A_2(\alpha_2)_{i,BC} M_A M_B M_C] (\mathbf{e}_i \otimes \mathbf{E}_A). \end{aligned} \quad (2.93)$$

Hence the Euler equation for the Mooney-Rivlin materials reinforced with bidirectional fiber in the frame of third gradient of deformation takes the form of

$$\begin{aligned}
P_{iA,A} &= \mu F_{iA,A} + \kappa F_{iA,A} F_{jC} F_{jC} - \kappa F_{iB,A} F_{jA} F_{jB} + \kappa F_{iB} (2F_{jC} F_{jC,A} - F_{jA,A} F_{jB} - \\
&F_{jA} F_{jB,A}) - p_{,A} F_{iA}^* + \frac{E_1}{2} (F_{iB,A} F_{jC} F_{jD} + F_{iB} F_{jC,A} F_{jD} + F_{iB} F_{jC} F_{jD,A}) D_A D_B D_C D_D \\
&- \frac{E_1}{2} F_{iB,A} D_A D_B - \frac{E_2}{2} F_{iB,A} M_A M_B + \frac{E_2}{2} (F_{iB,A} F_{jC} F_{jD} + F_{iB} F_{jC,A} F_{jD} + \\
&F_{iB} F_{jC} F_{jD,A}) M_A M_B M_C M_D - C_1 (g_1)_{i,AB} D_A D_B - C_2 (g_2)_{i,AB} M_A M_B \\
&+ A_1 (\alpha_1)_{i,ABC} D_A D_B D_C + A_2 (\alpha_2)_{i,ABC} M_A M_B M_C = 0. \quad (2.94)
\end{aligned}$$

Using Eq. (2.80), the above can be reduced as

$$\begin{aligned}
P_{iA,A} &= \mu F_{iA,A} + \kappa F_{iA,A} F_{jC} F_{jC} - \kappa F_{iB,A} F_{jA} F_{jB} + \kappa F_{iB} (2F_{jC} F_{jC,A} - F_{jA,A} F_{jB} - \\
&F_{jA} F_{jB,A}) - p_{,A} F_{iA}^* + \frac{E_1}{2} (F_{i1,1} F_{j1} F_{j1} + F_{i1} F_{j1,1} F_{j1} + F_{i1} F_{j1} F_{j1,1}) + \frac{E_2}{2} (F_{i2,2} F_{j2} F_{j2} \\
&+ F_{i2} F_{j2,2} F_{j2} + F_{i2} F_{j2} F_{j2,2}) - \frac{E_1}{2} F_{i1,1} - \frac{E_2}{2} F_{i2,2} - C_1 (g_1)_{i,11} - C_2 (g_2)_{i,22} + A_1 (\alpha_1)_{i,111} \\
&+ A_2 (\alpha_2)_{i,222} = 0. \quad (2.95)
\end{aligned}$$

Using Eq. (2.82), we obtain the following system of PDE's for the Mooney-Rivlin matrix materials reinforced with bidirectional fiber

$$\begin{aligned}
0 &= \mu \chi_{i,AA} + \kappa \chi_{i,AA} \chi_{j,C} \chi_{j,C} - \kappa \chi_{i,BA} \chi_{j,A} \chi_{j,B} + \kappa \chi_{i,B} (2\chi_{j,C} \chi_{j,C,A} - \chi_{j,AA} \chi_{j,B} - \\
&\chi_{j,AX} \chi_{j,BA}) - p_{,A} \varepsilon_{ij} \varepsilon_{AB} \chi_{j,B} + \frac{E_1}{2} (\chi_{i,11} \chi_{j,1} \chi_{j,1} + \chi_{i,1} \chi_{j,11} \chi_{j,1} + \chi_{i,1} \chi_{j,1} \chi_{j,11}) - \frac{E_1}{2} \chi_{i,11} \\
&+ \frac{E_2}{2} (\chi_{i,22} \chi_{j,2} \chi_{j,2} + \chi_{i,2} \chi_{j,22} \chi_{j,2} + \chi_{i,2} \chi_{j,2} \chi_{j,22}) - \frac{E_2}{2} \chi_{i,22} - C_1 \chi_{i,1111} - C_2 \chi_{i,2222} \\
&+ A_1 \chi_{i,111111} + A_2 \chi_{i,222222}, \quad (2.96)
\end{aligned}$$

and

$$\chi_{1,1} \chi_{2,2} - \chi_{1,2} \chi_{2,1} = 1. \quad (2.97)$$

2.4 Finite element analysis of the sixth-order coupled PDE

The resulting systems of PDEs (Eqs. (2.87)–(2.89)) are sixth-order coupled nonlinear differential equations. Demonstrating numerical analysis approaches for coupled PDE systems, especially those with higher order terms, is not trivial. For preprocessing, (Eqs. (2.87)–(2.89)) can be recast as:

$$\begin{aligned}
\mu(Q + \chi_{1,22}) - AS + BD + \frac{E_1}{2}(3QC^2 + QD^2 + 2CRD - Q) - C_1M + A_1M_{,11} &= 0, \\
\mu(R + \chi_{2,22}) + AG - BC + \frac{E_1}{2}(3RD^2 + RC^2 + 2CQD - R) - C_1N + A_1N_{,11} &= 0, \\
Q - \chi_{1,11} &= 0, \\
R - \chi_{2,11} &= 0, \\
C - \chi_{1,1} &= 0, \\
D - \chi_{2,1} &= 0, \\
G - \chi_{1,2} &= 0, \\
S - \chi_{2,2} &= 0, \\
M - Q_{,11} &= 0, \\
N - R_{,11} &= 0, \\
A - \mu(Q + \chi_{1,22}) - C_1M &= 0, \\
B - \mu(R + \chi_{2,22}) - C_1N &= 0,
\end{aligned} \tag{2.98}$$

where, $A = p_{,1}$, $B = p_{,2}$, $Q = \chi_{1,11}$, $R = \chi_{2,11}$, $C = \chi_{1,1}$, $D = \chi_{2,1}$, $G = \chi_{1,2}$, $S = \chi_{2,2}$, $M = Q_{,11}$ and $N = R_{,11}$. As a result, we were able to reduce a sixth-order partial differential coupled system of equations to a second-order system of coupled PDEs. The above non-linear terms(i.e., $A\chi_{2,2}$, $B\chi_{2,1}$ etc.) can be treated via the

Picard iterative procedure,

$$\begin{aligned}
-A_{initial}\chi_{2,2}^{initial} + B_{initial}\chi_{2,1}^{initial} &\Rightarrow -A_0\chi_{2,2}^0 + B_0\chi_{2,1}^0, \\
A_{initial}\chi_{1,2}^{initial} - B_{initial}\chi_{1,1}^{initial} &\Rightarrow A_0\chi_{1,2}^0 + B_0\chi_{1,1}^0, \\
-3Q_{initial}C_{initial}^2 + Q_{initial}D_{initial}^2 + 2C_{initial}R_{initial}D_{initial} &\Rightarrow 3Q_0C_0^2 + Q_0D_0^2 + 2C_0R_0D_0, \\
-3R_{initial}D_{initial}^2 + R_{initial}C_{initial}^2 + 2C_{initial}Q_{initial}D_{initial} &\Rightarrow 3R_0D_0^2 + R_0C_0^2 + 2C_0Q_0D_0,
\end{aligned} \tag{2.99}$$

where the values of A, B, C, D, G, S, Q , and R continue to be refreshed based on their previous estimations (i.e., $A_0, B_0, C_0, D_0, G_0, S_0, Q_0$ and R_0) as iteration progresses. As a result, the above expression can be generalised to N number of iterations as

$$\begin{aligned}
-A_{N-1}\chi_{2,2}^{N-1} + B_{N-1}\chi_{2,1}^{N-1} &\Rightarrow -A_N\chi_{2,2}^N + B_N\chi_{2,1}^N, \\
A_{N-1}\chi_{1,2}^{N-1} - B_{N-1}\chi_{1,1}^{N-1} &\Rightarrow A_N\chi_{1,2}^N + B_N\chi_{1,1}^N, \\
3Q_{N-1}C_{N-1}^2 + Q_{N-1}D_{N-1}^2 + 2C_{N-1}R_{N-1}D_{N-1} &\Rightarrow 3Q_NC_N^2 + Q_ND_N^2 + 2C_NR_ND_N, \\
3R_{N-1}D_{N-1}^2 + R_{N-1}C_{N-1}^2 + 2C_{N-1}Q_{N-1}D_{N-1} &\Rightarrow 3R_ND_N^2 + R_NC_N^2 + 2C_NQ_ND_N.
\end{aligned} \tag{2.100}$$

A convergence criteria can be used to determine the number of iterations. Thus,

the weak form of Eq. (2.98) is obtained by

$$\begin{aligned}
& \int_{\Omega^e} w_1 (\mu(Q + \chi_{1,22}) - A_0 S + B_0 D + \frac{E_1}{2} (3QC_0^2 + QD_0^2 + 2RC_0 D_0 - Q) - C_1 M \\
& \quad + A_1 M_{,11}) d\Omega = 0, \\
& \int_{\Omega^e} w_2 (\mu(R + \chi_{2,22}) + A_0 G - B_0 C + \frac{E_1}{2} (3RD_0^2 + RC_0^2 + 2QC_0 D_0 - R) - C_1 N \\
& \quad + A_1 N_{,11}) d\Omega = 0, \\
& \int_{\Omega^e} w_3 (Q - \chi_{1,11}) d\Omega = 0, \\
& \int_{\Omega^e} w_4 (R - \chi_{2,11}) d\Omega = 0, \\
& \int_{\Omega^e} w_5 (C - \chi_{1,1}) d\Omega = 0, \\
& \int_{\Omega^e} w_6 (D - \chi_{2,1}) d\Omega = 0, \\
& \int_{\Omega^e} w_7 (G - \chi_{1,2}) d\Omega = 0, \\
& \int_{\Omega^e} w_8 (S - \chi_{2,2}) d\Omega = 0, \\
& \int_{\Omega^e} w_9 (M - Q_{,11}) d\Omega = 0, \\
& \int_{\Omega^e} w_{10} (N - R_{,11}) d\Omega = 0, \\
& \int_{\Omega^e} w_{11} (A - \mu(Q + \chi_{1,22}) - C_1 M) d\Omega = 0, \\
& \int_{\Omega^e} w_{12} (B - \mu(R + \chi_{2,22}) - C_1 N) d\Omega = 0. \tag{2.101}
\end{aligned}$$

Using integration by parts and Green–Stoke’s theorem (e.g., $\int_{\Omega^e} w_1 \chi_{1,11} d\Omega =$

$\int_{\partial\Gamma^e} (w_1\chi_{1,1}) Nd\Gamma - \int_{\Omega^e} w_{1,1}\chi_{1,1}d\Omega$). We obtain from the above that

$$\begin{aligned}
& \int_{\Omega^e} w_1\mu Q - \mu w_{1,2}\chi_{1,2} - w_1A_0S + w_1B_0D + w_1\frac{E_1}{2}(3QC_0^2 + QD_0^2 + 2RC_0D_0 - Q) \\
& \quad - w_1C_1M - A_1w_{1,1}M_{,1})d\Omega + \int_{\partial\Gamma^e} (\mu w_1\chi_{1,2}) Nd\Gamma + \int_{\partial\Gamma^e} (A_1w_1M_{,1}) Nd\Gamma = 0, \\
& \int_{\Omega^e} (w_2\mu R - \mu w_{2,2}\chi_{2,2} + w_2A_0G - w_2B_0C + w_2\frac{E_1}{2}(3RD_0^2 + RC_0^2 + 2QC_0D_0 - R) \\
& \quad - w_2C_1N - A_1w_{2,1}N_{,1})d\Omega + \int_{\partial\Gamma^e} (\mu w_2\chi_{2,2}) Nd\Gamma + \int_{\partial\Gamma^e} (A_1w_2N_{,1}) Nd\Gamma = 0, \\
& \quad \int_{\Omega^e} (w_3Q + w_{3,1}\chi_{1,1})d\Omega - \int_{\partial\Gamma^e} (w_3\chi_{1,1}) Nd\Gamma = 0, \\
& \quad \int_{\Omega^e} (w_4R + w_{4,1}\chi_{2,1})d\Omega - \int_{\partial\Gamma^e} (w_4\chi_{2,1}) Nd\Gamma = 0, \\
& \quad \int_{\Omega^e} (w_5C - w_5\chi_{1,1}) d\Omega = 0, \\
& \quad \int_{\Omega^e} (w_6D - w_6\chi_{2,1}) d\Omega = 0, \\
& \quad \int_{\Omega^e} (w_7G - w_7\chi_{1,2}) d\Omega = 0, \\
& \quad \int_{\Omega^e} (w_8S - w_8\chi_{2,2}) d\Omega = 0, \\
& \quad \int_{\Omega^e} (w_9M + w_{9,1}Q_{,1})d\Omega - \int_{\partial\Gamma^e} (w_9Q_{,1}) Nd\Gamma = 0, \\
& \quad \int_{\Omega^e} (w_{10}N + w_{10,1}R_{,1})d\Omega - \int_{\partial\Gamma^e} (w_{10}R_{,1}) Nd\Gamma = 0, \\
& \quad \int_{\Omega^e} (w_{11}A - w_{11}\mu Q + \mu w_{11,2}\chi_{1,2} - w_{11}C_1M)d\Omega - \int_{\partial\Gamma^e} (\mu w_{11}\chi_{1,2}) Nd\Gamma = 0, \\
& \quad \int_{\Omega^e} (w_{12}B - w_{12}\mu R + \mu w_{12,2}\chi_{2,2} - w_{12}C_1N)d\Omega - \int_{\partial\Gamma^e} (\mu w_{12}\chi_{2,2}) Nd\Gamma = 0, \quad (2.102)
\end{aligned}$$

where Ω , $\partial\Gamma$ and \mathbf{N} are the domain of interest, the associated boundary, and the rightward unit normal to the boundary in the sense of the Green–Stoke’s theorem respectively. The unknowns χ_1 , χ_2 , Q , R , C , D , G , S , M , N , A and B can be expressed in the form of Lagrangian polynomial as

$$(*) = \sum_{j=1}^{n=4} \left[(*)_j \Psi_j(x, y) \right], \quad (2.103)$$

where $(*)$ represents any of the twelve unknowns. Therefore, The test function w

is obtained as

$$(w_k) = \sum_{i=1}^{n=4} [w_k^i \Psi_i(x, y)]; \quad k = 1, 2, 3, 4, \dots, 12, \quad (2.104)$$

where w_i is the weight of the test function and $\Psi_i(x, y)$ are the corresponding shape function for the four-node rectangular elements, such that

$$\Psi_1 = \frac{(x-2)(y-1)}{2}, \quad \Psi_2 = \frac{x(y-1)}{-2}, \quad \Psi_3 = \frac{xy}{2} \quad \text{and} \quad \Psi_4 = \frac{y(x-2)}{-2}. \quad (2.105)$$

Eq. (2.102) can be recast using Eqs.(2.103) and (2.104) as

$$\begin{aligned} & \sum_{i,j=1}^n \left\{ \int_{\Omega^e} \left(\mu \Psi_i \Psi_j + 3 \frac{E_1}{2} \Psi_i \Psi_j C_0^2 + \frac{E_1}{2} \Psi_i \Psi_j D_0^2 - \frac{E_1}{2} \Psi_i \Psi_j \right) d\Omega \right\} Q_j - \sum_{i,j=1}^n \left\{ \int_{\Omega^e} (\mu \Psi_{i,2} \right. \\ & \quad \left. \Psi_{j,2}) d\Omega \right\} \chi_{1j} - \sum_{i,j=1}^n \left\{ \int_{\Omega^e} (\Psi_i \Psi_j A_0) d\Omega \right\} S_j + \sum_{i,j=1}^n \left\{ \int_{\Omega^e} (\Psi_i \Psi_j B_0) d\Omega \right\} D_j \\ & - \sum_{i,j=1}^n \left\{ \int_{\Omega^e} (\Psi_i \Psi_j C_1 + \Psi_{i,1} \Psi_{j,1} A_1) d\Omega \right\} M_j + \sum_{i,j=1}^n \left\{ \int_{\Omega^e} \left(\frac{E_1}{2} \Psi_i^2 \Psi_j C_0 D_0 \right) d\Omega \right\} R_j \\ & \quad + \int_{\partial\Gamma^e} (\mu \Psi_i \chi_{1,2}) N d\Gamma + \left(\int_{\partial\Gamma^e} A_1 \Psi_i M_{,1} \right) N d\Gamma = 0, \\ & \sum_{i,j=1}^n \left\{ \int_{\Omega^e} \left(\mu \Psi_i \Psi_j + 3 \frac{E_1}{2} \Psi_i \Psi_j D_0^2 + \frac{E_1}{2} \Psi_i \Psi_j C_0^2 - \frac{E_1}{2} \Psi_i \Psi_j \right) d\Omega \right\} R_j - \sum_{i,j=1}^n \left\{ \int_{\Omega^e} (\mu \Psi_{i,2} \right. \\ & \quad \left. \Psi_{j,2}) d\Omega \right\} \chi_{2j} + \sum_{i,j=1}^n \left\{ \int_{\Omega^e} (\Psi_i \Psi_j A_0) d\Omega \right\} G_j - \sum_{i,j=1}^n \left\{ \int_{\Omega^e} (\Psi_i \Psi_j B_0) d\Omega \right\} C_j \\ & - \sum_{i,j=1}^n \left\{ \int_{\Omega^e} (\Psi_i \Psi_j C_1 + \Psi_{i,1} \Psi_{j,1} A_1) d\Omega \right\} N_j + \sum_{i,j=1}^n \left\{ \int_{\Omega^e} \left(\frac{E_1}{2} \Psi_i^2 \Psi_j C_0 D_0 \right) d\Omega \right\} Q_j \\ & \quad + \int_{\partial\Gamma^e} (\mu \Psi_i \chi_{2,2}) N d\Gamma + \int_{\partial\Gamma^e} (A_1 \Psi_i N_{,1}) N d\Gamma = 0, \\ & \sum_{i,j=1}^n \left\{ \int_{\Omega^e} (\Psi_i \Psi_j) d\Omega \right\} Q_j + \sum_{i,j=1}^n \left\{ \int_{\Omega^e} (\Psi_{i,1} \Psi_{j,1}) d\Omega \right\} \chi_{1j} - \int_{\partial\Gamma^e} (\Psi_i \chi_{1,1}) N d\Gamma = 0, \\ & \sum_{i,j=1}^n \left\{ \int_{\Omega^e} (\Psi_i \Psi_j) d\Omega \right\} R_j + \sum_{i,j=1}^n \left\{ \int_{\Omega^e} (\Psi_{i,1} \Psi_{j,1}) d\Omega \right\} \chi_{2j} - \int_{\partial\Gamma^e} (\Psi_i \chi_{2,1}) N d\Gamma = 0, \\ & \sum_{i,j=1}^n \left\{ \int_{\Omega^e} (\Psi_i \Psi_j) d\Omega \right\} C_j - \sum_{i,j=1}^n \left\{ \int_{\Omega^e} (\Psi_i \Psi_{j,1}) d\Omega \right\} \chi_{1j} = 0, \\ & \sum_{i,j=1}^n \left\{ \int_{\Omega^e} (\Psi_i \Psi_j) d\Omega \right\} D_j - \sum_{i,j=1}^n \left\{ \int_{\Omega^e} (\Psi_i \Psi_{j,1}) d\Omega \right\} \chi_{2j} = 0, \end{aligned}$$

$$\begin{aligned}
& \sum_{i,j=1}^n \left\{ \int_{\Omega^e} (\Psi_i \Psi_j) d\Omega \right\} G_j - \sum_{i,j=1}^n \left\{ \int_{\Omega^e} (\Psi_i \Psi_{j,2}) d\Omega \right\} \chi_{1j} = 0, \\
& \sum_{i,j=1}^n \left\{ \int_{\Omega^e} (\Psi_i \Psi_j) d\Omega \right\} S_j - \sum_{i,j=1}^n \left\{ \int_{\Omega^e} (\Psi_i \Psi_{j,2}) d\Omega \right\} \chi_{2j} = 0, \\
& \sum_{i,j=1}^n \left\{ \int_{\Omega^e} (\Psi_i \Psi_j) d\Omega \right\} M_j + \sum_{i,j=1}^n \left\{ \int_{\Omega^e} (\Psi_{i,1} \Psi_{j,1}) d\Omega \right\} Q_j - \int_{\partial\Gamma^e} (\Psi_i Q_{,1}) N d\Gamma = 0, \\
& \sum_{i,j=1}^n \left\{ \int_{\Omega^e} (\Psi_i \Psi_j) d\Omega \right\} N_j + \sum_{i,j=1}^n \left\{ \int_{\Omega^e} (\Psi_{i,1} \Psi_{j,1}) d\Omega \right\} R_j - \int_{\partial\Gamma^e} (\Psi_i R_{,1}) N d\Gamma = 0, \\
& \sum_{i,j=1}^n \left\{ \int_{\Omega^e} (\Psi_i \Psi_j) d\Omega \right\} A_j - \sum_{i,j=1}^n \left\{ \int_{\Omega^e} (\mu \Psi_i \Psi_j) d\Omega \right\} Q_j + \sum_{i,j=1}^n \left\{ \int_{\Omega^e} (\mu \Psi_{i,2} \Psi_{j,2}) d\Omega \right\} \chi_{1j} \\
& \quad - \sum_{i,j=1}^n \left\{ \int_{\Omega^e} (\Psi_i \Psi_j C_1) d\Omega \right\} M_j - \int_{\partial\Gamma^e} (\mu \Psi_i \chi_{1,2}) N d\Gamma = 0, \\
& \sum_{i,j=1}^n \left\{ \int_{\Omega^e} (\Psi_i \Psi_j) d\Omega \right\} B_j - \sum_{i,j=1}^n \left\{ \int_{\Omega^e} (\mu \Psi_i \Psi_j) d\Omega \right\} R_j + \sum_{i,j=1}^n \left\{ \int_{\Omega^e} (\mu \Psi_{i,2} \Psi_{j,2}) d\Omega \right\} \chi_{2j} \\
& \quad - \sum_{i,j=1}^n \left\{ \int_{\Omega^e} (\Psi_i \Psi_j C_1) d\Omega \right\} N_j - \int_{\partial\Gamma^e} (\mu \Psi_i \chi_{2,2}) N d\Gamma = 0. \tag{2.106}
\end{aligned}$$

The local stiffness matrix and forcing vector for each element can be found as

$$\begin{bmatrix} K_{11}^{11} & K_{12}^{11} & K_{13}^{11} & K_{14}^{11} \\ K_{21}^{11} & K_{22}^{11} & K_{23}^{11} & K_{24}^{11} \\ K_{31}^{11} & K_{32}^{11} & K_{33}^{11} & K_{34}^{11} \\ K_{41}^{11} & K_{42}^{11} & K_{43}^{11} & K_{44}^{11} \end{bmatrix}_{\text{Local}} \begin{bmatrix} \chi_1^1 \\ \chi_1^2 \\ \chi_1^3 \\ \chi_1^4 \end{bmatrix}_{\text{Local}} = \begin{bmatrix} F_1^1 \\ F_2^1 \\ F_3^1 \\ F_4^1 \end{bmatrix}_{\text{Local}}, \tag{2.107}$$

or alternatively, in a compact form,

$$\left[K_{ij}^{11} \right] \left[\chi_1^i \right] = \left[F_i^1 \right] \text{ for } i, j = 1, 2, 3, 4, \tag{2.108}$$

where

$$\left[K_{ij}^{11} \right] = - \int_{\Omega^e} (\mu \Psi_{i,2} \Psi_{j,2}) d\Omega, \tag{2.109}$$

and

$$\left[F_i^1 \right] = - \int_{\partial\Gamma^e} (\mu \Psi_i \chi_{1,2}) N d\Gamma - \left(\int_{\partial\Gamma^e} A_1 \Psi_i M_{,1} \right) N d\Gamma. \tag{2.110}$$

Finally, we obtain the following global systems of equations for each individual elements as

$$\begin{bmatrix}
 [K^{11}] & [K^{12}] & [K^{13}] & [K^{14}] & \dots & [K^{19}] & [K^{110}] & [K^{111}] & [K^{112}] \\
 [K^{21}] & [K^{22}] & [K^{23}] & [K^{24}] & \dots & [K^{29}] & [K^{210}] & [K^{211}] & [K^{212}] \\
 [K^{31}] & [K^{32}] & [K^{33}] & [K^{34}] & \dots & [K^{39}] & [K^{310}] & [K^{311}] & [K^{312}] \\
 [K^{41}] & [K^{42}] & [K^{43}] & [K^{44}] & \dots & [K^{49}] & [K^{410}] & [K^{411}] & [K^{412}] \\
 [K^{51}] & [K^{52}] & [K^{53}] & [K^{54}] & \dots & [K^{59}] & [K^{510}] & [K^{511}] & [K^{512}] \\
 [K^{61}] & [K^{62}] & [K^{63}] & [K^{64}] & \dots & [K^{69}] & [K^{610}] & [K^{611}] & [K^{612}] \\
 [K^{71}] & [K^{72}] & [K^{73}] & [K^{74}] & \dots & [K^{79}] & [K^{710}] & [K^{711}] & [K^{712}] \\
 [K^{81}] & [K^{82}] & [K^{83}] & [K^{84}] & \dots & [K^{89}] & [K^{810}] & [K^{811}] & [K^{812}] \\
 [K^{91}] & [K^{92}] & [K^{93}] & [K^{94}] & \dots & [K^{99}] & [K^{910}] & [K^{911}] & [K^{912}] \\
 [K^{101}] & [K^{102}] & [K^{103}] & [K^{104}] & \dots & [K^{109}] & [K^{1010}] & [K^{1011}] & [K^{1012}] \\
 [K^{111}] & [K^{112}] & [K^{113}] & [K^{114}] & \dots & [K^{119}] & [K^{1110}] & [K^{1111}] & [K^{1112}] \\
 [K^{121}] & [K^{122}] & [K^{123}] & [K^{124}] & \dots & [K^{129}] & [K^{1210}] & [K^{1211}] & [K^{1212}]
 \end{bmatrix}
 \begin{bmatrix}
 \chi_1^i \\
 \chi_2^i \\
 Q_i \\
 R_i \\
 C_i \\
 D_i \\
 G_i \\
 S_i \\
 M_i \\
 N_i \\
 A_i \\
 B_i
 \end{bmatrix}
 =
 \begin{bmatrix}
 \{F^1\} \\
 \{F^2\} \\
 \{F^3\} \\
 \{F^4\} \\
 \{F^5\} \\
 \{F^6\} \\
 \{F^7\} \\
 \{F^8\} \\
 \{F^9\} \\
 \{F^{10}\} \\
 \{F^{11}\} \\
 \{F^{12}\}
 \end{bmatrix}.
 \tag{2.111}$$

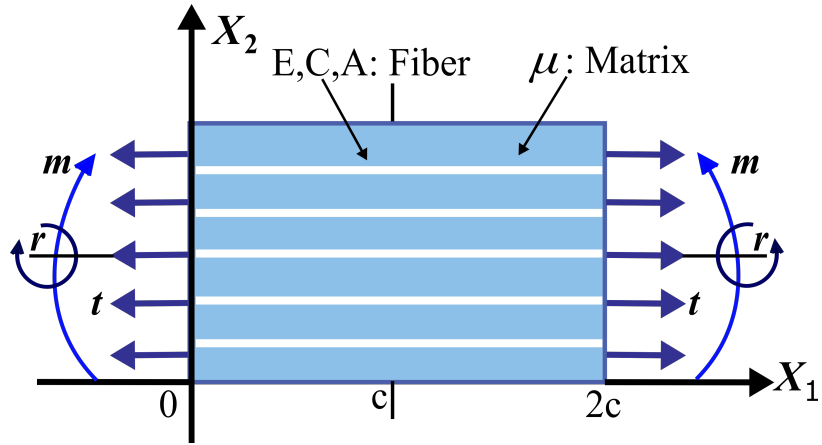


Figure 2.1: Schematic of the problem

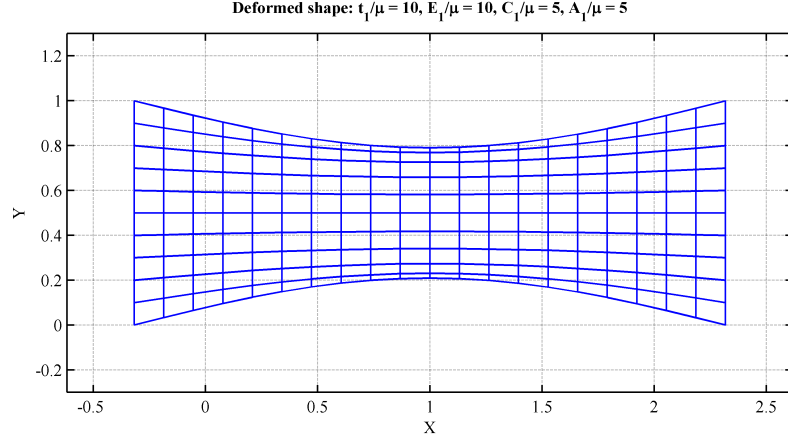


Figure 2.2: Deformation Configuration when $\frac{t_1}{\mu} = 10$, $\frac{E_1}{\mu} = 10$, $\frac{C_1}{\mu} = 5$ and $\frac{A_1}{\mu} = 5$

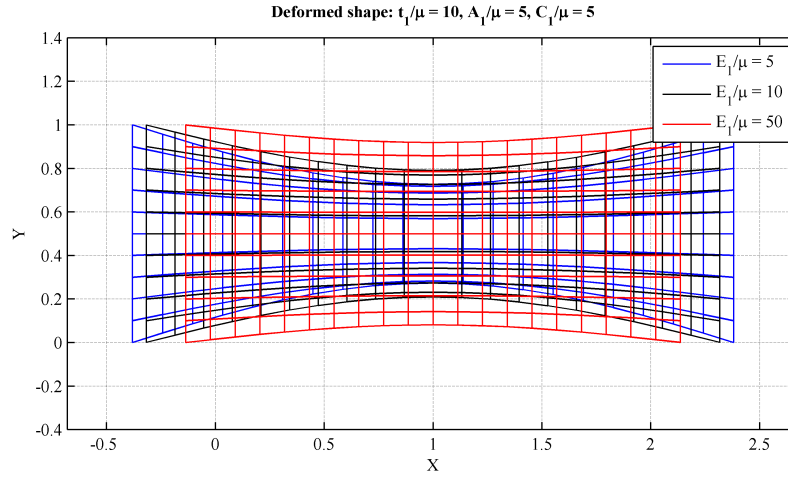


Figure 2.3: Deformed configuration with variation of $\frac{E_1}{\mu}$ when $\frac{t_1}{\mu} = 10$, $\frac{C_1}{\mu} = 5$, and $\frac{A_1}{\mu} = 5$

parameters as $\frac{E_1}{\mu} = 10$, $\frac{C_1}{\mu} = 5$, and $\frac{A_1}{\mu} = 5$. It is evident that the positive triple force ($\frac{t_1}{\mu}$) results clockwise point rotation. The effect is the opposite in the case of negative triple force. The values of θ_1, θ_2 and θ_3 correspond to the cases of negative, zero, and positive triple force, respectively (i.e. $\theta_1 < \theta_2 < \theta_3$).

Also, when we remove the triple stress parameter (i.e., $A_1 = 0$), the deformed configuration aligns closely (Figure 2.6) with the result obtained from the second gradient theory [67].

Figure 2.7 shows the deformed contour $\sqrt{\chi_1^2 + \chi_2^2}$ for different values of the triple

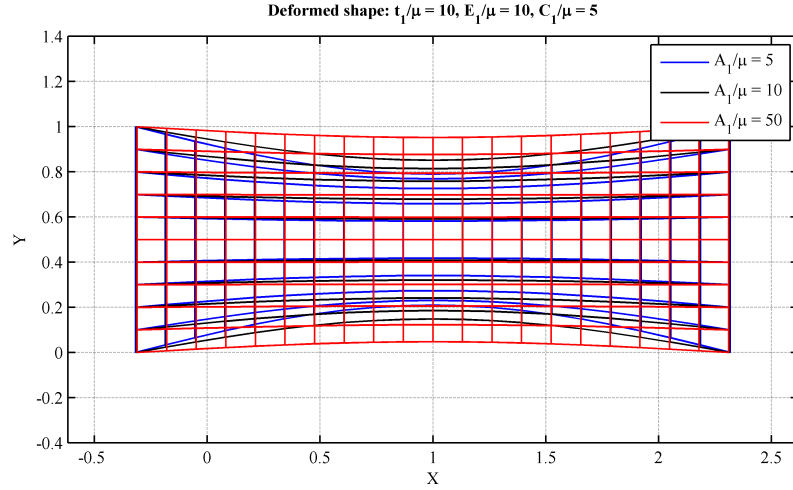


Figure 2.4: Deformed configuration with variation of $\frac{A_1}{\mu}$ when $\frac{t_1}{\mu} = 10$, $\frac{E_1}{\mu} = 10$, and $\frac{C_1}{\mu} = 5$

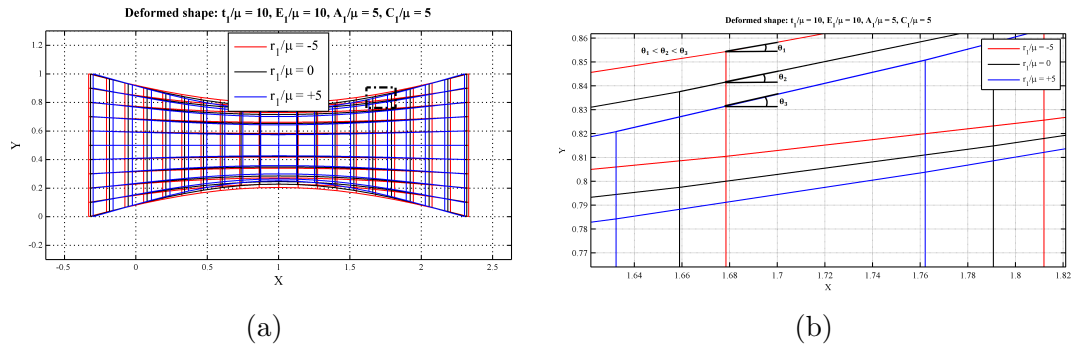


Figure 2.5: Deformed configuration with variation of triple force (a) when $\frac{t_1}{\mu} = 5$, $\frac{E_1}{\mu} = 10$, $\frac{C_1}{\mu} = 5$ and $\frac{A_1}{\mu} = 5$, (b) Zoomed section

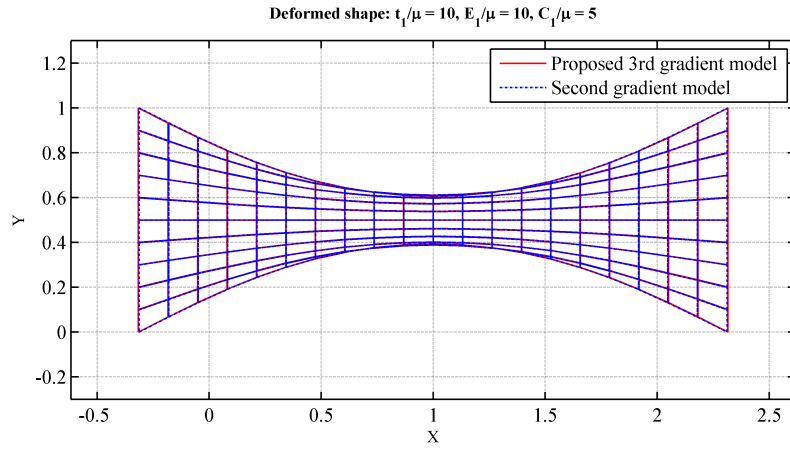
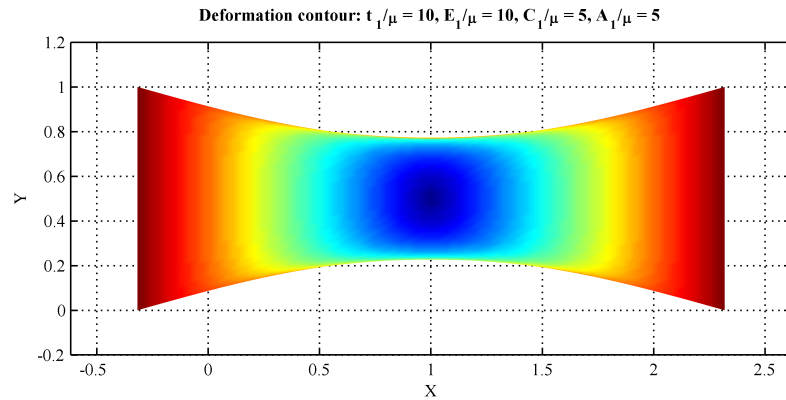
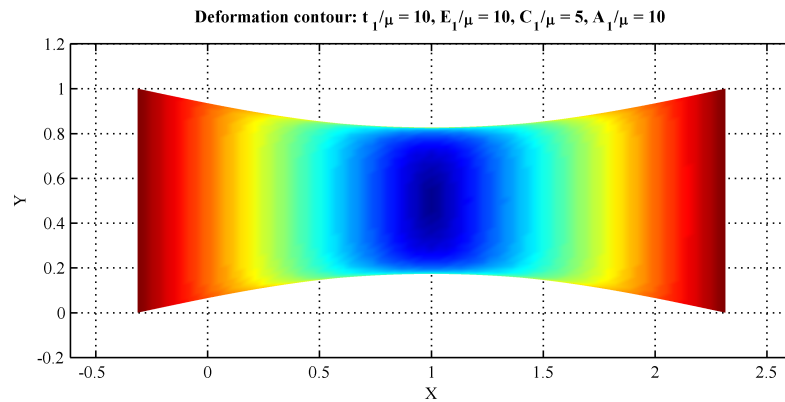


Figure 2.6: Comparison with the existing result [67]

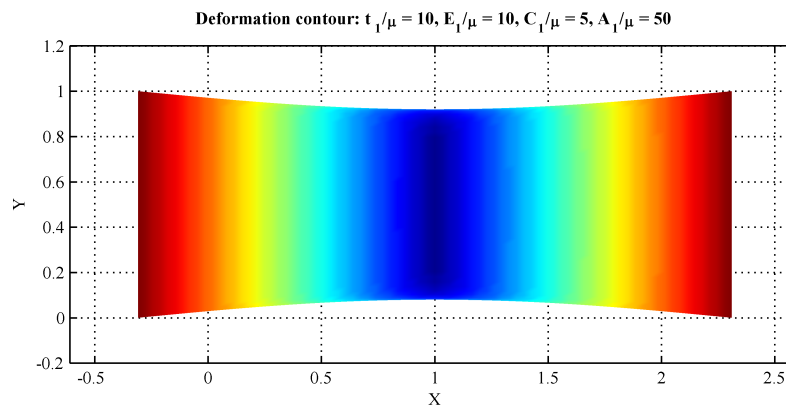
stress parameter. To gain a better understanding of the influences of the third gra-



(a)



(b)



(c)

Figure 2.7: Deformation contour $\sqrt{\chi_1^2 + \chi_2^2}$ (a) $\frac{A_1}{\mu} = 5$, (b) $\frac{A_1}{\mu} = 10$, (c) $\frac{A_1}{\mu} = 50$ when $\frac{t_1}{\mu} = 10$, $\frac{E_1}{\mu} = 10$, and $\frac{C_1}{\mu} = 5$

dient of deformations, we examine the shear strain fields and associated shear angle

distributions (see Figure 2.8) over the domain of interest for the uniaxial tension of a fiber-reinforced composite. The shear strain gradients and shear angles are computed in the analysis using the following relationships [85]:

$$\Phi' = \frac{u_2''(1 + u_1') - u_2' u_1''}{u_2'^2 + (1 + u_1')^2}, \quad (2.113)$$

$$\Phi = \tan^{-1}\left(\frac{\chi_{2,1} - \chi_{1,1}}{2 + \chi_{1,1} + \chi_{2,1}}\right). \quad (2.114)$$

We have shown earlier that the proposed third gradient model can reproduce the deformation anticipated from the second gradient model by vanishing the triple stress parameter (i.e., $A_1 = 0$), (see Figure 2.6). The shear angle distribution and corresponding shear strain gradient distribution predicted by the second gradient model is achieved by setting $\frac{A_1}{\mu} = 0$ and the associated plot is shown in Figure 2.8. It can be observed that when $\frac{A_1}{\mu} = 0$, the shear angle distribution is smooth, continuous but non-dilatational. The shear strain gradient field is found to be constant in this case. On the other hand, the shear angle distribution predicted by the third gradient model ($\frac{A_1}{\mu} \neq 0$) is smooth, continuous, and dilatational. The shear strain gradient field is also not constant (see Figure 2.8). The change in shear strain gradient can be interpreted as a sign of dilatation. Further, the dilatation increases as the triple stress parameter increases.

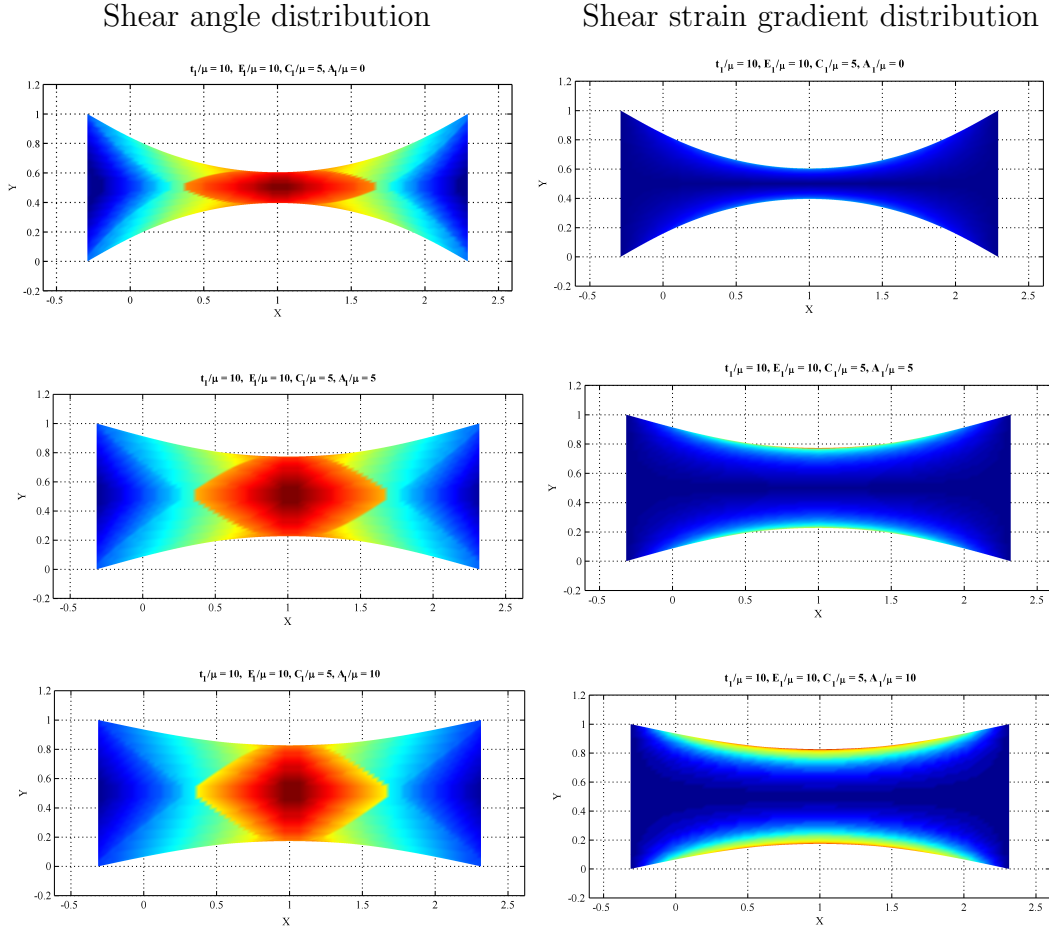


Figure 2.8: Shear angle and shear strain distribution for various triple stress parameter when $\frac{t_1}{\mu} = 10$, $\frac{E_1}{\mu} = 10$ and $\frac{C_1}{\mu} = 5$

2.5.1 Application of third gradient of deformation theory

The shear band is a narrow, intense shear strain zone that develops during large deformation. The shear band usually occurs in a wide range of metallic materials, including nanocrystalline metals and metallic glasses [86]. The thickness of the shear band is usually in the order of particle size [87]. The shear band can contain extremely large local deformation and frequently lead to failure [86, 88]. Hence, identifying the formation of the shear band is an entrancing topic for researchers. Shear band formation in metallic glasses under uniaxial tension has been well studied in [89–91]. It is found that the shear band inclination angle differs from 45 degrees [89]. In the case of uniaxial tension, the inclination angle is higher than 45 degrees, and in the

case of uniaxial compression, the value is lower than 45 degrees. Several theories have been proposed to describe the shear band inclination angle. In [92, 93], the author used the Coulomb-Mohr yield criterion to describe this behavior. Some extensions (see, for example, [91, 94]) to the Mohr-Coulomb criterion have been proposed. In [90], the author used the Oyane fracture criterion in their simulation and observed that a shear band was forming at an angle (59 degrees), which differed from their experimental result (62.9 degrees). This discrepancy is a result of local rotation during the damage process [90]. Moreover, In [91], the authors explain how the deviation from the standard 45 degrees is caused by the local friction. Also, the author in [89, 95] proposed that, since large deformation causes volume dilatation which results in atomic re-arrangement, the shear band inclination angle can be predicted using a formulation that incorporates the local volume dilatation. They incorporate a volume dilatation parameter ' a ' and find that the shear band inclination angle deviates more from 45 degrees with increasing the value of ' a '.

Local friction has an effect on shear band formation and shear band inclination angle. In this respect, we would like to discuss the utility of the proposed third gradient model in the analysis of the shear band's inclination angles and associated dilatation. Each particle rotates about its own axis, and the gradient of each unique revolution creates a relative rotation. Due to the relative rotation of the atoms, a local frictional force will be created. The friction describes the resistance of a system to shearing [96]. Because of the high internal friction, the rate of particle rotation is lower in highly coordinated materials [97]. In addition, for this type of highly coordinated dense material, dilatation is observed to be more intense [98].

From Figure 2.9(a), we can see that in a close-packed array, the aqua-colored atom is in direct contact with six adjacent atoms, whereas in a loose-packed array (see Figure 2.9(b), the number is four. In addition, in a close-packed array, the distance between neighboring atoms is smaller than in a loose-packed array. It is obvious that in the case of highly coordinated materials, the atoms have more internal friction

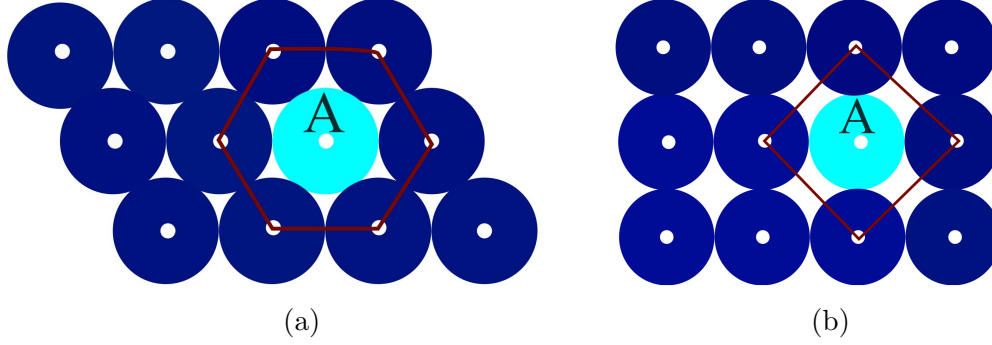


Figure 2.9: Material structure (a) Close packed array, (b) Loose packed array

because of the higher number of neighboring atoms. Due to high friction, point rotation or local rotation will be less in this case. For less coordinated materials, the friction force is less and the local rotation is greater. Now, from our model,

$$R = A \times \Phi, \quad (2.115)$$

where R , A and Φ are the applied triple force, triple stress parameter and induced point rotation, respectively. The induced point rotation is inversely related to the triple stress parameter. Accordingly, for a highly coordinated material where the point rotation is less [96] and the dilatation is more intense [98], the triple stress parameter will be large. From the simulation (see Figure 2.8), with varying triple stress parameter A_1 , we can observe that when $\frac{A_1}{\mu}$ is large the dilatation is more intense compared to the case when $\frac{A_1}{\mu}$ is small. Thus the third gradient model also implies the similar fact in terms of the dilatation of a highly coordinated material. Moreover, we have also applied the positive and negative triple force (\mathbf{r}) and have investigated its impact on shear dilatation. The positive triple force results in clockwise point rotation (see Figures 2.5(a) and 2.5(b)) and the shear dilatation for this case is less intensified in comparison to the negative ones (see Figure 2.10). Also, the average shear angle of the domain is higher in the case of positive triple force when it is compared to the negative triple force. Lastly, we obtain the shear band inclination angle using the formula provided in [89, 95]. In these papers, the authors introduce local atomic volume dilatation as a governing factor for the shear band inclination angle.

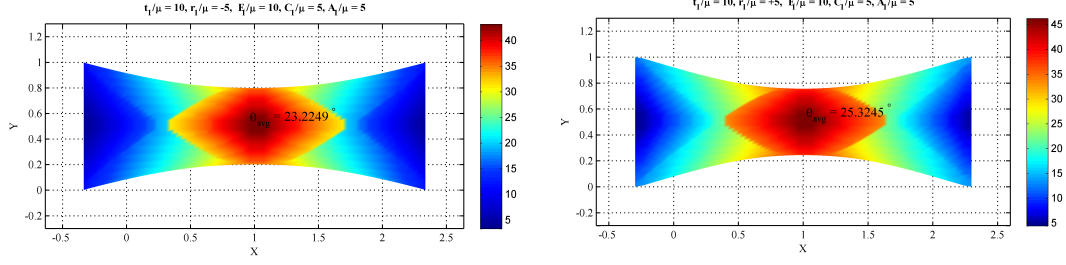


Figure 2.10: Shear angle distribution for various triple force $\mathbf{r} : \mathbf{r} < \mathbf{0}$ (left) and $\mathbf{r} > \mathbf{0}$ (right)

They have used a formulation based on the Drucker-Prager yield criterion with the volume change governed by Spaepen's free volume model [99]. A brief description of this model is presented in [89, 95]. The constitutive theory contains hydrostatic pressure originated from volume dilatation, $\sigma_e = aI_1 + \sqrt{J_2}$, where $I_1 = trace(\sigma)$, is the first invariant of the stress tensor, and the parameter a is constant related to the volume dilation sensitivity. $J_2 = \frac{ss}{2}$, $s = \sigma - trace(\sigma)I/3$ is the deviatoric stress with I being the identity tensor. The authors implemented the constitutive theory into the ABAQUS finite element software using the UMAT subroutine and obtained the shear band inclination angle from the contour plot of the shear strain field for various values of coefficient a (see Table 1). It is found that the shear band inclination angle deviates more with increasing the value of coefficient a which resembles more intense dilatation. The authors considered a sample under uniaxial tension and expressed the volume change rate as $\frac{\dot{v}}{v} = \dot{\varepsilon}_1 + \dot{\varepsilon}_2 + \dot{\varepsilon}_3$, where $\dot{\varepsilon}_1, \dot{\varepsilon}_2$, and $\dot{\varepsilon}_3$ are three principal strain rates. For plane strain condition $\dot{\varepsilon}_3 = 0$. The angle between the shear plane and the loading axis, denoted by α , is defined as

$$\cot(2\alpha) = -\frac{1}{2} \left(\dot{\varepsilon}_1 + \dot{\varepsilon}_2 \right) / \left(\dot{\gamma}/2 \right) = -\frac{\dot{v}}{v\dot{\gamma}}, \quad (2.116)$$

where $\dot{\gamma}$ is the shear strain rate. This expression explicitly incorporates the volume change rate. Hence, using the ratio between the volume change rate and the shearing rate, the shear band angle can be determined. For a particular time, the above

expression can be simplified as

$$\cot(2\alpha) = -\frac{1}{2} (\varepsilon_1 + \varepsilon_2) / (\gamma/2), \quad (2.117)$$

where, ε_1 and ε_2 are the principal strain and γ is the shear strain. We previously discussed how our triple stress parameter A_1 is related to the shear dilatation. We can see from [89, 95] that the shear band inclination angle varies with dilatation. In this respect, we compute the shear band inclination angle for different values of triple stress parameter A_1 using Eq. (2.117). We simulate our model with the following parameter settings of $\frac{E_1}{\mu} = 100$, $\frac{C_1}{\mu} = 100$, where 8% axial strain has been applied. We determine the shear angle at each nodal point of interest by using Eq. (2.114). The shear strain (γ) is calculated from the average shear angle of the domain.

Table 2.1: Shear band inclination angle obtained from [89, 95] and proposed third gradient model

Triple stress parameter, $\frac{A_1}{\mu}$	100	200	400	600	800
ε_1	0.211	0.149	0.104	0.096	0.091
ε_2	-0.233	-0.151	-0.097	-0.081	-0.071
θ_{avg} (deg) (see Figure 2.11)	21.94	14.05	7.053	5.276	3.982
$\gamma = \tan(\theta_{avg})$	0.4028	0.250	0.124	0.092	0.069
Shear band inclination angle, α (deg) (Using Eq. (2.117))	45.63	47.15	49.22	52.12	55.69
Drucker-Prager Coefficient, a [89, 95]	0.045	0.087	0.130	0.168	0.205
Shear band inclination angle, α (deg) [89, 95]	48	51	54	56	58

We compared our result to the shear band inclination angle reported in [89, 95]. Table 2.1 reveals that the shear band inclination angle deviates more as $\frac{A_1}{\mu}$ increased. Since the dilatation is more intense for the higher value of triple stress parameter A_1 (see Figure 2.8), it is evident that our model can successfully correlate the shear band inclination angle to the volume dilatation in a similar manner shown in [89, 95].

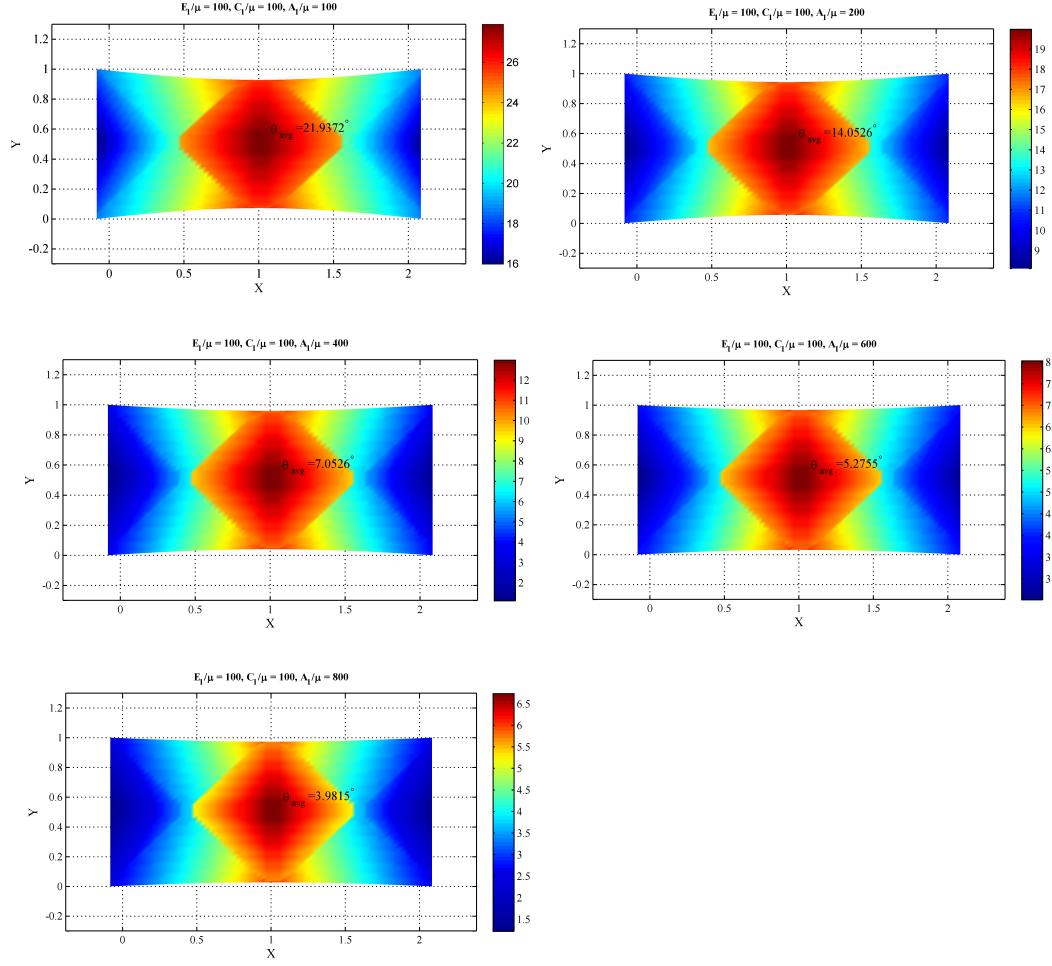


Figure 2.11: Shear angle distribution with the average shear angle of the domain

The triple stress parameter follows a similar trend to the Drucker-Prager coefficient, as shown in Figure 2.12. Both the triple stress parameter ($\frac{A_1}{\mu}$) and the coefficient a reported in [89, 95] characterize the deviation of shear band inclination angle and found that the deviation is more intense with the higher value of the triple stress parameter and drucker-prager coefficient. Thus, the triple stress parameter A_1 can be regarded as a new parameter characterizing volume dilatation and subsequently, the shear band inclination angle as specified by the coefficient a in [89, 95]. It should also be noted that the obtained model can be expanded to include more practical issues, such as determining the triple stress parameter and analyzing the residual triple stresses on the mechanical responses of higher-order continua.

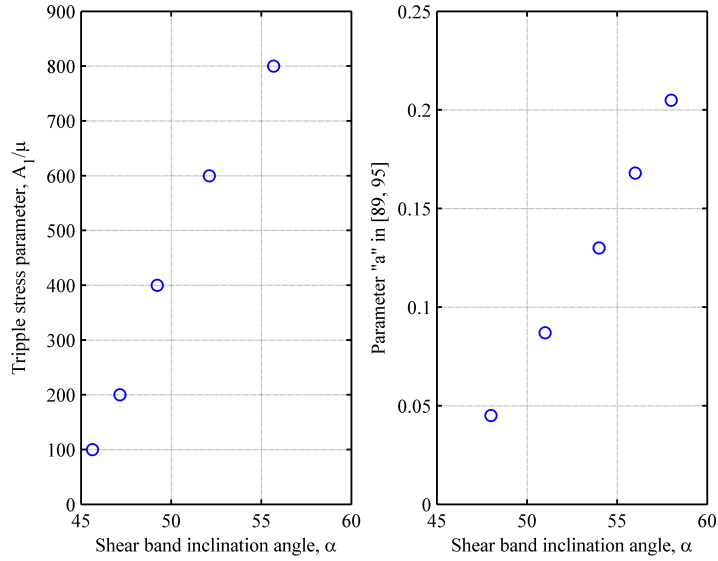


Figure 2.12: Variation of shear band inclination angle α with triple stress parameter $\frac{A_1}{\mu}$ and drucker prager coefficient a presented in [89, 95]

2.6 Conclusions

In this chapter, we present a continuum-based model describing the mechanics of third gradient continua reinforced with bidirectional fibers and subjected to finite plane deformations. The kinematics of fibers are obtained via the first, second, and third gradient of continuum deformations within the prescription of continuously distributed spatial rods of the Kirchhoff type. The variational principles and iterative integration by parts have been employed to obtain the Euler equations and the necessary boundary conditions. In particular, the energy density function of the Spencer and Soldatos type is refined within the framework of the second strain gradient theory to accommodate the kinematics and the associated bulk incompressibility arising in the third-gradient continua. The resulting systems of partial differential equations are solved using the custom-built numerical scheme.

The solution of the obtained model predicts smooth deformation profiles and dilatational shear angle distributions throughout the domain of interest when the composite is subjected to bias extension. Further, the introduction of the third gradient

of continuum deformation has resulted in the emergence of a constitutive parameter that is associated with the Piola-type triple stress and its energy couple (i.e., triple force) sustained by the third-gradient continua. Phenomenologically relevant results pertaining to the third gradient of continuum deformations has been discussed throughout the chapter, including; the increase of the triple stress parameter results in intensified volume dilatation and reduced local point rotations. We also computed the corresponding shear band inclination angles with respect to the different triple stress parameters indicating that the triple stress parameter follows a similar trend to the Drucker-Prager coefficients characterizing shear band inclination angle. More precisely, the deviations of the shear band inclination angle under uniaxial tension are intensified with the increasing triple stress parameter.

Chapter 3

A second strain gradient based continuum model for the composite reinforced with extensible nano-fibers resistant to flexure

In section 3.1, we define the kinematics of randomly distributed short fibers. Via the virtual work statement and iterative integration by parts, the corresponding Equilibrium equation and associated boundary conditions are derived in section 3.2. Following that, in sections 3.2.1 and 3.2.2, the governing equations for the mechanics of Neo-Hookean solids and Mooney-Rivlin solids reinforced with randomly distributed short fibers are delivered respectively. In section 3.3, Finite Element Analysis procedure is discussed to solve the governing Equations obtained for the case of the Neo-Hookean solid reinforced with randomly distributed short fiber. Finally, the obtained numerical results are discussed in section 3.4, and a summary of this chapter is provided at the end in section 3.5.

3.1 Kinematics

In this section, we derive the kinematics of randomly distributed short fibers. The transformation of unidirectional fiber composite into nano-fiber composite system is developed by Suprabha [100]. Here we used the similar transformation method which

is illustrated in Figure 3.1. We begin the derivation of the kinematics of continuously distributed unidirectional fibers within the similar framework used in chapter 2. Next, we transform the unidirectional fiber composite system into an aligned short fiber composite system by introducing the Shear Lag Parameter. Finally, this aligned short fiber system is transformed into a randomly distributed short fiber composite using the Krenchel Orientation Factor.

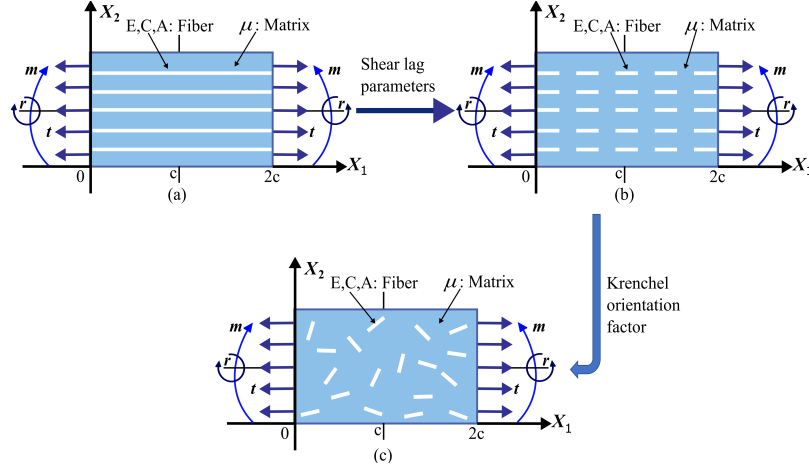


Figure 3.1: Schematic of the problem and demonstration of the model development (a) continuous unidirectional fiber, (b) aligned short fiber, (c) randomly distributed fiber

3.1.1 Defining energy potential for the unidirectional continuous fiber composite system

Let \mathbf{D} be the unit tangent to the fiber's trajectory in the reference configuration and \mathbf{d} is its equivalent in the deformed configuration. Following that, the configuration of a particular unidirectional fiber is determined as

$$\lambda = |\eta| = \frac{ds}{dS}, \text{ and } \mathbf{d} = \eta \lambda^{-1}, \quad (3.1)$$

where

$$\mathbf{F}\mathbf{D} = \lambda \mathbf{d}, \mathbf{F} = \lambda \mathbf{d} \otimes \mathbf{D}, \quad (3.2)$$

and \mathbf{F} is the first gradient of the deformation function, which is defined in Eq.

(2.3). Also, the above equation can be yielded to Eq. (2.6) using the orthonormal bases of the current and reference configurations.

In chapter 2, we have shown that (see Eq. 2.27) a third gradient based-energy density function in the description of an elastic solid reinforced with extensible fibers resistant to flexure can be expressed as

$$W(\mathbf{F}, \varepsilon(\mathbf{F}), \mathbf{g}(\mathbf{G}), \boldsymbol{\alpha}(\mathbf{H})) = W(\mathbf{F}) + W(\varepsilon(\mathbf{F})) + W(\mathbf{g}(\mathbf{G})) + W(\boldsymbol{\alpha}(\mathbf{H})), \quad (3.3)$$

where $W(\mathbf{F})$ is the strain energy function for the matrix material; using the similar manner as in Eqs. (2.7-2.27), the other terms can be defined for unidirectional fibers as follows:

For example, $W(\varepsilon(\mathbf{F}))$ is defined as

$$W(\varepsilon(\mathbf{F})) = \frac{1}{2}E\varepsilon^2, \quad (3.4)$$

where E is the fiber's elastic modulus, and the expression of ε is given by Eqs. (2.16)-(2.20) as

$$\varepsilon = \frac{1}{2}(\lambda^2 - 1) = \frac{1}{2}[(\mathbf{F}^T \mathbf{F}) \cdot \mathbf{D} \otimes \mathbf{D} - 1]. \quad (3.5)$$

Next, $W(\mathbf{g}(\mathbf{G}))$ can be defined as

$$W(\mathbf{g}(\mathbf{G})) \equiv \frac{1}{2}C(\mathbf{F})|\mathbf{g}(\mathbf{G})|^2, \quad (3.6)$$

where the geodesic curvature $\mathbf{g}(\mathbf{G})$ is defined in Eq. (2.7). For the present unidirectional case, it can be written as

$$\mathbf{g}(\mathbf{G}) = \mathbf{G}(\mathbf{D} \otimes \mathbf{D}), \quad (3.7)$$

and $C(\mathbf{F})$ is a constant material parameter. Thus Eq. 3.6 can be written as

$$W(\mathbf{g}(\mathbf{G})) \equiv \frac{1}{2}C|\mathbf{g}(\mathbf{G})|^2. \quad (3.8)$$

Also, the energy contribution related to the third gradient of deformation is defined as

$$W(\boldsymbol{\alpha}(\mathbf{H})) \equiv \frac{1}{2}A(\mathbf{H})|\boldsymbol{\alpha}(\mathbf{H})|^2, \quad (3.9)$$

where $\boldsymbol{\alpha}(\mathbf{H})$ is the third gradient of deformations. Using Eqs. (2.22)-(2.24), for an unidirectional fiber, $\boldsymbol{\alpha}(\mathbf{H})$ can be defined as

$$\boldsymbol{\alpha} = \frac{d^3 \mathbf{r}(S)}{dS^3} = \mathbf{H}(\mathbf{D} \otimes \mathbf{D} \otimes \mathbf{D}) = \boldsymbol{\alpha}(\mathbf{H}). \quad (3.10)$$

Also, by assuming $A(\mathbf{H})$ as a material constant, Eq. 3.9 can be recast as

$$W(\boldsymbol{\alpha}(\mathbf{H})) \equiv \frac{1}{2} A |\boldsymbol{\alpha}(\mathbf{H})|^2, \quad (3.11)$$

Thus, using Eqs. (3.3)-(3.4),(3.8),(3.11), we have defined the energy potential accommodating fiber extension, fiber bending, and the third gradient of deformations for the case of continuously distributed unidirectional fiber-composite system.

3.1.2 Development of randomly oriented short fiber composite system

To obtain the nano-fiber composite system, we followed the same procedure that was originally developed by Suprabha in [100]. In this section, we briefly discuss the theoretical development process. The continuously distributed unidirectional fiber composite is transformed into the short-fiber reinforced composite system via the shear lag parameter. In the case of a fiber-reinforced composite material, the load is transferred from the matrix material to the fiber by means of interfacial shear stress transfer. The theoretical background for the shear lag theory is well presented in [80, 81]. It is well known that the interfacial shear stress transfer is highly sensitive to the length scale of fiber. For example, if a fiber length is L , height is h , and aspect ratio S is defined as $\frac{2L}{h}$, it is shown that the interfacial shear stress transfer is more efficient for the higher value of aspect ratio, S [81]. Figure 3.2 represents the settings for the shear lag theory and displays the typical strain distribution along the fiber length. When the aspect ratio S is small, the maximum strain attains in the fiber is low. Also, the strain distribution is non-uniform throughout the entire fiber length. This is due to the poor interfacial shear stress transfer from the matrix material to the

fiber. In case of high aspect ratio, the strain in the fiber reaches its maximum value which is close to the strain of the matrix ($\frac{\epsilon_f}{\epsilon_m} \approx 1$) at the very corner and remains constant throughout the entire length.

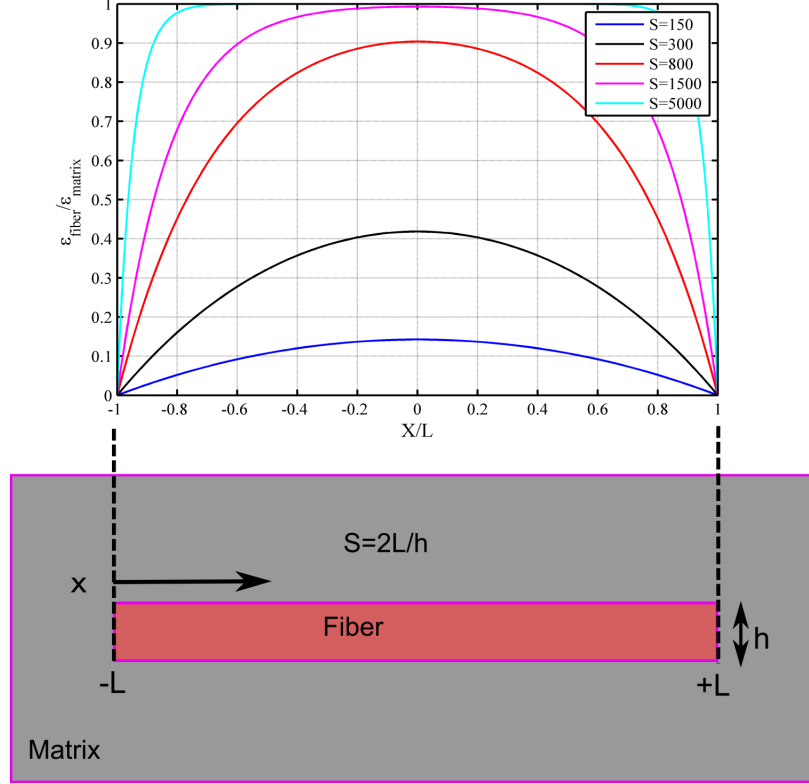


Figure 3.2: A typical strain distribution along the fiber length, and its dependence on the fiber aspect ratio

The dependence of the interfacial shear stress transfer on the aspect ratio of fiber is accommodated by the following relation [81]

$$\epsilon_f = \epsilon \left[1 - \frac{\cosh(\beta_s x)}{\cosh(\beta_s L)} \right], \quad (3.12)$$

where the shear lag parameter β_s is defined as, $\beta_s = \sqrt{\frac{K}{Eh}}$, K is the interfacial stiffness, h is the thickness, and L is the half-length of the fiber. To accommodate shear lag parameter into our model for the entire length of the fiber, we have modified our extension potential (see Eq. 3.4) using the similar method developed by Suprabha in

[100] as follows

$$\begin{aligned}
W(\varepsilon) &= \frac{1}{2}E\varepsilon_f^2 = \frac{1}{2}E\left[\frac{1}{2L}\int_{-L}^{+L}\varepsilon\left[1 - \frac{\cosh(\beta_s x)}{\cosh(\beta_s L)}\right]dx\right]^2 \\
&= \frac{1}{2}E\left[1 - \frac{\tanh(\beta_s L)}{\beta_s L}\right]^2\varepsilon^2 \\
&= \frac{1}{2}E\zeta\varepsilon^2,
\end{aligned} \tag{3.13}$$

where the modified shear lag parameter is defined as

$$\zeta = \left[1 - \frac{\tanh(\beta_s L)}{\beta_s L}\right]^2. \tag{3.14}$$

In Eq. (3.13), we have considered the energy potential for the uniformly distributed nano-fiber reinforcement. In most cases, the fibers are distributed randomly. Hence, the above fiber energy potential is further modified by Suprabha in [100] to accommodate randomly oriented fibers using the krenchel transformation function [82] as

$$W(\varepsilon(\mathbf{F})) = \frac{1}{2}E\eta_0\zeta\varepsilon^2, \tag{3.15}$$

where the term η_0 is defined as

$$\eta_0 = \frac{8}{15} + \frac{8}{21}\langle P_2 \cos \theta \rangle + \frac{8}{35}\langle P_4 \cos \theta \rangle, \tag{3.16}$$

for the perfectly oriented fiber, $P_2 \cos \theta = P_4 \cos \theta = 1$, and for the randomly oriented fiber $P_2 \cos \theta = P_4 \cos \theta = 0$. A similar fashion is widely used in micromechanics of randomly oriented fibers (see, for example, [101–104]).

Now, the energy fraction of fiber indicated as β , is accommodated to the model as

$$W(\mathbf{F}, \varepsilon(\mathbf{F}), \mathbf{g}(\mathbf{G}), \boldsymbol{\alpha}(\mathbf{H})) = (1-\beta)W(\mathbf{F}) + \beta[W(\varepsilon(\mathbf{F})) + W(\mathbf{g}(\mathbf{G})) + W(\boldsymbol{\alpha}(\mathbf{H}))]. \tag{3.17}$$

The induced energy variation can be evaluated from Eq. (3.17) as,

$$\dot{W}(\mathbf{F}, \varepsilon, \mathbf{g}, \boldsymbol{\alpha}) = (1 - \beta)W_{\mathbf{F}} \cdot \dot{\mathbf{F}} + \beta(W_{\varepsilon}\dot{\varepsilon} + W_{\mathbf{g}} \cdot \dot{\mathbf{g}} + W_{\boldsymbol{\alpha}} \cdot \dot{\boldsymbol{\alpha}}), \tag{3.18}$$

Recalling the procedures used in Eqs. (2.29)-(2.38), we obtain the desired induced energy variation for the present case. For example, using Eqs. (3.4), (3.5),(3.7)-(3.8)

and (3.10)-(3.11), we define the following terms as

$$W_\varepsilon \dot{\varepsilon} = \left[\frac{E}{2} \eta_0 \zeta (F_{jC} F_{jD} D_C D_D - 1) (F_{iB} D_B D_A) \right] \dot{F}_{iA}, \quad (3.19)$$

$$W_{\mathbf{g}} \cdot \dot{\mathbf{g}} = C g_i \dot{G}_{iAB} D_A D_B, \quad (3.20)$$

$$W_{\boldsymbol{\alpha}} \cdot \dot{\boldsymbol{\alpha}} = A \alpha_i \dot{H}_{iABC} D_A D_B D_C. \quad (3.21)$$

Now put back the values from Eqs. (3.19)-(3.21) into Eq. (3.18), the induced energy potential variation is obtained as

$$\begin{aligned} \dot{W}(\mathbf{F}, \varepsilon, \mathbf{g}, \boldsymbol{\alpha}) &= (1 - \beta) W_{F_{iA}} \dot{F}_{iA} + \frac{E}{2} \eta_0 \zeta \beta (F_{jC} F_{jD} D_C D_D - 1) F_{iB} D_B D_A \dot{F}_{iA} \\ &\quad + C g_i \beta \dot{G}_{iAB} D_A D_B + A \alpha_i \beta \dot{H}_{iABC} D_A D_B D_C. \end{aligned} \quad (3.22)$$

Thus, we obtain the variational derivative of the energy potential in Eq. (3.22).

3.2 Equilibrium and Boundary Conditions

The weak form of the equilibrium equations can be obtained by the virtual-work statement (see, for example, [24, 34, 35, 67]) as described in Eq. (2.40). In this thesis, we also adopt the framework of the virtual work statement to formulate the Euler equilibrium equations and the associated boundary conditions arising in the third gradient of the continuum deformation. For the present case, we evaluate the potential energy of the system as

$$E = \int_{\Omega} U(\mathbf{F}, \varepsilon, \mathbf{g}, \boldsymbol{\alpha}) dA, \quad (3.23)$$

where Ω is the referential domain occupied by a fiber-matrix material. The variational derivative of the potential energy of the system is

$$\dot{E} = \int_{\Omega} \dot{U}(\mathbf{F}, \varepsilon, \mathbf{g}, \boldsymbol{\alpha}) dA. \quad (3.24)$$

The energy potential in Eq. (3.23) is augmented as $U(\mathbf{F}, \varepsilon, \mathbf{g}, \boldsymbol{\alpha}, p) = W(\mathbf{F}, \varepsilon, \mathbf{g}, \boldsymbol{\alpha}) - p(J - 1)$ to overcome the constraint of bulk incompressibility, where J is determinant

of deformation gradient \mathbf{F} and p is an indeterminate Lagrange multiplier field. Therefore Eq. (3.24) becomes

$$\dot{E} = \int_{\Omega} \dot{U}(\mathbf{F}, \varepsilon, \mathbf{g}, \boldsymbol{\alpha}, p) dA. \quad (3.25)$$

Now, using Eq. (3.22) and the relation $\dot{J} = J_{\mathbf{F}} \dot{\mathbf{F}} \cdot \dot{\mathbf{F}} = \mathbf{F}^* \cdot \dot{\mathbf{F}}$, we evaluated the variational derivative of the augmented energy potential as

$$\begin{aligned} \dot{U} &= \dot{W} - p\dot{J} \\ &= (1 - \beta)W_{F_{iA}} \dot{F}_{iA} + \frac{E}{2}\eta_0\zeta\beta(F_{jC}F_{jD}D_C D_D - 1)(F_{iB}D_B D_A)\dot{F}_{iA} + Cg_i\beta\dot{G}_{iAB}D_A D_B \\ &\quad + A\alpha_i\beta\dot{H}_{iABC}D_A D_B D_C - pF_{iA}^* \dot{F}_{iA}. \end{aligned} \quad (3.26)$$

Let us define $\dot{\chi}_i = u_i$. Thus Eq. (3.25) can be recast as

$$\begin{aligned} \dot{E} &= \int_{\Omega} [(1 - \beta)W_{F_{iA}} u_{i,A} + \frac{E}{2}\eta_0\zeta\beta(F_{jC}F_{jD}D_C D_D - 1)(F_{iB}D_B D_A)u_{i,A} \\ &\quad + Cg_i\beta D_A D_B u_{i,AB} + A\alpha_i\beta D_A D_B D_C u_{i,ABC} - pF_{iA}^* u_{i,A}] dA. \end{aligned} \quad (3.27)$$

Applying integration by parts (see Eqs. (2.46) and (2.47))

$$Cg_i D_A D_B u_{i,AB} = (Cg_i D_A D_B u_{i,A})_{,B} - (Cg_i D_A D_B)_{,B} u_{i,A}, \quad (3.28)$$

and

$$A\alpha_i D_A D_B D_C u_{i,ABC} = (A\alpha_i D_A D_B D_C u_{i,AB})_{,C} - (A\alpha_i D_A D_B D_C)_{,C} u_{i,AB}. \quad (3.29)$$

Now using the expressions from Eqs. (3.28)-(3.29) into the Eq. (3.27) we obtain

$$\begin{aligned} \dot{E} &= \int_{\Omega} [(1 - \beta)W_{F_{iA}} u_{i,A} + \frac{E}{2}\eta_0\zeta\beta(F_{jC}F_{jD}D_C D_D - 1)(F_{iB}D_B D_A)u_{i,A} \\ &\quad + (Cg_i\beta D_A D_B u_{i,A})_{,B} - (Cg_i\beta D_A D_B)_{,B} u_{i,A} + (A\alpha_i\beta D_A D_B D_C u_{i,AB})_{,C} \\ &\quad - (A\alpha_i\beta D_A D_B D_C)_{,C} u_{i,AB} - pF_{iA}^* u_{i,A}] dA. \end{aligned} \quad (3.30)$$

This can be written as

$$\begin{aligned} \dot{E} &= \int_{\Omega} [(1 - \beta)W_{F_{iA}} - pF_{iA}^* + \frac{E}{2}\eta_0\zeta\beta(F_{jC}F_{jD}D_C D_D - 1)(F_{iB}D_B D_A) \\ &\quad - (Cg_i\beta D_A D_B)_{,B}] u_{i,A} dA - \int_{\Omega} [(A\alpha_i\beta D_A D_B D_C)_{,C} u_{i,AB}] dA \\ &\quad + \int_{\partial\Omega} (Cg_i\beta D_A D_B) u_{i,A} N_B dS + \int_{\partial\Omega} (A\alpha_i\beta D_A D_B D_C) u_{i,AB} N_C dS. \end{aligned} \quad (3.31)$$

By applying integration by parts and Green-Stoke's theorem, we find the expression of second integral term of Eq. (3.31) as

$$\begin{aligned}
& \int_{\Omega} \left[(A\alpha_i D_A D_B D_C)_{,C} u_{i,AB} \right] dA \\
&= \int_{\Omega} \left[\{ (A\alpha_i D_A D_B D_C)_{,C} u_{i,A} \}_{,B} - (A\alpha_i D_A D_B D_C)_{,CB} u_{i,A} \right] dA, \\
&= \int_{\partial\Omega} (A\alpha_i D_A D_B D_C)_{,C} u_{i,A} N_B dS - \int_{\Omega} (A\alpha_i D_A D_B D_C)_{,CB} u_{i,A} dA. \quad (3.32)
\end{aligned}$$

In Eqs. (3.31) and (3.32), \mathbf{N} is the rightward unit normal to the boundary $\partial\Omega$. We substitute the Eq. (3.32) into Eq. (3.31) and furnish

$$\begin{aligned}
\dot{E} &= \int_{\Omega} \left[(1 - \beta) W_{F_{iA}} - p F_{iA}^* + \frac{E}{2} \eta_0 \zeta \beta (F_{jC} F_{jD} D_C D_D - 1) (F_{iB} D_B D_A) \right. \\
&\quad \left. - (C g_i \beta D_A D_B)_{,B} + (A\alpha_i \beta D_A D_B D_C)_{,CB} \right] u_{i,A} dA + \int_{\partial\Omega} (C g_i \beta D_A D_B u_{i,A}) N_B dS \\
&\quad + \int_{\partial\Omega} [(A\alpha_i \beta D_A D_B D_C) u_{i,AB}] N_C dS - \int_{\partial\Omega} [(A\alpha_i \beta D_A D_B D_C)_{,C} u_{i,A}] N_B dS. \quad (3.33)
\end{aligned}$$

Finally, we obtain

$$\begin{aligned}
\dot{E} &= \int_{\Omega} P_{iA} u_{i,A} dA + \int_{\partial\Omega} \left[\left\{ C g_i \beta D_A D_B - A (\alpha_i \beta D_A D_B D_C)_{,C} \right\} u_{i,A} N_B \right. \\
&\quad \left. + A \alpha_i \beta D_A D_B D_C u_{i,AB} N_C \right] dS, \quad (3.34)
\end{aligned}$$

where

$$\begin{aligned}
P_{iA} (\mathbf{e}_i \otimes \mathbf{E}_A) &= \left[(1 - \beta) W_{F_{iA}} - p F_{iA}^* + \frac{E}{2} \eta_0 \zeta \beta (F_{jC} F_{jD} D_C D_D - 1) (F_{iB} D_A D_B) \right. \\
&\quad \left. - C (g_i \beta D_A D_B)_{,B} + A (\alpha_i \beta D_A D_B D_C)_{,BC} \right] (\mathbf{e}_i \otimes \mathbf{E}_A). \quad (3.35)
\end{aligned}$$

To obtain the admissible boundary conditions, we apply integration by parts (i.e.

$P_{iA} u_{i,A} = (P_{iA} u_i)_{,A} - P_{iA,A} u_i$) in Eq. (3.34) and obtain

$$\begin{aligned}
\dot{E} &= \int_{\partial\Omega} P_{iA} u_i N_A dS - \int_{\Omega} P_{iA,A} u_i dA + \int_{\partial\Omega} \left[\left\{ C g_i \beta D_A D_B - A (\alpha_i \beta D_A D_B D_C)_{,C} \right\} u_{i,A} N_B \right. \\
&\quad \left. + A \alpha_i \beta D_A D_B D_C u_{i,AB} N_C \right] dS. \quad (3.36)
\end{aligned}$$

Now, we define

$$W_{G_{iAB}} \equiv C g_i D_A D_B \text{ and } W_{H_{iABC}} \equiv A \alpha_i D_A D_B D_C. \quad (3.37)$$

Using Eqs. (3.37) and (2.56), we can rewrite Eq. (3.36) as

$$\dot{E} = \int_{\partial\Omega} P_{iA} u_i N_A dS + \int_{\partial\Omega} [\beta (W_{G_{iAB}} - (W_{H_{iABC}})_{,C}) u_{i,A} N_B + \beta W_{H_{iABC}} u_{i,AB} N_C] dS. \quad (3.38)$$

Eq. (3.38) can be recast using Eqs. (2.58)-(2.61) as

$$\begin{aligned} \dot{E} &= \int_{\partial\Omega} P_{iA} u_i N_A dS + \int_{\partial\Omega} \beta [W_{G_{iAB}} - (W_{H_{iABC}})_{,C}] (u'_i T_A + u_{i,N} N_A) N_B dS \\ &+ \int_{\partial\Omega} \beta W_{H_{iABC}} [u''_i T_A T_B + u'_i (T'_A T_B + T_{A,N} N_B) + u'_{i,N} (T_A N_B + N_A T_B) \\ &+ u_{i,N} (N'_A T_B + N_{A,N} N_B) + u_{i,NN} N_A N_B] N_C dS. \end{aligned} \quad (3.39)$$

Now, we apply the iterated integrations by parts (see, for example, Eqs. (2.63)-(2.67)) and obtain

$$\begin{aligned} \dot{E} &= \int_{\partial\Omega} P_{iA} u_i N_A dS + \int_{\partial\Omega} \beta [(W_{G_{iAB}} T_A N_B u_i)' - (W_{G_{iAB}} T_A N_B)' u_i] dS \\ &- \int_{\partial\Omega} \beta [((W_{H_{iABC}})_{,C} T_A N_B u_i)' - ((W_{H_{iABC}})_{,C} T_A N_B)' u_i] dS + \int_{\partial\Omega} \beta [W_{G_{iAB}} N_A N_B \\ &- (W_{H_{iABC}})_{,C} N_A N_B] u_{i,N} dS + \int_{\partial\Omega} \beta [(W_{H_{iABC}} T_A T_B N_C u_i)'' + (W_{H_{iABC}} T_A T_B N_C)'' u_i \\ &- 2 [(W_{H_{iABC}} T_A T_B N_C)' u_i]'] dS + \int_{\partial\Omega} \beta [(W_{H_{iABC}} (T'_A T_B N_C + T_{A,N} N_B N_C) u_i)' \\ &- (W_{H_{iABC}} (T'_A T_B N_C + T_{A,N} N_B N_C))' u_i] dS + \int_{\partial\Omega} \beta W_{H_{iABC}} [u_{i,N} (N'_A T_B N_C \\ &+ N_{A,N} N_B N_C)] dS + \int_{\partial\Omega} \beta [(W_{H_{iABC}} (T_A N_B N_C + N_A T_B N_C) u_{i,N})' - (W_{H_{iABC}} (T_A N_B N_C \\ &+ N_A T_B N_C))' u_{i,N}] dS + \int_{\partial\Omega} \beta (W_{H_{iABC}} u_{i,NN} N_A N_B N_C) dS. \end{aligned} \quad (3.40)$$

We can rearrange the above as

$$\begin{aligned}
\dot{E} &= \int_{\partial\Omega} [P_{iA}N_A - \beta(W_{G_{iAB}}T_A N_B)' + \beta((W_{H_{iABC}})_{,C}T_A N_B)' + \beta(W_{H_{iABC}}T_A T_B N_C)'' \\
&\quad - \beta(W_{H_{iABC}}(T_A' T_B N_C + T_{A,N}N_B N_C))'] u_i dS + \int_{\partial\Omega} \beta[W_{G_{iAB}}N_A N_B - (W_{H_{iABC}})_{,C}N_A N_B \\
&\quad + W_{H_{iABC}}(N_A' T_B N_C + N_{A,N}N_B N_C) - (W_{H_{iABC}}(T_A N_B N_C + N_A T_B N_C))'] u_{i,N} dS \\
&\quad + \int_{\partial\Omega} \beta[\{W_{G_{iAB}}T_A N_B - (W_{H_{iABC}})_{,C}T_A N_B - 2(W_{H_{iABC}}T_A T_B N_C)'\} u_i]' dS \\
&\quad + \int_{\partial\Omega} \beta[(W_{H_{iABC}}T_A T_B N_C u_i)''] dS + \int_{\partial\Omega} \beta[W_{H_{iABC}}(T_A' T_B N_C + T_{A,N}N_B N_C) u_i]' dS \\
&\quad + \int_{\partial\Omega} \beta[W_{H_{iABC}}(T_A N_B N_C + N_A T_B N_C) u_{i,N}]' dS + \int_{\partial\Omega} \beta(W_{H_{iABC}} u_{i,NN} N_A N_B N_C) dS, \tag{3.41}
\end{aligned}$$

which may be recast as

$$\begin{aligned}
\dot{E} &= \int_{\partial\Omega} [P_{iA}N_A - \beta(Cg_i D_A T_A D_B N_B)' + \beta(A\alpha_{i,C} D_A T_A D_B N_B D_C)' \\
&\quad + \beta(A\alpha_i D_A T_A D_B T_B D_C N_C)'' - (\beta A\alpha_i D_C N_C (D_A T_A' D_B T_B + D_A T_{A,N} D_B N_B))'] u_i dS \\
&\quad + \int_{\partial\Omega} \beta[Cg_i D_A N_A D_B N_B - A\alpha_{i,C} D_A N_A D_B N_B D_C + A\alpha_i D_C N_C (D_A N_A' D_B T_B \\
&\quad + D_A N_{A,N} D_B N_B) - \{A\alpha_i D_A D_B D_C (T_A N_B N_C + N_A T_B N_C)\}] u_{i,N} dS \\
&\quad + \sum \| \beta\{Cg_i D_A T_A D_B N_B - A\alpha_{i,C} D_A T_A D_B N_B D_C - 2(A\alpha_i D_A T_A D_B T_B D_C N_C)'\} u_i \| \\
&\quad + \sum \| \frac{d}{dS} [(\beta A\alpha_i D_A T_A D_B T_B D_C N_C) u_i] \| + \sum \| [A\alpha_i \beta (D_A T_A' D_B T_B D_C N_C \\
&\quad + D_A T_{A,N} D_B N_B D_C N_C) u_i \| + \sum \| [A\alpha_i \beta (D_A T_A D_B N_B D_C N_C \\
&\quad + D_A N_A D_B T_B D_C N_C) u_{i,N} \| + \int_{\partial\Omega} (A\alpha_i \beta D_A N_A D_B N_B D_C N_C) u_{i,NN} dS, \tag{3.42}
\end{aligned}$$

By comparing Eqs. (3.42) and (2.71), we obtain

$$\begin{aligned}
t_i &= P_{iA}N_A - \beta \frac{d}{ds} [Cg_i D_A T_A D_B N_B - A\alpha_{i,C} D_A T_A D_B N_B D_C \\
&\quad + A\alpha_i D_C N_C (D_A T'_A D_B T_B + D_A T_{A,N} D_B N_B)] + \frac{d^2}{ds^2} (A\alpha_i \beta D_A T_A D_B T_B D_C N_C), \\
m_i &= C(g)_i \beta D_A N_A D_B N_B - A(\alpha)_{i,C} \beta D_A N_A D_B N_B D_C \\
&\quad + A\alpha_i \beta D_C N_C (D_A N'_A D_B T_B + D_A N_{A,N} D_B N_B) - \frac{d}{ds} \{2(A\alpha_i \beta D_A D_B D_C N_A T_B N_C)\}, \\
r_i &= A\alpha_i \beta D_A N_A D_B N_B D_C N_C, \\
f_i &= Cg_i \beta D_A T_A D_B N_B - A\alpha_{i,C} \beta D_A T_A D_B N_B D_C - 2\beta \frac{d}{ds} [A\alpha_i D_A T_A D_B T_B D_C N_C] \\
&\quad + A\alpha_i \beta (D_A T'_A D_B T_B D_C N_C + D_A T_{A,N} D_B N_B D_C N_C), \\
\frac{d}{ds}(f_i) &= \frac{d}{ds} (A\alpha_i \beta D_A T_A D_B T_B D_C N_C), \\
h_i &= 2A\alpha_i \beta D_A N_A D_B T_B D_C N_C, \tag{3.43}
\end{aligned}$$

where t_i , m_i , and f_i are the expressions of edge tractions, edge moments, and corner forces, respectively. Similar boundary conditions are formulated in [69, 70] for the third gradient continua. In the present case, the local point rotations are obtained via the computation of the third gradient of continuum deformation, i.e., the rate of changes in curvature which is determined by the imposition of triple forces (i.e. r_i , h_i) on the desired boundaries.

Now, using Eq. (2.73), we reduce the Eq. (3.43) to

$$\begin{aligned}
t_i &= P_{iA}N_A, \\
m_i &= (Cg_i \beta - A\alpha_{i,C} \beta D_C) D_A N_A D_B N_B, \\
r_i &= A\alpha_i \beta D_A N_A D_B N_B D_C N_C, \\
f_i &= 0, \\
\frac{d}{ds}(f_i) &= 0, \\
h_i &= 0. \tag{3.44}
\end{aligned}$$

Further, Eq. (3.35) can be written as

$$P_{iA}(\mathbf{e}_i \otimes \mathbf{E}_A) = [(1 - \beta)W_{F_{iA}} - pF_{iA}^* + \frac{E}{2}\eta_0\zeta\beta(F_{jC}F_{jD}D_CD_D - 1)(F_{iB}D_AD_B) - Cg_{i,B}\beta D_AD_B + A\alpha_{i,BC}\beta D_AD_B D_C](\mathbf{e}_i \otimes \mathbf{E}_A). \quad (3.45)$$

3.2.1 Example: Neo-Hookean materials

So far, we have discussed the kinematics of the reinforcement phase (i.e. fibers) of a composite. The response of matrix material is assimilated by the energy density function of Neo-Hookean materials which is given by Eqs. (2.76) and (2.77).

Taking the derivative of Eq. (2.77) with respect to deformation gradient \mathbf{F} and substituting it into Eq. (3.45), we find

$$P_{iA}(\mathbf{e}_i \otimes \mathbf{E}_A) = [(1 - \beta)\mu F_{iA} - pF_{iA}^* + \frac{E}{2}\eta_0\zeta\beta(F_{jC}F_{jD}D_CD_D - 1)(F_{iB}D_AD_B) - Cg_{i,B}\beta D_AD_B + A\alpha_{i,BC}\beta D_AD_B D_C](\mathbf{e}_i \otimes \mathbf{E}_A). \quad (3.46)$$

By using the Piola's identity $F_{iA,A}^* = 0$, Eq. (2.56), and Eq. (3.46), the Euler equilibrium equation is obtained as

$$P_{iA,A} = (1 - \beta)\mu F_{iA,A} - p_{,A}F_{iA}^* + \frac{E}{2}\eta_0\zeta\beta(F_{iB,A}F_{jC}F_{jD} + F_{iB}F_{jC,A}F_{jD} + F_{iB}F_{jC}F_{jD,A})D_AD_B D_CD_D - \frac{E}{2}\eta_0\zeta\beta F_{iB,A}D_AD_B - Cg_{i,AB}\beta D_AD_B + A\alpha_{i,ABC}\beta D_AD_B D_C = 0. \quad (3.47)$$

In case of initially orthonormal set of fibers

$$\mathbf{D} = \mathbf{E}_1, D_1 = 1, D_2 = 0, \quad (3.48)$$

and Eq. (3.47) can be recast as

$$P_{iA,A} = (1 - \beta)\mu F_{iA,A} - p_{,A}F_{iA}^* + \frac{E}{2}\eta_0\zeta\beta(F_{i1,1}F_{j1}F_{j1} + F_{i1}F_{j1,1}F_{j1} + F_{i1}F_{j1}F_{j1,1}) - \frac{E}{2}\eta_0\zeta\beta F_{i1,1} - \beta Cg_{i,11} + \beta A\alpha_{i,111} = 0, \quad (3.49)$$

where

$$g_i = F_{i1,1}, \alpha_i = F_{i1,11}, F_{iA} = \chi_{i,A}, F_{iA}^* = \varepsilon_{ij}\varepsilon_{AB}F_{jB}, \quad (3.50)$$

and ε_{ij} is a 2-D permutation. Now, using Eqs. (3.49)-(3.50) and the constraint of the bulk incompressibility (i.e., $\det \mathbf{F} = 1$), we deliver the following system of PDEs for the case of Neo-Hookean materials reinforced with randomly distributed nano-fibers,

$$0 = (1 - \beta)\mu\chi_{i,AA} - p_{,A}\varepsilon_{ij}\varepsilon_{AB}\chi_{j,B} + \frac{E}{2}\eta_0\zeta\beta(\chi_{i,11}\chi_{j,1}\chi_{j,1} + \chi_{i,1}\chi_{j,11}\chi_{j,1} + \chi_{i,1}\chi_{j,1}\chi_{j,11}) - \frac{E}{2}\eta_0\zeta\beta\chi_{i,11} - \beta C\chi_{i,1111} + \beta A\chi_{i,111111}, \quad (3.51)$$

$$\text{for } i = 1; \quad (1 - \beta)\mu(\chi_{1,11} + \chi_{1,22}) - p_{,1}\chi_{2,2} + p_{,2}\chi_{2,1} + \frac{E}{2}\eta_0\zeta\beta(3\chi_{1,11}\chi_{1,1}\chi_{1,1} + \chi_{1,11}\chi_{2,1}\chi_{2,1} + 2\chi_{2,11}\chi_{1,1}\chi_{2,1}) - \frac{E}{2}\eta_0\zeta\beta\chi_{1,11} - \beta C\chi_{1,1111} + \beta A\chi_{1,111111} = 0, \quad (3.52)$$

$$\text{for } i = 2; \quad (1 - \beta)\mu(\chi_{2,11} + \chi_{2,22}) + p_{,1}\chi_{1,2} - p_{,2}\chi_{1,1} + \frac{E}{2}\eta_0\zeta\beta(3\chi_{2,11}\chi_{2,1}\chi_{2,1} + \chi_{2,11}\chi_{1,1}\chi_{1,1} + 2\chi_{1,11}\chi_{1,1}\chi_{2,1}) - \frac{E}{2}\eta_0\zeta\beta\chi_{2,11} - \beta C\chi_{2,1111} + \beta A\chi_{2,111111} = 0, \quad (3.53)$$

and

$$\chi_{1,1}\chi_{2,2} - \chi_{1,2}\chi_{2,1} - 1 = 0. \quad (3.54)$$

The details of the numerical solution process of the above (Eqs. (3.52)-(3.54)) system of Partial Differentiation Equations (PDEs) are reserved in section 3.3.

3.2.2 Example: Mooney-Rivlin materials

In case of Mooney-Rivlin materials, the energy density function and its derivative with respect to \mathbf{F} are given by Eqs. (2.90)-(2.92).

Now, substituting Eq. (2.92) into Eq. (3.45), we find

$$P_{iA}(\mathbf{e}_i \otimes \mathbf{E}_A) = [(1 - \beta)\{\mu F_{iA} + \kappa F_{iB}(F_{jC}F_{jC}\delta_{AB} - F_{jA}F_{jB})\} - pF_{iA}^* + \frac{E}{2}\eta_0\zeta\beta(F_{jC}F_{jD}D_C D_D - 1)(F_{iB}D_A D_B) - Cg_{i,B}\beta D_A D_B + A\alpha_{i,BC}\beta D_A D_B D_C](\mathbf{e}_i \otimes \mathbf{E}_A). \quad (3.55)$$

The Euler equations for the Mooney-Rivlin materials reinforced with randomly oriented nano-fibers are obtained using Eq. (2.56) as

$$\begin{aligned}
P_{iA,A} = & (1 - \beta)\{\mu F_{iA,A} + \kappa F_{iA,A} F_{jC} F_{jC} - \kappa F_{iB,A} F_{jA} F_{jB} + \kappa F_{iB}(2F_{jC} F_{jC,A} \\
& - F_{jA,A} F_{jB} - F_{jA} F_{jB,A})\} - p_{,A} F_{iA}^* - \left(\frac{E}{2}\eta_0 \zeta \beta F_{iB,A} D_A D_B\right) + \frac{E}{2}\eta_0 \zeta \beta (F_{iB,A} F_{jC} F_{jD} \\
& + F_{iB} F_{jC,A} F_{jD} + F_{iB} F_{jC} F_{jD,A}) D_A D_B D_C D_D - C g_{i,AB} \beta D_A D_B + A \alpha_{i,ABC} \beta D_A D_B D_C = 0,
\end{aligned} \tag{3.56}$$

which can be reduced by using Eq. (3.48) as

$$\begin{aligned}
P_{iA,A} = & (1 - \beta)\{\mu F_{iA,A} + \kappa F_{iA,A} F_{jC} F_{jC} - \kappa F_{iB,A} F_{jA} F_{jB} + \kappa F_{iB}(2F_{jC} F_{jC,A} - F_{jA,A} F_{jB} \\
& - F_{jA} F_{jB,A})\} - p_{,A} F_{iA}^* + \frac{E}{2}\eta_0 \zeta \beta (F_{i1,1} F_{j1} F_{j1} + F_{i1} F_{j1,1} F_{j1} + F_{i1} F_{j1} F_{j1,1}) - \frac{E}{2}\eta_0 \zeta \beta F_{i1,1} \\
& - C \beta g_{i,11} + A \beta \alpha_{i,111} = 0,
\end{aligned} \tag{3.57}$$

where g_i , α_i , and F_{iA}^* are defined in Eq. (3.50). Thus we deliver the following governing equations for the Mooney-Rivlin matrix materials reinforced with randomly oriented nano-fibers

$$\begin{aligned}
0 = & (1 - \beta)\{\mu \chi_{i,AA} + \kappa \chi_{i,AA} \chi_{j,C} \chi_{j,C} - \kappa \chi_{i,BA} \chi_{j,A} \chi_{j,B} + \kappa \chi_{i,B}(2\chi_{j,C} \chi_{j,CA} - \chi_{j,AA} \chi_{j,B} \\
& - \chi_{j,A} \chi_{j,BA})\} - p_{,A} \varepsilon_{ij} \varepsilon_{AB} \chi_{j,B} + \frac{E}{2}\eta_0 \zeta \beta (\chi_{i,11} \chi_{j,1} \chi_{j,1} + \chi_{i,1} \chi_{j,11} \chi_{j,1} + \chi_{i,1} \chi_{j,1} \chi_{j,11}) \\
& - \frac{E}{2}\eta_0 \zeta \beta \chi_{i,11} - C \beta \chi_{i,1111} + A \beta \chi_{i,111111},
\end{aligned} \tag{3.58}$$

3.3 Custom-built FEA of the nonlinear coupled PDE

The resulting PDE systems (Eqs. (3.52)–(3.54)) are coupled nonlinear differential equations of sixth order. For the purpose of preprocessing, Eqs. (3.52)–(3.54) has

been recast as:

$$\begin{aligned}
\beta' \mu(Q + \chi_{1,22}) - PS + BD + \frac{E}{2} \Gamma(3QT^2 + QD^2 + 2TRD - Q) - \beta CM + \beta AM_{,11} &= 0, \\
\beta' \mu(R + \chi_{2,22}) + PG - BT + \frac{E}{2} \Gamma(3RD^2 + RT^2 + 2TQD - R) - \beta CN + \beta AN_{,11} &= 0, \\
Q - \chi_{1,11} &= 0, \\
R - \chi_{2,11} &= 0, \\
T - \chi_{1,1} &= 0, \\
D - \chi_{2,1} &= 0, \\
G - \chi_{1,2} &= 0, \\
S - \chi_{2,2} &= 0, \\
M - Q_{,11} &= 0, \\
N - R_{,11} &= 0, \\
P - \mu(Q + \chi_{1,22}) - CM &= 0, \\
B - \mu(R + \chi_{2,22}) - CN &= 0,
\end{aligned} \tag{3.59}$$

where $\Gamma = \beta\eta_0\zeta$, $1 - \beta = \beta'$, $P = p_{,1}$, $B = p_{,2}$, $Q = \chi_{1,11}$, $R = \chi_{2,11}$, $T = \chi_{1,1}$, $D = \chi_{2,1}$, $G = \chi_{1,2}$, $S = \chi_{2,2}$, $M = Q_{,11}$, and $N = R_{,11}$. Thus, we transform a system of coupled sixth-order partial differential equations into a system of coupled second-order PDEs. The above non-linear terms(i.e., $P\chi_{2,2}$, $B\chi_{2,1}$ etc.) has been treated via the Picard iterative procedure,

$$\begin{aligned}
-P_{initial}\chi_{2,2}^{initial} + B_{initial}\chi_{2,1}^{initial} &\Rightarrow -P_0\chi_{2,2}^0 + B_0\chi_{2,1}^0, \\
P_{initial}\chi_{1,2}^{initial} - B_{initial}\chi_{1,1}^{initial} &\Rightarrow P_0\chi_{1,2}^0 + B_0\chi_{1,1}^0, \\
3Q_{initial}T_{initial}^2 + Q_{initial}D_{initial}^2 + 2T_{initial}R_{initial}D_{initial} &\Rightarrow 3Q_0T_0^2 + Q_0D_0^2 + 2T_0R_0D_0, \\
3R_{initial}D_{initial}^2 + R_{initial}T_{initial}^2 + 2T_{initial}Q_{initial}D_{initial} &\Rightarrow 3R_0D_0^2 + R_0T_0^2 + 2T_0Q_0D_0.
\end{aligned} \tag{3.60}$$

With the progress of iteration, values of P, B, T, D, G, S, Q , and R continue to be refreshed based on their previous estimations (i.e., $P_0, B_0, T_0, D_0, G_0, S_0, Q_0$ and R_0).

Hence, for N th number iteration, we can write

$$\begin{aligned}
-P_{N-1}\chi_{2,2}^{N-1} + B_{N-1}\chi_{2,1}^{N-1} &\Rightarrow -P_N\chi_{2,2}^N + B_N\chi_{2,1}^N, \\
P_{N-1}\chi_{1,2}^{N-1} - B_{N-1}\chi_{1,1}^{N-1} &\Rightarrow P_N\chi_{1,2}^N + B_N\chi_{1,1}^N, \\
3Q_{N-1}T_{N-1}^2 + Q_{N-1}D_{N-1}^2 + 2T_{N-1}R_{N-1}D_{N-1} &\Rightarrow 3Q_NT_N^2 + Q_ND_N^2 + 2T_NR_ND_N, \\
3R_{N-1}D^2 + R_{N-1}T_{N-1}^2 + 2T_{N-1}Q_{N-1}D_{N-1} &\Rightarrow 3R_ND_N^2 + R_NT_N^2 + 2T_NQ_ND_N.
\end{aligned} \tag{3.61}$$

Thus, the weak form of Eq. (3.59) is obtained by

$$\begin{aligned}
\int_{\Omega^e} w_1(\beta' \mu(Q + \chi_{1,22}) - P_0S + B_0D + \frac{E}{2}\Gamma(3QT_0^2 + QD_0^2 + 2RT_0D_0 - Q) - \beta CM \\
+ \beta AM_{,11})d\Omega = 0, \\
\int_{\Omega^e} w_2(\beta' \mu(R + \chi_{2,22}) + P_0G - B_0T + \frac{E}{2}\Gamma(3RD_0^2 + RT_0^2 + 2QT_0D_0 - R) - \beta CN \\
+ \beta AN_{,11})d\Omega = 0, \\
\int_{\Omega^e} w_3(Q - \chi_{1,11})d\Omega = 0, \\
\int_{\Omega^e} w_4(R - \chi_{2,11})d\Omega = 0, \\
\int_{\Omega^e} w_5(T - \chi_{1,1})d\Omega = 0, \\
\int_{\Omega^e} w_6(D - \chi_{2,1})d\Omega = 0, \\
\int_{\Omega^e} w_7(G - \chi_{1,2})d\Omega = 0, \\
\int_{\Omega^e} w_8(S - \chi_{2,2})d\Omega = 0, \\
\int_{\Omega^e} w_9(M - Q_{,11})d\Omega = 0, \\
\int_{\Omega^e} w_{10}(N - R_{,11})d\Omega = 0, \\
\int_{\Omega^e} w_{11}(P - \mu(Q + \chi_{1,22}) - CM)d\Omega = 0, \\
\int_{\Omega^e} w_{12}(B - \mu(R + \chi_{2,22}) - CN)d\Omega = 0,
\end{aligned} \tag{3.62}$$

Using integration by parts and Green–Stoke’s theorem, we obtain that

$$\begin{aligned}
& \int_{\Omega^e} \beta' w_1 \mu Q - \beta' \mu w_{1,2} \chi_{1,2} - w_1 P_0 S + w_1 B_0 D + w_1 \frac{E}{2} \Gamma (3QT_0^2 + QD_0^2 + 2RT_0 D_0 - Q) \\
& \quad - w_1 \beta C M - \beta A w_{1,1} M_{,1} d\Omega + \int_{\partial\Gamma^e} \left(\beta' \mu w_1 \chi_{1,2} \right) N d\Gamma + \int_{\partial\Gamma^e} \left(\beta A w_1 M_{,1} \right) N d\Gamma = 0, \\
& \int_{\Omega^e} \left(w_2 \beta' \mu R - \beta' \mu w_{2,2} \chi_{2,2} + w_2 P_0 G - w_2 B_0 T + w_2 \frac{E}{2} \Gamma (3RD_0^2 + RT_0^2 + 2QT_0 D_0 - R) \right. \\
& \quad \left. - w_2 \beta C N - \beta A w_{2,1} N_{,1} \right) d\Omega + \int_{\partial\Gamma^e} \left(\beta' \mu w_2 \chi_{2,2} \right) N d\Gamma + \int_{\partial\Gamma^e} \left(\beta A w_2 N_{,1} \right) N d\Gamma = 0, \\
& \int_{\Omega^e} \left(w_3 Q + w_{3,1} \chi_{1,1} \right) d\Omega - \int_{\partial\Gamma^e} \left(w_3 \chi_{1,1} \right) N d\Gamma = 0, \\
& \int_{\Omega^e} \left(w_4 R + w_{4,1} \chi_{2,1} \right) d\Omega - \int_{\partial\Gamma^e} \left(w_4 \chi_{2,1} \right) N d\Gamma = 0, \\
& \int_{\Omega^e} \left(w_5 T - w_5 \chi_{1,1} \right) d\Omega = 0, \\
& \int_{\Omega^e} \left(w_6 D - w_6 \chi_{2,1} \right) d\Omega = 0, \\
& \int_{\Omega^e} \left(w_7 G - w_7 \chi_{1,2} \right) d\Omega = 0, \\
& \int_{\Omega^e} \left(w_8 S - w_8 \chi_{2,2} \right) d\Omega = 0, \\
& \int_{\Omega^e} \left(w_9 M + w_{9,1} Q_{,1} \right) d\Omega - \int_{\partial\Gamma^e} \left(w_9 Q_{,1} \right) N d\Gamma = 0, \\
& \int_{\Omega^e} \left(w_{10} N + w_{10,1} R_{,1} \right) d\Omega - \int_{\partial\Gamma^e} \left(w_{10} R_{,1} \right) N d\Gamma = 0, \\
& \int_{\Omega^e} \left(w_{11} P - w_{11} \mu Q + \mu w_{11,2} \chi_{1,2} - w_{11} C M \right) d\Omega - \int_{\partial\Gamma^e} \left(\mu w_{11} \chi_{1,2} \right) N d\Gamma = 0, \\
& \int_{\Omega^e} \left(w_{12} B - w_{12} \mu R + \mu w_{12,2} \chi_{2,2} - w_{12} C N \right) d\Omega - \int_{\partial\Gamma^e} \left(\mu w_{12} \chi_{2,2} \right) N d\Gamma = 0, \quad (3.63)
\end{aligned}$$

where Ω , $\partial\Gamma$ and \mathbf{N} are the domain of interest, the associated boundary, and the rightward unit normal to the boundary. Now, the unknowns can be expressed in the form of Lagrangian polynomial as

$$(*) = \sum_{j=1}^{n=4} \left[(*)_j \Psi_j(x, y) \right], \quad (3.64)$$

where $(*)$ represents any of the twelve $(\chi_1, \chi_2, Q, R, T, D, G, S, M, N, P, B)$ unknowns. Thus, The test function w is obtained as

$$(w_k) = \sum_{i=1}^{n=4} \left[w_k^i \Psi_i(x, y) \right]; \quad k = 1, 2, 3, 4, \dots, 12, \quad (3.65)$$

where w_i is the weight of the test function and $\Psi_i(x, y)$ are the corresponding shape function, such that

$$\Psi_1 = \frac{(x-2)(y-1)}{2}, \Psi_2 = \frac{x(y-1)}{-2}, \Psi_3 = \frac{xy}{2} \text{ and } \Psi_4 = \frac{y(x-2)}{-2}. \quad (3.66)$$

Eq. (3.63) can be recast using Eqs. (3.64) and (3.65) as

$$\begin{aligned} & \sum_{i,j=1}^n \left\{ \int_{\Omega^e} \left(\beta' \mu \Psi_i \Psi_j + 3 \frac{E}{2} \Gamma \Psi_i \Psi_j T_0^2 + \frac{E}{2} \Gamma \Psi_i \Psi_j D_0^2 - \frac{E}{2} \Gamma \Psi_i \Psi_j \right) d\Omega \right\} Q_j - \\ & \sum_{i,j=1}^n \left\{ \int_{\Omega^e} (\beta' \mu \Psi_{i,2} \Psi_{j,2}) d\Omega \right\} \chi_{1j} - \sum_{i,j=1}^n \left\{ \int_{\Omega^e} (\Psi_i \Psi_j P_0) d\Omega \right\} S_j + \sum_{i,j=1}^n \left\{ \int_{\Omega^e} (\Psi_i \Psi_j B_0) \right. \\ & \left. d\Omega \right\} D_j - \sum_{i,j=1}^n \left\{ \int_{\Omega^e} (\Psi_i \Psi_j \beta C + \Psi_{i,1} \Psi_{j,1} \beta A) d\Omega \right\} M_j + \sum_{i,j=1}^n \left\{ \int_{\Omega^e} \left(\frac{E}{2} \Gamma \Psi_i 2 \Psi_j \right. \right. \\ & \left. \left. T_0 D_0 \right) d\Omega \right\} R_j + \int_{\partial \Gamma^e} (\beta' \mu \Psi_i \chi_{1,2}) N d\Gamma + \left(\int_{\partial \Gamma^e} \beta A \Psi_i M_{,1} \right) N d\Gamma = 0, \\ & \sum_{i,j=1}^n \left\{ \int_{\Omega^e} \left(\beta' \mu \Psi_i \Psi_j + 3 \Gamma \frac{E}{2} \Psi_i \Psi_j D_0^2 + \frac{E}{2} \Gamma \Psi_i \Psi_j T_0^2 - \frac{E}{2} \Gamma \Psi_i \Psi_j \right) d\Omega \right\} R_j \\ & - \sum_{i,j=1}^n \left\{ \int_{\Omega^e} (\beta' \mu \Psi_{i,2} \Psi_{j,2}) d\Omega \right\} \chi_{2j} + \sum_{i,j=1}^n \left\{ \int_{\Omega^e} (\Psi_i \Psi_j P_0) d\Omega \right\} G_j \\ & - \sum_{i,j=1}^n \left\{ \int_{\Omega^e} (\Psi_i \Psi_j B_0) d\Omega \right\} T_j - \sum_{i,j=1}^n \left\{ \int_{\Omega^e} (\Psi_i \Psi_j \beta C + \Psi_{i,1} \Psi_{j,1} \beta A) d\Omega \right\} N_j \\ & + \sum_{i,j=1}^n \left\{ \int_{\Omega^e} \left(\frac{E}{2} \Gamma \Psi_i 2 \Psi_j T_0 D_0 \right) d\Omega \right\} Q_j + \int_{\partial \Gamma^e} (\beta' \mu \Psi_i \chi_{2,2}) N d\Gamma \\ & + \int_{\partial \Gamma^e} (\beta A \Psi_i N_{,1}) N d\Gamma = 0, \\ & \sum_{i,j=1}^n \left\{ \int_{\Omega^e} (\Psi_i \Psi_j) d\Omega \right\} Q_j + \sum_{i,j=1}^n \left\{ \int_{\Omega^e} (\Psi_{i,1} \Psi_{j,1}) d\Omega \right\} \chi_{1j} - \int_{\partial \Gamma^e} (\Psi_i \chi_{1,1}) N d\Gamma = 0, \\ & \sum_{i,j=1}^n \left\{ \int_{\Omega^e} (\Psi_i \Psi_j) d\Omega \right\} R_j + \sum_{i,j=1}^n \left\{ \int_{\Omega^e} (\Psi_{i,1} \Psi_{j,1}) d\Omega \right\} \chi_{2j} - \int_{\partial \Gamma^e} (\Psi_i \chi_{2,1}) N d\Gamma = 0, \\ & \sum_{i,j=1}^n \left\{ \int_{\Omega^e} (\Psi_i \Psi_j) d\Omega \right\} T_j - \sum_{i,j=1}^n \left\{ \int_{\Omega^e} (\Psi_i \Psi_{j,1}) d\Omega \right\} \chi_{1j} = 0, \\ & \sum_{i,j=1}^n \left\{ \int_{\Omega^e} (\Psi_i \Psi_j) d\Omega \right\} D_j - \sum_{i,j=1}^n \left\{ \int_{\Omega^e} (\Psi_i \Psi_{j,1}) d\Omega \right\} \chi_{2j} = 0, \\ & \sum_{i,j=1}^n \left\{ \int_{\Omega^e} (\Psi_i \Psi_j) d\Omega \right\} G_j - \sum_{i,j=1}^n \left\{ \int_{\Omega^e} (\Psi_i \Psi_{j,2}) d\Omega \right\} \chi_{1j} = 0, \end{aligned}$$

$$\begin{aligned}
& \sum_{i,j=1}^n \left\{ \int_{\Omega^e} (\Psi_i \Psi_j) d\Omega \right\} S_j - \sum_{i,j=1}^n \left\{ \int_{\Omega^e} (\Psi_i \Psi_{j,2}) d\Omega \right\} \chi_{2j} = 0 \\
& \sum_{i,j=1}^n \left\{ \int_{\Omega^e} (\Psi_i \Psi_j) d\Omega \right\} M_j + \sum_{i,j=1}^n \left\{ \int_{\Omega^e} (\Psi_{i,1} \Psi_{j,1}) d\Omega \right\} Q_j - \int_{\partial\Gamma^e} (\Psi_i Q_{,1}) N d\Gamma = 0, \\
& \sum_{i,j=1}^n \left\{ \int_{\Omega^e} (\Psi_i \Psi_j) d\Omega \right\} N_j + \sum_{i,j=1}^n \left\{ \int_{\Omega^e} (\Psi_{i,1} \Psi_{j,1}) d\Omega \right\} R_j - \int_{\partial\Gamma^e} (\Psi_i R_{,1}) N d\Gamma = 0, \\
& \sum_{i,j=1}^n \left\{ \int_{\Omega^e} (\Psi_i \Psi_j) d\Omega \right\} P_j - \sum_{i,j=1}^n \left\{ \int_{\Omega^e} (\mu \Psi_i \Psi_j) d\Omega \right\} Q_j + \sum_{i,j=1}^n \left\{ \int_{\Omega^e} (\mu \Psi_{i,2} \Psi_{j,2}) d\Omega \right\} \chi_{1j} \\
& \quad - \sum_{i,j=1}^n \left\{ \int_{\Omega^e} (\Psi_i \Psi_j C) d\Omega \right\} M_j - \int_{\partial\Gamma^e} (\mu \Psi_i \chi_{1,2}) N d\Gamma = 0, \\
& \sum_{i,j=1}^n \left\{ \int_{\Omega^e} (\Psi_i \Psi_j) d\Omega \right\} B_j - \sum_{i,j=1}^n \left\{ \int_{\Omega^e} (\mu \Psi_i \Psi_j) d\Omega \right\} R_j + \sum_{i,j=1}^n \left\{ \int_{\Omega^e} (\mu \Psi_{i,2} \Psi_{j,2}) d\Omega \right\} \chi_{2j} \\
& \quad - \sum_{i,j=1}^n \left\{ \int_{\Omega^e} (\Psi_i \Psi_j C) d\Omega \right\} N_j - \int_{\partial\Gamma^e} (\mu \Psi_i \chi_{2,2}) N d\Gamma = 0, \tag{3.67}
\end{aligned}$$

Now, we obtain the local stiffness matrix and the forcing vector for each element

as

$$\begin{bmatrix} K_{11}^{11} & K_{12}^{11} & K_{13}^{11} & K_{14}^{11} \\ K_{21}^{11} & K_{22}^{11} & K_{23}^{11} & K_{24}^{11} \\ K_{31}^{11} & K_{32}^{11} & K_{33}^{11} & K_{34}^{11} \\ K_{41}^{11} & K_{42}^{11} & K_{43}^{11} & K_{44}^{11} \end{bmatrix}_{\text{Local}} \begin{bmatrix} \chi_1^1 \\ \chi_1^2 \\ \chi_1^3 \\ \chi_1^4 \end{bmatrix}_{\text{Local}} = \begin{bmatrix} F_1^1 \\ F_2^1 \\ F_3^1 \\ F_4^1 \end{bmatrix}_{\text{Local}}. \tag{3.68}$$

Which can be written in compact form as

$$\left[K_{ij}^{11} \right] \left[\chi_1^i \right] = \left[F_i^1 \right] \text{ for } i, j = 1, 2, 3, 4, \tag{3.69}$$

where

$$\left[K_{ij}^{11} \right] = - \int_{\Omega^e} \left(\beta' \mu \Psi_{i,2} \Psi_{j,2} \right) d\Omega, \tag{3.70}$$

and

$$\left[F_i^1 \right] = - \int_{\partial\Gamma^e} \left(\beta' \mu \Psi_i \chi_{1,2} \right) N d\Gamma - \left(\int_{\partial\Gamma^e} \beta A \Psi_i M_{,1} \right) N d\Gamma. \tag{3.71}$$

Finally, the global systems of equations for each individual elements can be obtained as

$$\begin{bmatrix}
[K^{11}] & [K^{12}] & [K^{13}] & [K^{14}] & \dots & [K^{19}] & [K^{110}] & [K^{111}] & [K^{112}] \\
[K^{21}] & [K^{22}] & [K^{23}] & [K^{24}] & \dots & [K^{29}] & [K^{210}] & [K^{211}] & [K^{212}] \\
[K^{31}] & [K^{32}] & [K^{33}] & [K^{34}] & \dots & [K^{39}] & [K^{310}] & [K^{311}] & [K^{312}] \\
[K^{41}] & [K^{42}] & [K^{43}] & [K^{44}] & \dots & [K^{49}] & [K^{410}] & [K^{411}] & [K^{412}] \\
[K^{51}] & [K^{52}] & [K^{53}] & [K^{54}] & \dots & [K^{59}] & [K^{510}] & [K^{511}] & [K^{512}] \\
[K^{61}] & [K^{62}] & [K^{63}] & [K^{64}] & \dots & [K^{69}] & [K^{610}] & [K^{611}] & [K^{612}] \\
[K^{71}] & [K^{72}] & [K^{73}] & [K^{74}] & \dots & [K^{79}] & [K^{710}] & [K^{711}] & [K^{712}] \\
[K^{81}] & [K^{82}] & [K^{83}] & [K^{84}] & \dots & [K^{89}] & [K^{810}] & [K^{811}] & [K^{812}] \\
[K^{91}] & [K^{92}] & [K^{93}] & [K^{94}] & \dots & [K^{99}] & [K^{910}] & [K^{911}] & [K^{912}] \\
[K^{101}] & [K^{102}] & [K^{103}] & [K^{104}] & \dots & [K^{109}] & [K^{1010}] & [K^{1011}] & [K^{1012}] \\
[K^{111}] & [K^{112}] & [K^{113}] & [K^{114}] & \dots & [K^{119}] & [K^{1110}] & [K^{1111}] & [K^{1112}] \\
[K^{121}] & [K^{122}] & [K^{123}] & [K^{124}] & \dots & [K^{129}] & [K^{1210}] & [K^{1211}] & [K^{1212}]
\end{bmatrix}
\begin{bmatrix}
\chi_1^i \\
\chi_2^i \\
Q_i \\
R_i \\
T_i \\
D_i \\
G_i \\
S_i \\
M_i \\
N_i \\
P_i \\
B_i
\end{bmatrix}
=
\begin{bmatrix}
\{F^1\} \\
\{F^2\} \\
\{F^3\} \\
\{F^4\} \\
\{F^5\} \\
\{F^6\} \\
\{F^7\} \\
\{F^8\} \\
\{F^9\} \\
\{F^{10}\} \\
\{F^{11}\} \\
\{F^{12}\}
\end{bmatrix}
\tag{3.72}$$

3.4 Results and discussion

The delivered system of PDEs (Eqs. (3.52)-(3.54)) which govern the mechanics of the Neo-Hookean material reinforced with nano-fibers has been solved using a custom-built numerical analysis scheme. The schematic of the problem is demonstrated in Figure 3.1. It is to be noted that, data are obtained under the normalized setting $\frac{t}{\mu} = 10$, $\frac{E}{\mu} = 100$, $\frac{C}{\mu} = 10$, $\frac{A}{\mu} = 10$, $S = 100$ unless otherwise specified. The fiber energy fraction is taken as equivalent to the volume fraction of fiber ($\beta = 4.6\%$). The various aspect ratios S are obtained by varying the fiber length $2L$ while keeping the thickness $h = 0.34nm$ as a constant. Typical strain distribution along the fiber length for three different types of graphene i.e., Pristine, Hydroxylated, and TSW defected is shown in Figure 3.3. The relevant parameters (i.e., interfacial stiffness K , Young's modulus E etc.) for the different types of graphene are taken from [100].

As the aspect ratio of graphene increases, the strain distribution becomes uniform throughout the entire length of nano-fiber for all the three cases shown in Figure 3.3.

Table 3.1: Interfacial parameters and properties of graphene [100]

Graphene	$K(GPa)$	$E(GPa)$	$h(nm)$
Pristine	0.173	1023	0.34
Hydroxylated	3.03	956	0.34
TSW defected	0.931	335	0.34

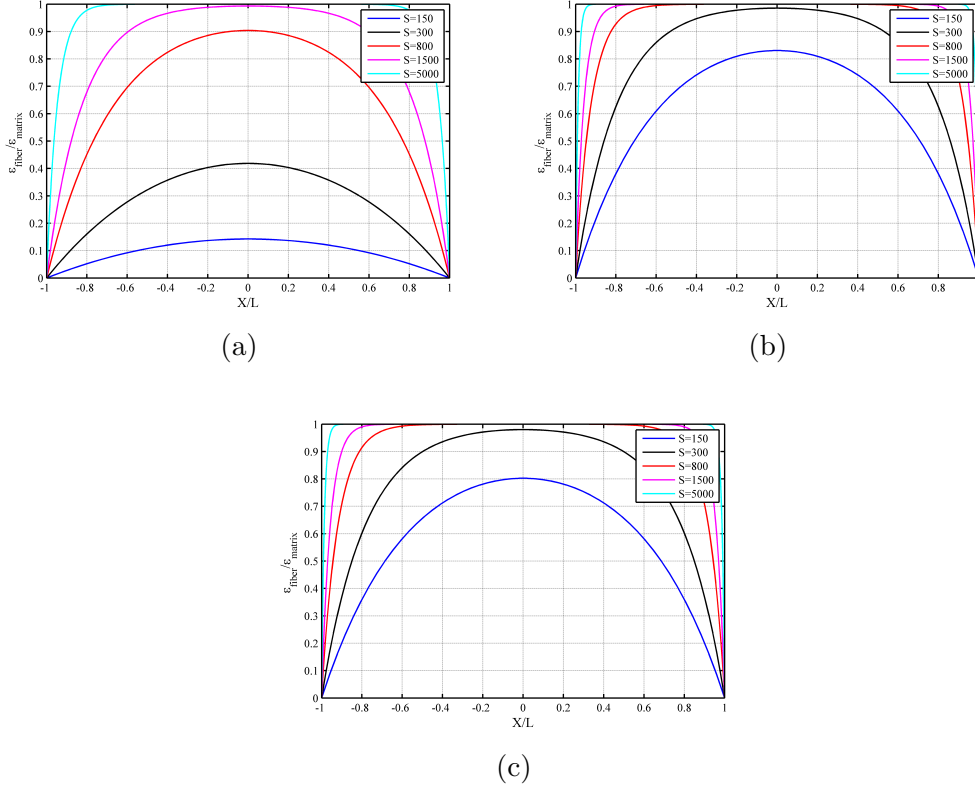


Figure 3.3: Strain distribution along the fiber length for (a) Pristine, (b) Hydroxylated and (c) TSW-defected cases with various aspect ratios S

The uniform strain distribution along the fiber length obtained for higher aspect ratio (S) indicates a greater efficiency of interfacial shear stress transfer from the matrix material to the fiber. In later section, we will discuss how this high interfacial stress transfer efficiency affects the effective Young's modulus of a nano-fiber reinforced composite.

A general deformation configuration of a nano-fiber reinforced composite material subjected to the uniaxial tension under the normalized parameter setting (i.e. $\frac{t}{\mu} =$

10, $\frac{E}{\mu} = 100$, $\frac{C}{\mu} = 10$, $\frac{A}{\mu} = 10$, $S = 100$) is displayed in Figure 3.4. The expression of the applied load t is obtained from Eqs. (3.44)-(3.45) as follows

$$t = P_{11} = (1-\beta)\mu\chi_{1,1}-p\chi_{2,2}+\frac{E}{2}\eta_0\zeta\beta(\chi_{1,1}\chi_{1,1}+\chi_{2,1}\chi_{2,1}-1)\chi_{1,1}-C\beta\chi_{1,111}+A\beta\chi_{1,11111}. \quad (3.73)$$

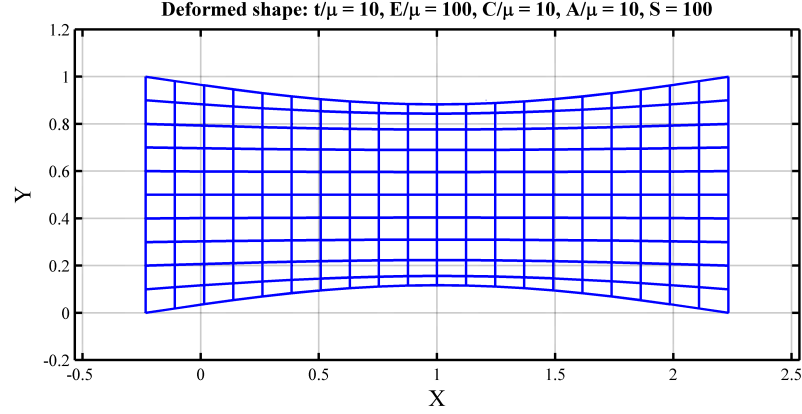


Figure 3.4: Deformation configuration: $\frac{t}{\mu} = 10$, $\frac{E}{\mu} = 100$, $\frac{C}{\mu} = 10$, $\frac{A}{\mu} = 10$, $S = 100$

The variation of the deformation profile with fiber axial stiffness is shown in Figure 3.5. In chapter 2, we have discussed the effect of fiber's elastic modulus (see, for example, Figure 2.3) for the case of unidirectional fiber reinforcement. We observed a similar result in the present nano-fiber reinforcement case, which refers that the axial extension of the composite is sensitive to the modulus pertaining to the fiber's extension. When the fiber stiffness is reduced, the amount of axial strain in the composite increases. The result is closely aligned with the findings in [67]. Figure 3.6 indicates that the composite's axial extension is also sensitive to the fiber aspect ratio S . The axial extension of the composite is less for a higher fiber aspect ratio (i.e., $S = 5000$) compared to the lower fiber aspect ratio (i.e., $S = 100$) under the same applied tension. As we have seen from Figure 3.3 that the interfacial shear stress transfer from the matrix material to the fiber is less effective for the lower aspect ratio, most of the load is carried by the matrix itself. Therefore, the resistance to the axial tension is poor and the axial strain of the composite becomes more in case of low aspect ratio S .

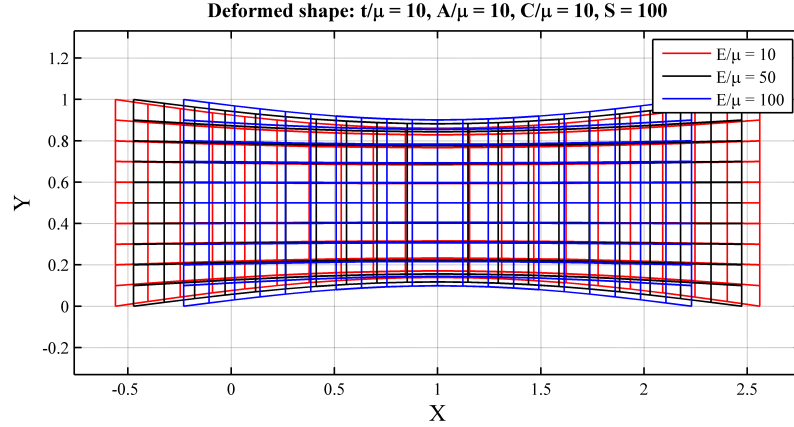


Figure 3.5: Deformed configuration with variation of $\frac{E}{\mu}$ when $\frac{t}{\mu} = 10$, $\frac{C}{\mu} = 10$, $\frac{A}{\mu} = 10$, $S = 100$

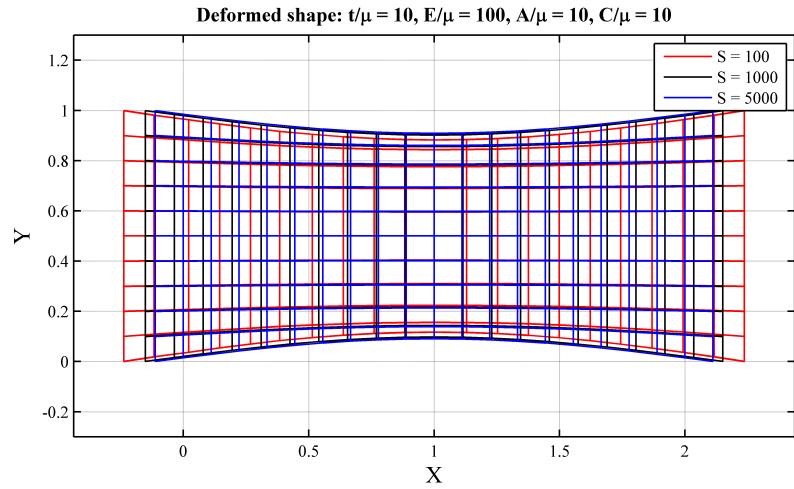


Figure 3.6: Deformed configuration with variation of S when $\frac{t}{\mu} = 10$, $\frac{E}{\mu} = 100$, $\frac{C}{\mu} = 10$, $\frac{A}{\mu} = 10$

The deformation configuration is also affected by the varying triple stress modulus ($\frac{A}{\mu}$). Figure 3.7 depicts the change in deformation configuration with the various triple stress parameter ($\frac{A}{\mu}$) for the case of nano-fiber reinforcement. In this case, the axial strain is also found to be insensitive to the triple stress parameter, whereas the lateral strain decreases as the triple stress parameter increases. The obtained result is similar to the unidirectional fiber reinforcement case that we have discussed in section 2.5 (see Figure 2.4). Moreover, the solution obtained from the proposed third gradient model accommodates the solutions from the second gradient model [67]

in the limit of vanishing triple stress modulus (i.e., $\frac{A}{\mu} = 0$, see, Figure 3.8). It is to be noted here that, to compare the deformation configuration obtained from the third gradient model to the second gradient model [67], we set the shear lag parameter $\zeta = 1$ and the krenzel orientation factor $\eta_0 = 1$.

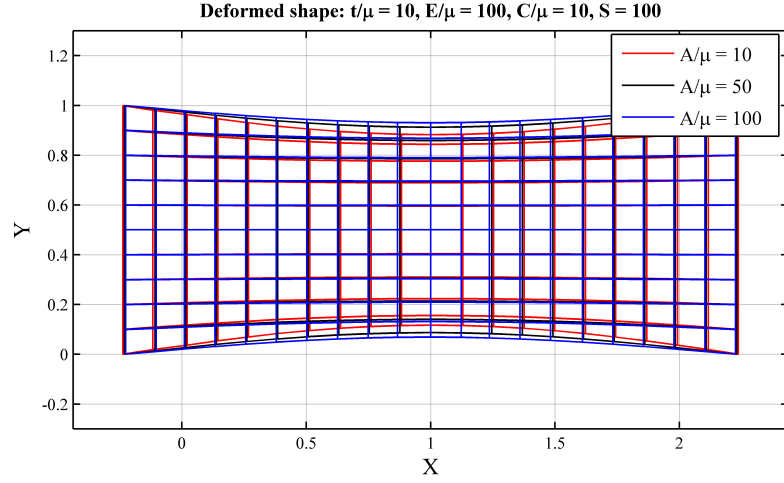


Figure 3.7: Deformed configuration with variation of $\frac{A}{\mu}$ when $\frac{t}{\mu} = 10$, $\frac{E}{\mu} = 100$, $\frac{C}{\mu} = 10$, $S = 100$

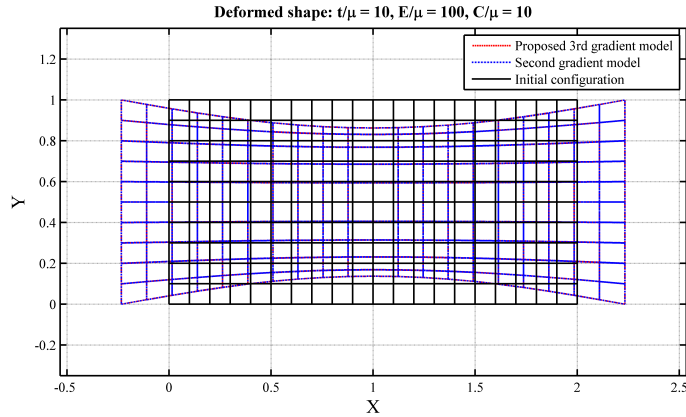


Figure 3.8: Comparison with the existing results [67]

To get a better understanding of the effect of fiber aspect ratio S , the deformation contour ($\sqrt{\chi_1^2 + \chi_2^2}$) is plotted in Figure 3.9. The resulting deformation contours due to the bias extension of the composite demonstrates that the proposed model can predict the smooth transitions throughout the entire domain of interest. The

maximum deformation is observed at the two ends of the composite, and with a smooth transition, the minimum is attained at the center. In addition, the maximum deformation in case of a higher fiber aspect ratio is small compared to the lower fiber aspect ratio. For example, the maximum deformation ($\sqrt{\chi_1^2 + \chi_2^2}$) for the fiber aspect ratio $S = 5000$ is almost 50% lower compared to the case when $S = 1000$ (see Figure 3.9).

It is clear from Figs. (3.5-3.9) that the net amount of axial (longitudinal) extension decreases with increasing the values of fiber's young's modulus E and aspect ratio S . In particular, to examine the effects of the fiber aspect ratios within the framework of the third gradient of deformations onto the shear responses of the nano-fiber reinforced composite material, we evaluate the shear angle distributions over the domain of interest. The corresponding shear angles are computed by using Eq. (2.114). As we discussed in chapter 2, in case of first-order theory, there is a significant discontinuity in the shear strain field, whereas the second-gradient model predicts a smooth but non-dilatational transition (see, for example, Fig. 5 in [67]). The results in Figure 3.10 indicate that the proposed third gradient theory predicts continuous, smooth, and dilatational shear angle distribution over the domain of interest for the nano-fiber reinforcement case. The shear angle is calculated at each node, and the average (θ_{avg}) is presented in Figure 3.10. The obtained value of the average shear angle (θ_{avg}) decreases with increasing fiber aspect ratio S . The compatible results can also be found in [85], which demonstrate a close agreement with the presented results. In addition, the dilatational shear angle distribution is reported in [70], where a linearized third gradient model is implemented.

Finally, we simulate our proposed model with various fiber aspect ratios (S) and triple stress parameters ($\frac{A}{\mu}$) to find the effect of S and $\frac{A}{\mu}$ on the effective Young's modulus of the nanofiber-reinforced composite. The Euclidean norm is used to calculate the effective strain. Upon giving the axial extension, the effective Young's modulus of composite is obtained from the applied stress divided by the effective strain. It is

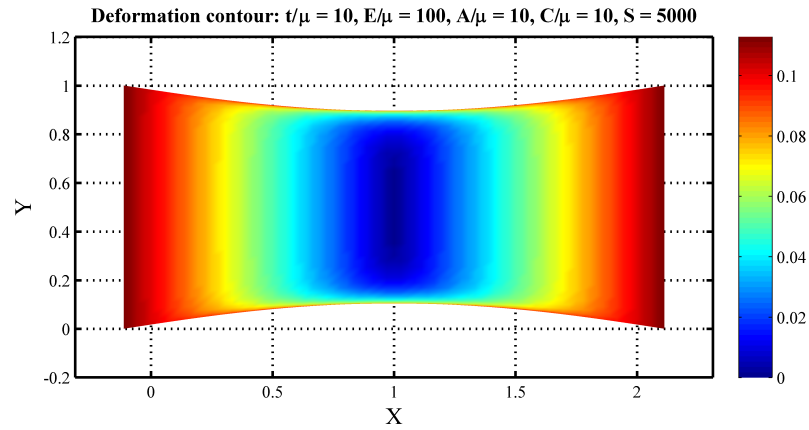
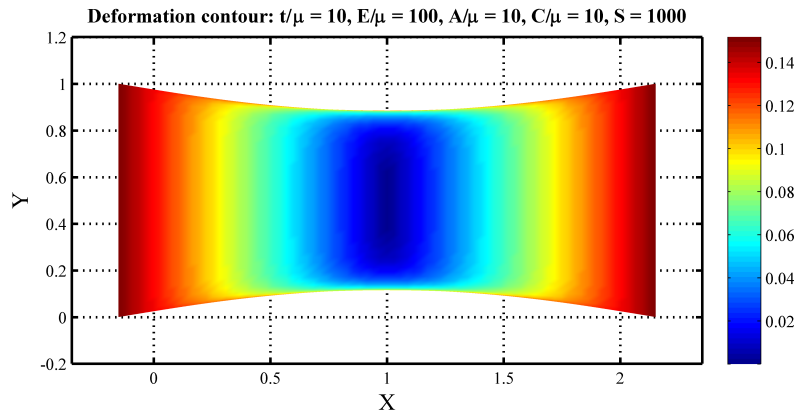
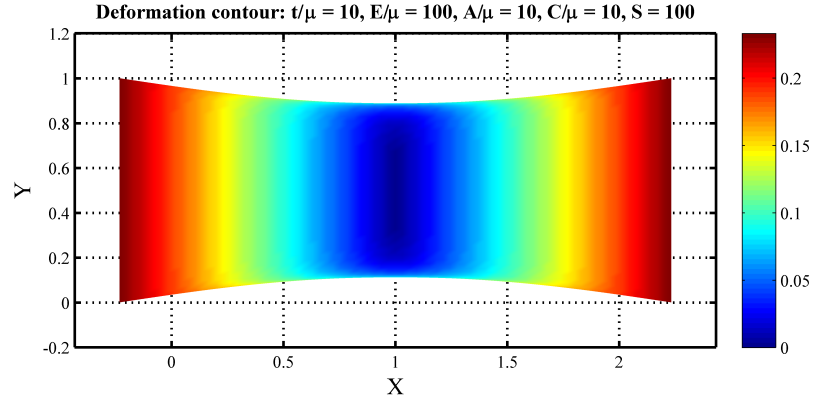


Figure 3.9: Deformation contour $\sqrt{\chi_1^2 + \chi_2^2}$ (a) $S = 100$, (b) $S = 1000$, (c) $S = 5000$ when $\frac{t}{\mu} = 10, \frac{E}{\mu} = 100, \frac{C}{\mu} = 10, \frac{A}{\mu} = 10$

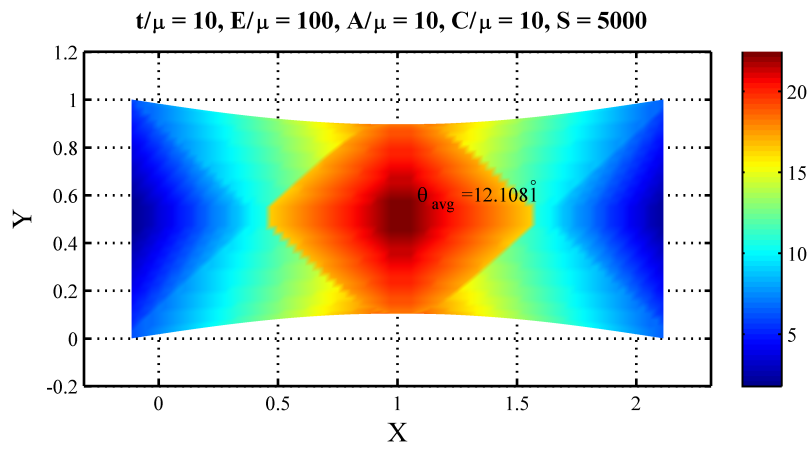
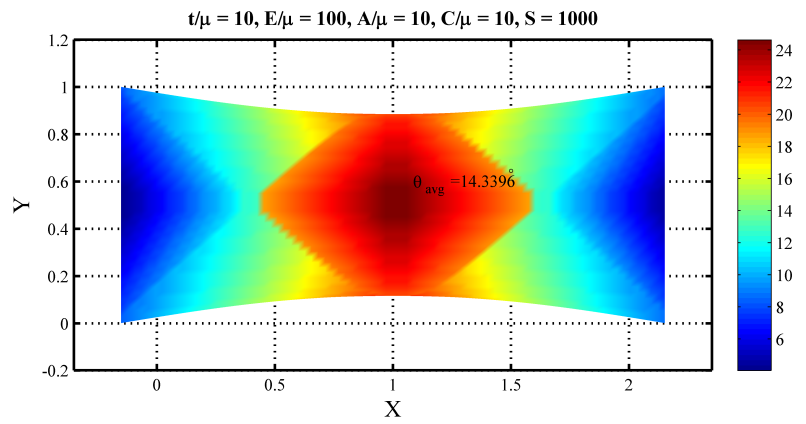
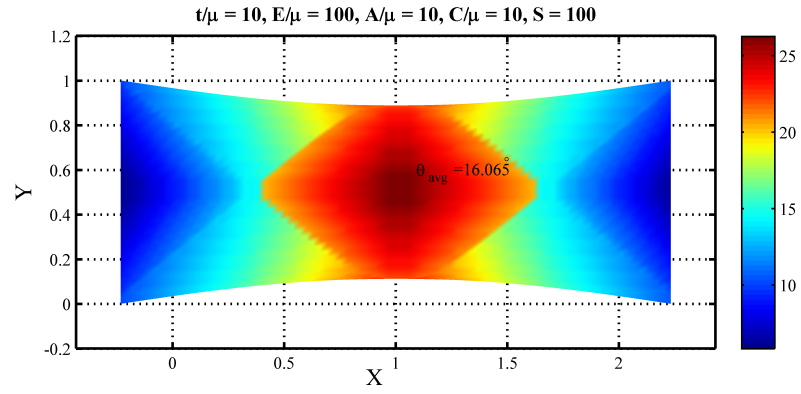


Figure 3.10: Shear angle distribution for various fiber aspect ratios S ((a) $S = 100$, (b) $S = 1000$, (c) $S = 5000$) when $\frac{t}{\mu} = 10, \frac{E}{\mu} = 100, \frac{C}{\mu} = 10, \frac{A}{\mu} = 10$

clear from Figure 3.11 that, Young's modulus of composite E_C increases with the fiber aspect ratio. The rate of increment is high until a certain level of fiber aspect ratio and Young's modulus gets saturated beyond that level. For example, when $\frac{A}{\mu} = 100$, the Young's modulus increases sharply until the fiber aspect ratio value $S = 750$, then it increases slowly up to $S = 2000$. Beyond that limit Young's modulus converges to nearly $40GPa$ and becomes saturated (i.e. insensitive to the fiber aspect ratio).

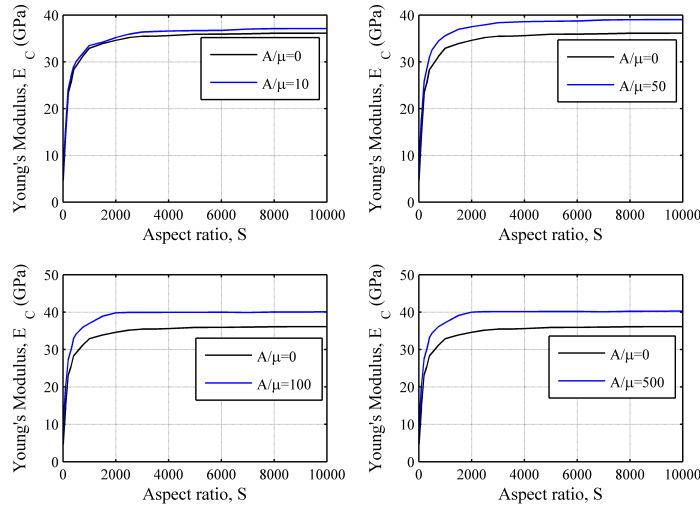


Figure 3.11: Variation of effective Young's modulus of composite with fiber aspect ratio S

We mentioned earlier that the proposed third gradient model can accommodate the solutions predicted by the second gradient theory in the limit of the vanishing triple stress modulus (see, for example, Figure 3.8). In this respect, we compare Young's modulus of composite E_C obtained from the proposed third gradient model ($\frac{A}{\mu} \neq 0$) to Young's modulus of composite E_C obtained from second gradient model ($\frac{A}{\mu} = 0$). Figure 3.11 indicates that Young's modulus E_C converges to a higher value in the case of the third gradient model approximation than that of the second gradient model. For example, in case of the second gradient model ($\frac{A}{\mu} = 0$), the Young's modulus E_C converges to nearly $36GPa$, whereas it converges to nearly $40GPa$ when $\frac{A}{\mu} = 100$.

The relationship between Young's modulus of composite E_C and triple stress pa-

parameter $\frac{A}{\mu}$ is also investigated. In particular, the modulus of elasticity of a highly coordinated material is high compared to the less coordinated material [105]. In [105], the authors determined the modulus of elasticity for various planar densities and showed that the higher the planar density, the larger the modulus of elasticity. In section 2.5.1, we have discussed that, for highly coordinated materials, the rate of particle rotation is less and the triple stress parameter value is high. Since the higher triple stress parameter is a characteristic of highly coordinated material, the modulus of elasticity will essentially be large for the high value of the triple stress parameter. Figure 3.12 indicates that Young's modulus of composite E_C increases with the higher value of the triple stress parameter. When the triple stress parameter $\frac{A}{\mu}$ is small, the Young's modulus E_C converges to a lower value compared to the case when $\frac{A}{\mu}$ is high. Again, Young's modulus E_C gets saturated at a certain limit of the triple stress parameter. If the triple stress parameter is increased from $\frac{A}{\mu} = 100$ to $\frac{A}{\mu} = 500$, the Young's modulus E_C converges to nearly $40GPa$ in both cases, as shown in Figure 3.12

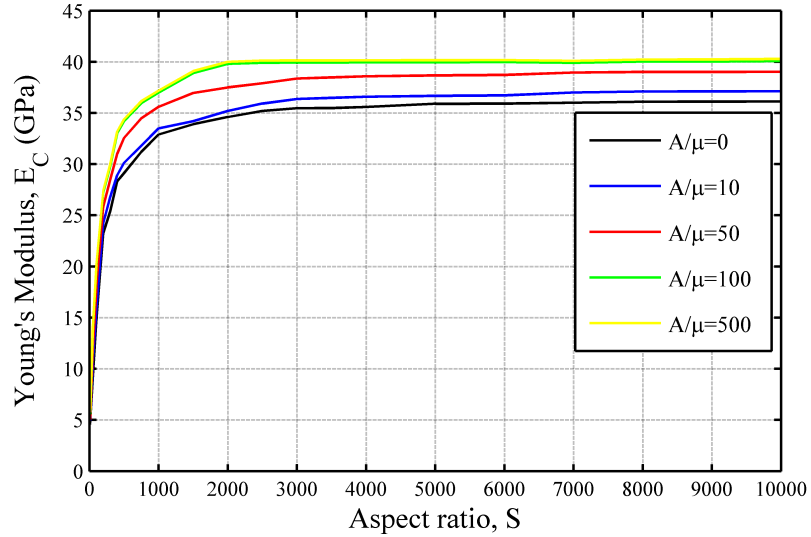


Figure 3.12: Variation of effective Young's modulus of composite with triple stress parameter $\frac{A}{\mu}$

3.5 Conclusions

In this chapter, we present a third gradient-based continuum model for the mechanics of nanofiber-reinforced composite material subjected to plane deformations. The fibers are initially assumed as continuously distributed spatial rods of Kirchhoff type, in which the kinematics of fibers is obtained via the first, second and third gradient of continuum deformations. The shear lag parameter is incorporated into the model to transform the continuously distributed unidirectional fibers into the aligned nanofibers reinforcement, which is subsequently transformed into a randomly oriented nanofiber composite system by introducing the Krenchel orientation factor. The variational principles and iterative integration by parts are employed to derive the Euler equations and associated boundary conditions. The energy density function of Spencer and Soldatos type is modified within the framework of the third gradient theory to accommodate the third-gradient continua and the associated bulk incompressibility. These, in turn, furnish a system of nonlinear coupled partial differential equations which have been solved using the custom-built FEA procedure to obtain the mechanical responses of nanofiber composites.

The mechanical response of nanofiber composite for the various fiber aspect ratios is presented throughout the chapter. The effective Young's modulus of the composite is found to be increased with the fiber aspect ratio up to a certain limit. Beyond that limit, Young's modulus gets saturated and converges to a constant value. Moreover, the obtained model predicts continuous, smooth and dilatational shear angle distributions of the composite subjected to plane bias extension. A constitutive parameter associated with Piola-type triple stress and its energy couple (i.e., triple force), designated as the triple stress parameter, emerges due to the introduction of the third gradient of continuum deformation. The relationship between Young's modulus of composite and triple stress parameter is discussed within the scope of the third gradient theory. The effective Young's modulus of the composite increases with the

triple stress parameter even when the elastic modulus of the nanofiber remains constant. However, The value of Young's modulus is nearly the same for all values of the triple-stress parameter above a certain limit.

Chapter 4

Conclusions & Future Works

4.1 Conclusions

In this thesis, we have presented a second strain gradient-based continuum model for the mechanics of elastic solid reinforced with unidirectional fibers (see chapter 2 and chapter 3), bidirectional fibers (see chapter 2), and randomly distributed nanofibers (see chapter 3) in finite plane elastostatics. The conclusions can be drawn as follows:

- We have developed a second strain gradient model for the composite and solved it numerically. We formulated the kinematics of embedded fibers by their position and director fields and eliminated the constraints of fibers by means of modeling them as Kirchhoff's rods so that the fibers can bend and stretch within the medium. Then, we obtained the Euler equations and associated boundary conditions arising from the third gradient of continuum deformations using iterative integrations by parts and variational formulations.
- We modified the energy density function of Spencer and Soldatos type within the framework of the third gradient theory to accommodate the fiber's extension, bending and point rotation.
- Finally, we obtained the governing equations, which are sixth-order nonlinear coupled PDE systems from which a set of numerical solutions describing mechanical responses of fiber composites are obtained using the custom-built

numerical scheme.

- To validate the model, we compared the deformation fields obtained from the proposed model with deformation fields predicted by the second gradient model in the limit of vanishing triple stress parameter. The results are found to be consistent.
- We obtained a new constitutive parameter called the triple stress parameter due to the introduction of the third gradient of deformations into the model. The obtained triple stress parameter is related to the variation in the curvature change rate. More precisely, the rate of change in curvature at a particular point on the convex surface, which provides implicit information about the point rotation, decreases when the triple stress parameter is increased. Moreover, we observed that the positive triple force results in clockwise point rotation.
- The shear angle distribution is found to be smooth and dilatational, in contrast to the first and second gradient of deformation models, where the distribution is either non-smooth or non-dilatational. The dilatation becomes intensified, as the triple stress parameter gets higher. The results further suggest that the proposed third gradient model leads to a more comprehensive analysis of the characterization of the dilatation process in fiber composites. In the case of highly coordinated materials, the triple stress parameter is high and the dilatation is more intense. Also, the deviations of the shear band inclination angle under uniaxial tension are found to be intensified with the increasing triple stress parameter. Moreover, we simulate our model for various triple stress parameters and compute the corresponding shear band inclination angles. It is observed that the triple stress parameter follows a similar trend to the Drucker-Prager coefficients with shear band inclination angle.
- We also provide a comprehensive analytical platform for the nanofiber-reinforced

composite. To do so, we incorporated the Shear Lag Parameter into the model to transform the continuously distributed unidirectional fibers into the aligned nano-fibers reinforcement. After that, we transformed the aligned nano-fibers composite into a randomly oriented nanofiber composite system by introducing the Krenchel Orientation Factor. The effect of fiber aspect ratio on the mechanical response of a nanocomposite is discussed. The interfacial shear stress transfer from the matrix to the fiber becomes more efficient with the higher value of the fiber aspect ratio. The effective Young's modulus of nanocomposite is found to be sensitive to the fiber's aspect ratio and triple stress parameter. More precisely, with increasing the fiber aspect ratio, the effective Young's modulus of composite starts increasing initially and eventually converges to a certain constant value. In addition, up to a certain limit, the effective Young's modulus is observed to converge at higher values with increasing the triple stress parameter. Above that certain limit of the triple stress parameter, the effective Young's modulus converges to a similar value.

4.2 Future Work

In this thesis, we used the second strain gradient framework for the analysis of fiber-reinforced composites. The present work can be further extended into various aspects. Such as,

- In this thesis, we have provided the governing equations using both Neo-Hookean and Mooney-Rivlin hyperelastic models. However, we have only implemented the Neo-Hookean case. To characterize the large deformation of soft materials more accurately, the Mooney-Rivlin case can be solved.
- Since we get an explicit idea of point rotation from this model, with further investigations, it can be used as an alternative to the micropolar elasticity.
- Experimentation and/or molecular dynamics study is needed to specify the

numerical value of the obtained new constitutive material parameter called the triple stress parameter.

- Other forms of energy potential, especially the polynomial and exponential forms may be used to explore the behavior of fiber.

Bibliography

- [1] D Hull and T. W. Clyne, *An Introduction to Composite Materials*, 2nd ed. Cambridge: Cambridge University Press, 1996. DOI: [10.1017/CBO9781139170130](https://doi.org/10.1017/CBO9781139170130).
- [2] V. Serifi, M. Tarić, D. Jevtic, A. Ristovski, and M. Šahinagić-Isović, “HISTORICAL DEVELOPMENT OF COMPOSITE MATERIALS,” *Ann. Univ. Oradea. Econ. Sci.*, vol. Vol. XXVII (XVII), 2018. DOI: [10.15660/AUOFMTE.2018-3.3392](https://doi.org/10.15660/AUOFMTE.2018-3.3392).
- [3] R. R. Nagavally, “Composite Materials - History , Types , Fabrication Techniques , Advantages , and Applications,” *Int. J. Adv. Sci. Eng. Technol.*, vol. 4, no. 2, pp. 87–92, 2016.
- [4] S. S. Godara, A. Yadav, B. Goswami, and R. S. Rana, “Review on history and characterization of polymer composite materials,” *Mater. Today Proc.*, vol. 44, pp. 2674–2677, 2021. DOI: <https://doi.org/10.1016/j.matpr.2020.12.680>.
- [5] T. G. Yashas Gowda, M. R. Sanjay, K. Subrahmanya Bhat, P. Madhu, P. Senthamaraiannan, and B. Yogesha, “Polymer matrix-natural fiber composites: An overview,” *Cogent Engineering*, vol. 5, no. 1, p. 1446667, 2018. DOI: [10.1080/23311916.2018.1446667](https://doi.org/10.1080/23311916.2018.1446667).
- [6] G. Sherif, D. Chukov, V. Tcherdyntsev, and V. Torokhov, “Effect of formation route on the mechanical properties of the polyethersulfone composites reinforced with glass fibers,” *Polymers*, vol. 11, no. 8, p. 1364, 2019. DOI: [10.3390/polym11081364](https://doi.org/10.3390/polym11081364).
- [7] M. May, G. D. Rupakula, and P. Matura, “Non-polymer-matrix composite materials for space applications,” *Composites Part C: Open Access*, vol. 3, no. September, p. 100057, 2020. DOI: [10.1016/j.jcomc.2020.100057](https://doi.org/10.1016/j.jcomc.2020.100057).
- [8] F. Ortega, F. Versino, O. V. López, and M. A. García, “Biobased composites from agro-industrial wastes and by-products,” *Emergent Materials*, vol. 5, no. 3, pp. 873–921, 2022. DOI: [10.1007/s42247-021-00319-x](https://doi.org/10.1007/s42247-021-00319-x).
- [9] M. Airliners, “*what are the boeing 787 dreamliner specs?*”, Available at <https://modernairliners.com/boeing-787-dreamliner/boeing-787-dreamliner-specs/> (10/11/2022).
- [10] A. Kaw, *Mechanics of Composite Materials*, 2nd ed. CRC Press, 2005. DOI: [10.1201/9781420058291](https://doi.org/10.1201/9781420058291).

- [11] M. Shahzad, A. Kamran, M. Z. Siddiqui, and M. Farhan, “Mechanical characterization and FE modelling of a hyperelastic material,” *Mater. Res.*, vol. 18, no. 5, pp. 918–924, 2015. DOI: [10.1590/1516-1439.320414](https://doi.org/10.1590/1516-1439.320414).
- [12] R. S. Rivlin and E. K. Rideal, “Large elastic deformations of isotropic materials IV. further developments of the general theory,” *Philosophical Transactions of the Royal Society of London. Series A, Mathematical and Physical Sciences*, vol. 241, no. 835, pp. 379–397, Oct. 1948. DOI: [10.1098/rsta.1948.0024](https://doi.org/10.1098/rsta.1948.0024).
- [13] T. J. Pence and K. Gou, “On compressible versions of the incompressible neo-Hookean material,” *Math. Mech. Solids*, vol. 20, no. 2, pp. 157–182, 2014. DOI: [10.1177/1081286514544258](https://doi.org/10.1177/1081286514544258).
- [14] M Mooney, “A Theory of Large Elastic Deformation,” *Journal of Applied Physics*, vol. 11, no. 9, pp. 582–592, Sep. 1940. DOI: [10.1063/1.1712836](https://doi.org/10.1063/1.1712836).
- [15] B. Kim *et al.*, “A comparison among Neo-Hookean model, Mooney-Rivlin model, and Ogden model for Chloroprene rubber,” *Int. J. Precis. Eng. Manuf.*, vol. 13, no. 5, pp. 759–764, 2012. DOI: [10.1007/s12541-012-0099-y](https://doi.org/10.1007/s12541-012-0099-y).
- [16] M. Zeidi, “Gradient elasticity modelling and analysis for the mechanics of unidirectional and bidirectional fiber reinforced composites,” M.S. thesis, University of Alberta, Canada, 2018.
- [17] A. Kelly and G. J. Davies, “The principles of the fibre reinforcement of metals,” *Metallurgical Reviews*, vol. 10, no. 1, pp. 1–77, 1965. DOI: [10.1179/mtrlr.1965.10.1.1](https://doi.org/10.1179/mtrlr.1965.10.1.1).
- [18] A. Kelly, *Strong Solids*. Oxford: Clarendon Press, 1966.
- [19] A. J. Spencer, “A theory of the failure of ductile materials reinforced by elastic fibres,” *International Journal of Mechanical Sciences*, vol. 7, no. 3, pp. 197–209, 1965. DOI: [10.1016/0020-7403\(65\)90018-4](https://doi.org/10.1016/0020-7403(65)90018-4).
- [20] J. F. Mulhern, T. G. Rogers, and A. J. M. Spencer, “A continuum model for fibre-reinforced plastic materials,” in *Proceedings of the Royal Society of London. Series A. Mathematical and Physical Sciences*, vol. 301, 1967, pp. 473–492. DOI: [10.1098/rspa.1967.0220](https://doi.org/10.1098/rspa.1967.0220).
- [21] Z. Hashin and B. Rosen, “The elastic moduli of fiber-reinforced materials,” *Journal of Applied Mechanics*, vol. 31, pp. 223–232, 1964. DOI: [10.1115/1.3629590](https://doi.org/10.1115/1.3629590).
- [22] Z Hashin, “On elastic behaviour of fibre reinforced materials of arbitrary transverse phase geometry,” *Journal of the Mechanics and Physics of Solids*, vol. 13, no. 3, pp. 119–134, 1965. DOI: [10.1016/0022-5096\(65\)90015-3](https://doi.org/10.1016/0022-5096(65)90015-3).
- [23] J. E. Adkins and R. S. Rivlin, “Large Elastic Deformations of Isotropic Materials X. Reinforcement by Inextensible Cords,” *Philosophical Transactions of the Royal Society of London. Series A, Mathematical and Physical Sciences*, vol. 248, no. 944, pp. 201–223, 1955. DOI: [10.1098/rsta.1955.0014](https://doi.org/10.1098/rsta.1955.0014).

- [24] P Germain, “Method of virtual power in continuum mechanics. Part 2: Microstructure,” *SIAM J. Appl. Math.*, vol. 25, no. 3, pp. 556–575, 1973. DOI: [10.1137/0125053](https://doi.org/10.1137/0125053).
- [25] C. Papenfuss and P. Ván, “Scalar, vectorial, and tensorial damage parameters from the mesoscopic background,” *Proceedings of the Estonian Academy of Sciences*, vol. 57, no. 3, pp. 132–141, 2008. DOI: [10.3176/proc.2008.3.03](https://doi.org/10.3176/proc.2008.3.03).
- [26] N. Kirchner and P. Steinmann, “A unifying treatise on variational principles for gradient and micromorphic continua,” *Philosophical Magazine*, vol. 85, no. 33–35, pp. 3875–3895, 2005. DOI: [10.1080/14786430500362421](https://doi.org/10.1080/14786430500362421).
- [27] M. Charlotte and L. Truskinovsky, “Linear elastic chain with a hyper-prestress,” *Journal of the Mechanics and Physics of Solids*, vol. 50, no. 2, pp. 217–251, 2002. DOI: [10.1016/S0022-5096\(01\)00054-0](https://doi.org/10.1016/S0022-5096(01)00054-0).
- [28] S Forest, “Mechanics of generalized continua: construction by homogenization,” *J. Phys. IV France*, vol. 08, no. PR4, pp. 4–39, Jun. 1998. DOI: [10.1051/jp4:1998405](https://doi.org/10.1051/jp4:1998405).
- [29] N. Kirchner and P. Steinmann, “On the material setting of gradient hyperelasticity,” *Mathematics and Mechanics of Solids*, vol. 12, no. 5, pp. 559–580, 2007. DOI: [10.1177/1081286506067073](https://doi.org/10.1177/1081286506067073).
- [30] S. Forest, “Homogenization methods and mechanics of generalized continua - part 2,” *Theoretical and Applied Mechanics*, vol. 28, no. 28–29, pp. 113–144, 2002. DOI: [10.2298/tam0229113f](https://doi.org/10.2298/tam0229113f).
- [31] A. S. J. Suiker and C. S. Chang, “Application of higher-order tensor theory for formulating enhanced continuum models,” *Acta Mechanica*, vol. 142, no. 1, pp. 223–234, 2000. DOI: [10.1007/BF01190020](https://doi.org/10.1007/BF01190020).
- [32] R. D. Mindlin, “Second gradient of strain and surface-tension in linear elasticity,” *International Journal of Solids and Structures*, vol. 1, no. 4, pp. 417–438, 1965. DOI: [10.1016/0020-7683\(65\)90006-5](https://doi.org/10.1016/0020-7683(65)90006-5).
- [33] F. Dell’Isola, A. Della Corte, and I. Giorgio, “Higher-gradient continua: The legacy of Piola, Mindlin, Sedov and Toupin and some future research perspectives,” *Mathematics and Mechanics of Solids*, vol. 22, no. 4, pp. 852–872, 2017. DOI: [10.1177/1081286515616034](https://doi.org/10.1177/1081286515616034).
- [34] R. A. Toupin, “Theories of elasticity with couple-stress,” *Archive for Rational Mechanics and Analysis*, vol. 17, no. 2, pp. 85–112, 1964. DOI: [10.1007/BF00253050](https://doi.org/10.1007/BF00253050).
- [35] W. T. Koiter, “Couple Stresses in the Theory of Elasticity, I & II,” *Philosophical Transactions of the Royal Society of London B*, vol. 67, pp. 17–44, 1964.
- [36] C Pideri and P Seppecher, “A second gradient material resulting from the homogenization of an heterogeneous linear elastic medium,” *Continuum Mechanics and Thermodynamics*, vol. 9, no. 5, pp. 241–257, 1997. DOI: [10.1007/s001610050069](https://doi.org/10.1007/s001610050069).

- [37] A. S. J. Suiker, R. de Borst, and C. S. Chang, “Micro-mechanical modelling of granular material. Part 1: Derivation of a second-gradient micro-polar constitutive theory,” *Acta Mechanica*, vol. 149, no. 1, pp. 161–180, 2001. DOI: [10.1007/BF01261670](https://doi.org/10.1007/BF01261670).
- [38] M. El Jarroudi, “Homogenization of a nonlinear elastic fibre-reinforced composite: A second gradient nonlinear elastic material,” *Journal of Mathematical Analysis and Applications*, vol. 403, no. 2, pp. 487–505, 2013. DOI: [10.1016/j.jmaa.2013.02.042](https://doi.org/10.1016/j.jmaa.2013.02.042).
- [39] F. dell’Isola, P. Seppecher, and A. Madeo, “How contact interactions may depend on the shape of Cauchy cuts in Nth gradient continua: Approach ”à la D’Alembert”,” *Zeitschrift fur Angewandte Mathematik und Physik*, vol. 63, no. 6, pp. 1119–1141, 2012. DOI: [10.1007/s00033-012-0197-9](https://doi.org/10.1007/s00033-012-0197-9).
- [40] H.-T. Thai, T. P. Vo, T.-K. Nguyen, and S.-E. Kim, “A review of continuum mechanics models for size-dependent analysis of beams and plates,” *Compos. Struct.*, vol. 177, pp. 196–219, 2017. DOI: <https://doi.org/10.1016/j.compstruct.2017.06.040>.
- [41] A. Battista, L. Rosa, R. Dell’Erba, and L. Greco, “Numerical investigation of a particle system compared with first and second gradient continua: Deformation and fracture phenomena*,” *Mathematics and Mechanics of Solids*, vol. 22, no. 11, pp. 2120–2134, Jul. 2016. DOI: [10.1177/1081286516657889](https://doi.org/10.1177/1081286516657889).
- [42] M. Cuomo, F. Dell’Isola, L. Greco, and N. L. Rizzi, “First versus second gradient energies for planar sheets with two families of inextensible fibres: Investigation on deformation boundary layers, discontinuities and geometrical instabilities,” *Composites Part B: Engineering*, vol. 115, pp. 423–448, 2017. DOI: [10.1016/j.compositesb.2016.08.043](https://doi.org/10.1016/j.compositesb.2016.08.043).
- [43] R. S. Rivlin, “The solution of problems in second order elasticity theory,” *Journal of Rational Mechanics and Analysis*, vol. 2, pp. 53–81, 1953.
- [44] J. Adkins, “Cylindrically Symmetrical Deformations of Incompressible Elastic Materials Reinforced with Inextensible Cords,” *Journal of Rational Mechanics and Analysis*, vol. 5, no. 1, pp. 189–202, 1956. DOI: [10.1512/iumj.1956.5.55005](https://doi.org/10.1512/iumj.1956.5.55005).
- [45] J. E. Adkins and E. K. Rideal, “Finite plane deformation of thine elastic sheets reinforced with inextensible cords,” *Philosophical Transactions of the Royal Society of London. Series A, Mathematical and Physical Sciences*, vol. 249, no. 961, pp. 125–150, May 1956. DOI: [10.1098/rsta.1956.0017](https://doi.org/10.1098/rsta.1956.0017).
- [46] J. Adkins, “A three-dimensional problem for highly elastic materials subject to constraints,” *Quarterly Journal of Mechanics and Applied Mathematics*, vol. 11, no. 1, pp. 88–97, 1958. DOI: [10.1093/qjmam/11.1.88](https://doi.org/10.1093/qjmam/11.1.88).
- [47] A. Spencer, *Deformations of fibre-reinforced materials*. Oxford: Oxford University Press, 1972.

- [48] G. A. Holzapfel and R. W. Ogden, *Mechanics of Biological Tissue*, G. A. Holzapfel and R. W. Ogden, Eds. Springer Berlin, Heidelberg, 2006, vol. 1. DOI: [10.1007/3-540-31184-X](https://doi.org/10.1007/3-540-31184-X).
- [49] A. J. Spencer and K. P. Soldatos, “Finite deformations of fibre-reinforced elastic solids with fibre bending stiffness,” *International Journal of Non-Linear Mechanics*, vol. 42, no. 2, pp. 355–368, 2007. DOI: [10.1016/j.ijnonlinmec.2007.02.015](https://doi.org/10.1016/j.ijnonlinmec.2007.02.015).
- [50] I. Stewart, *The Static and Dynamic Continuum Theory of Liquid Crystals*, I. Stewart, Ed. Taylor & Francis, London, 2004. DOI: [10.4324/9780203646335](https://doi.org/10.4324/9780203646335).
- [51] M. G. Hilgers and A. C. Pipkin, “Elastic sheets with bending stiffness,” *Quarterly Journal of Mechanics and Applied Mathematics*, vol. 45, no. 1, pp. 57–75, 1992. DOI: [10.1093/qjmam/45.1.57](https://doi.org/10.1093/qjmam/45.1.57).
- [52] D. J. Steigmann, “Theory of elastic solids reinforced with fibers resistant to extension, flexure and twist,” *International Journal of Non-Linear Mechanics*, vol. 47, no. 7, pp. 734–742, 2012. DOI: [10.1016/j.ijnonlinmec.2012.04.007](https://doi.org/10.1016/j.ijnonlinmec.2012.04.007).
- [53] D. J. Steigmann, “Equilibrium of elastic lattice shells,” *Journal of Engineering Mathematics*, vol. 109, no. 1, pp. 47–61, 2018. DOI: [10.1007/s10665-017-9905-y](https://doi.org/10.1007/s10665-017-9905-y).
- [54] D. J. Steigmann and F. Dell’Isola, “Mechanical response of fabric sheets to three-dimensional bending, twisting, and stretching,” *Acta Mechanica Sinica/Lixue Xuebao*, vol. 31, no. 3, pp. 373–382, 2015. DOI: [10.1007/s10409-015-0413-x](https://doi.org/10.1007/s10409-015-0413-x).
- [55] D. J. Steigmann and A. C. Pipkin, “Equilibrium of Elastic Nets,” *Philosophical Transactions: Physical Sciences and Engineering*, vol. 335, no. 1639, pp. 419–454, Oct. 1991. DOI: [10.1098/rsta.1991.0056](https://doi.org/10.1098/rsta.1991.0056).
- [56] F. dell’Isola *et al.*, “Advances in pantographic structures: design, manufacturing, models, experiments and image analyses,” *Continuum Mechanics and Thermodynamics*, vol. 31, no. 4, pp. 1231–1282, 2019. DOI: [10.1007/s00161-019-00806-x](https://doi.org/10.1007/s00161-019-00806-x).
- [57] R. D. Mindlin and H. F. Tiersten, “Effects of couple-stresses in linear elasticity,” *Archive for Rational Mechanics and Analysis*, vol. 11, no. 1, pp. 415–448, 1962. DOI: [10.1007/BF00253946](https://doi.org/10.1007/BF00253946).
- [58] F. Yang, A. C. M. Chong, D. C. C. Lam, and P. Tong, “Couple stress based strain gradient theory for elasticity,” *Int. J. Solids Struct.*, vol. 39, no. 10, pp. 2731–2743, 2002. DOI: [https://doi.org/10.1016/S0020-7683\(02\)00152-X](https://doi.org/10.1016/S0020-7683(02)00152-X).
- [59] D. C. C. Lam, F. Yang, A. C. M. Chong, J. Wang, and P. Tong, “Experiments and theory in strain gradient elasticity,” *J. Mech. Phys. Solids*, vol. 51, no. 8, pp. 1477–1508, 2003. DOI: [https://doi.org/10.1016/S0022-5096\(03\)00053-X](https://doi.org/10.1016/S0022-5096(03)00053-X).
- [60] R. Asaro and V. Lubarda, “Micropolar Elasticity,” in *Mech. Solids Mater.* R. Asaro and V. Lubarda, Eds., Cambridge: Cambridge University Press, 2006, pp. 375–406. DOI: [10.1017/CBO9780511755514.023](https://doi.org/10.1017/CBO9780511755514.023).

- [61] A. Eringen, “Theory of Micropolar Plates,” *Journal of Applied Mathematics and Physics*, vol. 18, pp. 12–31, 1967. DOI: [10.1007/BF01593891](https://doi.org/10.1007/BF01593891).
- [62] V. A. Eremeyev, A. Skrzat, and A. Vinakurava, “Application of the Micropolar Theory to the Strength Analysis of Bioceramic Materials for Bone Reconstruction,” *Strength Mater.*, vol. 48, no. 4, pp. 573–582, 2016. DOI: [10.1007/s11223-016-9800-1](https://doi.org/10.1007/s11223-016-9800-1).
- [63] R. Lakes, “*cosserat elasticity; micropolar elasticity*”, Available at <http://silver.neep.wisc.edu/~lakes/Coss.html> (10/11/2022).
- [64] E Kröner, “Elasticity theory of materials with long range cohesive forces,” *Int. J. Solids Struct.*, vol. 3, no. 5, pp. 731–742, 1967. DOI: [https://doi.org/10.1016/0020-7683\(67\)90049-2](https://doi.org/10.1016/0020-7683(67)90049-2).
- [65] A. Eringen and D. Edelen, “On Nonlocal Elasticity,” *International Journal of Engineering Science*, vol. 10, pp. 233–248, 1972. DOI: [10.1016/0020-7225\(72\)90039-0](https://doi.org/10.1016/0020-7225(72)90039-0).
- [66] A. C. Eringen, “On differential equations of nonlocal elasticity and solutions of screw dislocation and surface waves,” *Journal of Applied Physics*, vol. 54, no. 9, pp. 4703–4710, Sep. 1983. DOI: [10.1063/1.332803](https://doi.org/10.1063/1.332803).
- [67] C. I. Kim and M. Zeidi, “Gradient elasticity theory for fiber composites with fibers resistant to extension and flexure,” *International Journal of Engineering Science*, vol. 131, pp. 80–99, 2018. DOI: <https://doi.org/10.1016/j.ijengsci.2018.06.002>.
- [68] P Boisse, N Hamila, and A Madeo, “Modelling the development of defects during composite reinforcements and prepreg forming,” *Philos. Trans. R. Soc. A Math. Phys. Eng. Sci.*, vol. 374, no. 2071, p. 20150269, 2016. DOI: [10.1098/rsta.2015.0269](https://doi.org/10.1098/rsta.2015.0269).
- [69] C. I. Kim and S. Islam, “Mechanics of third-gradient continua reinforced with fibers resistant to flexure in finite plane elastostatics,” *Continuum Mechanics and Thermodynamics*, vol. 32, no. 6, pp. 1595–1617, 2020. DOI: [10.1007/s00161-020-00867-3](https://doi.org/10.1007/s00161-020-00867-3).
- [70] S. E. S. Bolouri and C. I. Kim, “A model for the second strain gradient continua reinforced with extensible fibers in plane elastostatics,” *Continuum Mechanics and Thermodynamics*, vol. 33, no. 5, pp. 2141–2165, 2021. DOI: [10.1007/s00161-021-01015-1](https://doi.org/10.1007/s00161-021-01015-1).
- [71] G. A. Francfort and J.-J. Marigo, “Cracks in Fracture Mechanics : A Time Indexed Family of Energy Minimizers,” in *IUTAM symposium on variations of domain and free-boundary problems in solid mechanics*, January, P. Argoul, M. Frémond, and Q. Nguyen, Eds., Kluwer Academic Publishers, 1999, pp. 197–202. DOI: [10.1007/978-94-011-4738-5_{_}23](https://doi.org/10.1007/978-94-011-4738-5_{_}23).

- [72] H. Askes and E. C. Aifantis, “Gradient elasticity in statics and dynamics: An overview of formulations, length scale identification procedures, finite element implementations and new results,” *International Journal of Solids and Structures*, vol. 48, no. 13, pp. 1962–1990, 2011. DOI: [10.1016/j.ijsolstr.2011.03.006](https://doi.org/10.1016/j.ijsolstr.2011.03.006).
- [73] A. Paolone, M. Vasta, and A. Luongo, “Flexural-torsional bifurcations of a cantilever beam under potential and circulatory forces I: Non-linear model and stability analysis,” *International Journal of Non-Linear Mechanics*, vol. 41, no. 4, pp. 586–594, 2006. DOI: [10.1016/j.ijnonlinmec.2006.02.006](https://doi.org/10.1016/j.ijnonlinmec.2006.02.006).
- [74] A. Luongo and G. Piccardo, “Linear instability mechanisms for coupled translational galloping,” *Journal of Sound and Vibration*, vol. 288, no. 4-5, pp. 1027–1047, 2005. DOI: [10.1016/j.jsv.2005.01.056](https://doi.org/10.1016/j.jsv.2005.01.056).
- [75] A. Luongo and F. Romeo, “Real wave vectors for dynamic analysis of periodic structures,” *Journal of Sound and Vibration*, vol. 279, no. 1-2, pp. 309–325, 2005. DOI: [10.1016/j.jsv.2003.11.011](https://doi.org/10.1016/j.jsv.2003.11.011).
- [76] L. I. Sedov, “MATHEMATICAL METHODS FOR CONSTRUCTING NEW MODELS OF CONTINUOUS MEDIA,” *Russian Mathematical Surveys*, vol. 20, no. 5, pp. 123–182, 1965. DOI: [10.1070/rm1965v020n05abeh001191](https://doi.org/10.1070/rm1965v020n05abeh001191).
- [77] S. C. Cowin, “Bone poroelasticity,” *Journal of Biomechanics*, vol. 32, no. 3, pp. 217–238, 1999. DOI: [10.1016/S0021-9290\(98\)00161-4](https://doi.org/10.1016/S0021-9290(98)00161-4).
- [78] S. Federico and T. C. Gasser, “Nonlinear elasticity of biological tissues with statistical fibre orientation,” *Journal of The Royal Society Interface*, vol. 7, no. 47, pp. 955–966, Jun. 2010. DOI: [10.1098/rsif.2009.0502](https://doi.org/10.1098/rsif.2009.0502).
- [79] E. H. Dill, “Kirchhoff’s Theory of Rods,” *Archive for History of Exact Sciences*, vol. 44, no. 1, pp. 1–23, Oct. 1992.
- [80] H. L. Cox, “The elasticity and strength of paper and other fibrous materials,” *British Journal of Applied Physics*, vol. 3, no. 3, pp. 72–79, Mar. 1952. DOI: [10.1088/0508-3443/3/3/302](https://doi.org/10.1088/0508-3443/3/3/302).
- [81] G. Guo and Y. Zhu, “Cohesive-Shear-Lag Modeling of Interfacial Stress Transfer between a Monolayer Graphene and a Polymer Substrate,” *Journal of Applied Mechanics, Transactions ASME*, vol. 82, no. 3, p. 031005, 2015. DOI: [10.1115/1.4029635](https://doi.org/10.1115/1.4029635).
- [82] H Krenchel, *Fibre Reinforcement: Theoretical and Practical Investigations of the Elasticity and Strength of Fibre-reinforced Materials*. Copenhagen, Denmark: Akademisk forlag, 1964.
- [83] A. Javili, F. Dell’Isola, and P. Steinmann, “Geometrically nonlinear higher-gradient elasticity with energetic boundaries,” *Journal of the Mechanics and Physics of Solids*, vol. 61, no. 12, pp. 2381–2401, 2013. DOI: [10.1016/j.jmps.2013.06.005](https://doi.org/10.1016/j.jmps.2013.06.005).
- [84] D. J. Steigmann, “Invariants of the stretch tensors and their application to finite elasticity theory,” *Mathematics and Mechanics of Solids*, vol. 7, no. 4, pp. 393–404, 2002. DOI: [10.1177/108128028481](https://doi.org/10.1177/108128028481).

- [85] F. dell’Isola, I. Giorgio, M. Pawlikowski, and N. L. Rizzi, “Large deformations of planar extensible beams and pantographic lattices: heuristic homogenization, experimental and numerical examples of equilibrium,” *Proceedings of the Royal Society A: Mathematical, Physical and Engineering Sciences*, vol. 472, no. 2185, p. 20150790, Jan. 2016. DOI: [10.1098/rspa.2015.0790](https://doi.org/10.1098/rspa.2015.0790).
- [86] T. Nizolek, T. Pollock, and R. McMeeking, “Kink band and shear band localization in anisotropic perfectly plastic solids,” *J. Mech. Phys. Solids*, vol. 146, p. 104183, 2021. DOI: [10.1016/j.jmps.2020.104183](https://doi.org/10.1016/j.jmps.2020.104183).
- [87] M. R. Kuhn, “Loading, Movement, and Strength,” in *Granular Geomechanics*, M. R. Kuhn, Ed., Elsevier, 2017, pp. 153–227. DOI: [10.1016/b978-1-78548-071-3.50004-9](https://doi.org/10.1016/b978-1-78548-071-3.50004-9).
- [88] Q. Wei, D. Jia, K. T. Ramesh, and E. Ma, “Evolution and microstructure of shear bands in nanostructured Fe,” *Appl. Phys. Lett.*, vol. 81, no. 7, pp. 1240–1242, 2002. DOI: [10.1063/1.1501158](https://doi.org/10.1063/1.1501158).
- [89] M. Zhao and M. Li, “Interpreting the change in shear band inclination angle in metallic glasses,” *Applied Physics Letters*, vol. 93, no. 24, p. 241906, 2008. DOI: [10.1063/1.3050462](https://doi.org/10.1063/1.3050462).
- [90] X. J. Duan, M. K. Jain, M. Bruhis, and D. S. Wilkinson, “Experimental and Numerical Study of Intense Shear Banding for Al-Alloy under Uniaxial Tension,” *Advanced Materials Research*, vol. 6-8, no. May, pp. 737–744, 2005. DOI: [10.4028/www.scientific.net/amr.6-8.737](https://doi.org/10.4028/www.scientific.net/amr.6-8.737).
- [91] K. Karimi and J. L. Barrat, “Correlation and shear bands in a plastically deformed granular medium,” *Scientific Reports*, vol. 8, no. 1, p. 4021, 2018. DOI: [10.1038/s41598-018-22310-z](https://doi.org/10.1038/s41598-018-22310-z).
- [92] L. Anand and C. Su, “A theory for amorphous viscoplastic materials undergoing finite deformations, with application to metallic glasses,” *Journal of the Mechanics and Physics of Solids*, vol. 53, no. 6, pp. 1362–1396, 2005. DOI: [10.1016/j.jmps.2004.12.006](https://doi.org/10.1016/j.jmps.2004.12.006).
- [93] A. C. Lund and C. A. Schuh, “The Mohr–Coulomb criterion from unit shear processes in metallic glass,” *Intermetallics*, vol. 12, no. 10, pp. 1159–1165, 2004. DOI: [10.1016/j.intermet.2004.07.001](https://doi.org/10.1016/j.intermet.2004.07.001).
- [94] D. Vandembroucq and S. Roux, “Mechanical noise dependent aging and shear banding behavior of a mesoscopic model of amorphous plasticity,” *Physical Review B - Condensed Matter and Materials Physics*, vol. 84, no. 13, p. 134210, 2011. DOI: [10.1103/PhysRevB.84.134210](https://doi.org/10.1103/PhysRevB.84.134210).
- [95] M. Zhao and M. Li, “A constitutive theory and modeling on deviation of shear band inclination angles in bulk metallic glasses,” *Journal of Materials Research*, vol. 24, no. 8, pp. 2688–2696, 2009. DOI: [10.1557/jmr.2009.0306](https://doi.org/10.1557/jmr.2009.0306).

- [96] N. Makedonska, D. W. Sparks, E. Aharonov, and L. Goren, “Friction versus dilation revisited: Insights from theoretical and numerical models,” *Journal of Geophysical Research: Solid Earth*, vol. 116, no. 9, B09302, 2011. DOI: [10.1029/2010JB008139](https://doi.org/10.1029/2010JB008139).
- [97] S. A. McDonald, C. Holzner, E. M. Lauridsen, P. Reischig, A. P. Merkle, and P. J. Withers, “Microstructural evolution during sintering of copper particles studied by laboratory diffraction contrast tomography (LabDCT),” *Scientific Reports*, vol. 7, no. 1, p. 5251, 2017. DOI: [10.1038/s41598-017-04742-1](https://doi.org/10.1038/s41598-017-04742-1).
- [98] M. Kobayakawa, S. Miyai, T. Tsuji, and T. Tanaka, “Local dilation and compaction of granular materials induced by plate drag,” *Physical Review E*, vol. 98, no. 5, p. 052907, 2018. DOI: [10.1103/PhysRevE.98.052907](https://doi.org/10.1103/PhysRevE.98.052907).
- [99] F. Spaepen, “A microscopic mechanism for steady state inhomogeneous flow in metallic glasses,” *Acta Metallurgica*, vol. 25, no. 4, pp. 407–415, 1977. DOI: [10.1016/0001-6160\(77\)90232-2](https://doi.org/10.1016/0001-6160(77)90232-2).
- [100] S. Islam, S. Yang, and C. I. Kim, “A multiscale continuum model for the mechanics of hyperelastic composite reinforced with nanofibers,” *Compos. Sci. Technol.*, [Under revision].
- [101] S. K. Garkhail, R. W. H. Heijenrath, and T. Peijs, “Mechanical Properties of Natural-Fibre-Mat- Reinforced Thermoplastics based on Flax Fibres and Polypropylene,” *Applied Composite Materials*, vol. 7, no. 5, pp. 351–372, 2000. DOI: [10.1023/A:1026590124038](https://doi.org/10.1023/A:1026590124038).
- [102] H. Stang, V. C. Li, and H. Krenchel, “Design and structural applications of stress-crack width relations in fibre reinforced concrete,” *Materials and Structures*, vol. 28, no. 4, pp. 210–219, 1995. DOI: [10.1007/BF02473251](https://doi.org/10.1007/BF02473251).
- [103] F. Serra-parareda, F. Vilaseca, R. Aguado, F. X. Espinach, Q. Tarrés, and M. Delgado-aguilar, “Effective young’s modulus estimation of natural fibers through micromechanical models: The case of henequen fibers reinforced-pp composites,” *Polymers*, vol. 13, no. 22, p. 3947, 2021. DOI: [10.3390/polym13223947](https://doi.org/10.3390/polym13223947).
- [104] N. Andre and Z. M. Ishak, “Predicting the Tensile Modulus of Randomly Oriented Nonwoven Kenaf/Epoxy Composites,” *Procedia Chemistry*, vol. 19, pp. 419–425, 2016. DOI: [10.1016/j.proche.2016.03.033](https://doi.org/10.1016/j.proche.2016.03.033).
- [105] M. Rabiei *et al.*, “Measurement modulus of elasticity related to the atomic density of planes in unit cell of crystal lattices,” *Materials*, vol. 13, no. 19, p. 4380, 2020, ISSN: 19961944. DOI: [10.3390/ma13194380](https://doi.org/10.3390/ma13194380).